Composition and Biodegradation of DOM Leached from Permafrost End-members across the Western Canadian Arctic

by

Erin MacDonald

A thesis submitted in partial fulfillment of the requirements for the degree of

Master of Science

in

Ecology

Department of Biological Sciences
University of Alberta

ABSTRACT

Organic matter, upon dissolution into the aqueous state as dissolved organic matter (DOM), can undergo mineralization by microbes (biodegradation). There has been increasing effort to characterize DOM released from thawing permafrost because it may perpetuate a permafrost carbon feedback. Permafrost-derived DOM has a composition that can be highly susceptible to biodegradation (biolabile), but studies to date have been limited in scope. Importantly, diversity in deposit type and thaw modification processes have led to spatial and stratigraphic variability in permafrost, but our understanding of how the composition and biolability of DOM derived from differing permafrost types (end-members) is poor. Furthermore, few studies couple biolability measurements with assessing the microbial community structure, despite the important role that these microbes play in degrading DOM. This project aims to investigate how the composition of DOM leached from diverse permafrost end-members may vary, how compositional differences may relate to biodegradation rates, and how microbial communities sourced from contrasting thaw-affected areas may differ in their structure, or enable differences in biodegradation rates. Using Fourier transform ion cyclotron resonance mass spectrometry, we identified marked variation in DOM composition among permafrost end-member types. Permafrost leachates were generally higher in aliphatics, lower in aromatics, and were less oxygenated than active layer leachates. Tills were compositionally dissimilar to all other permafrost end-members. Compounds unique to Yedoma were predominantly aliphatic, while compounds unique to peat, lacustrine, and diamicton spanned saturation and oxygenation. DOM compositional differences were linked to varying carbon-normalized biodegradation rates in the incubation experiment. Though there was variation by site, DOM compositional shifts demonstrated that microbially-produced/protein-like components

were preferentially consumed over terrestrially-derived/humic-like components. Biodegradation rates were slightly elevated in samples treated with microbial communities from aqueous environments, and the source of the inocula influenced the direction and extent of structural divergence of the communities over time. In all cases, compositional differences appear to reflect not only variation in permafrost parent materials, but also a strong effect from thaw-driven modification processes. Constraining DOM composition, biolability, and assessing its stratigraphic variability, linked with assessing microbial communities, will become more pressing as the spatial and stratigraphic extent of thaw increases with future warming.

PREFACE

This thesis is the result of a collaborative effort between co-authors, where the contribution of each collaborator is described in detail below. I was responsible for writing the introductory and concluding chapters (1 and 4, respectively), with insight provided by Dr. Suzanne Tank.

For Chapter 2, Dr. Suzanne Tank and I developed the experimental design, which used permafrost core samples that were previously collected by Dr. Duane Froese, Dr. Steve Kokelj, and their colleagues (as part of a larger geotechnical program to characterize permafrost conditions along a northern highway). I was responsible for collecting active layer and near-surface permafrost cores, as well as completing data collection, data analysis, and manuscript composition, with oversight from Dr. Suzanne Tank. Dr. Ryan Hutchins provided methodological assistance for the detailed compositional analysis.

MacDonald, E., Tank, S., Froese, D., Kokelj, S. and R. Hutchins. DOM Composition Varies with Permafrost Type across the Western Canadian Arctic. In preparation for submission to *Environmental Research Letters*.

For Chapter 3, I was responsible for the experimental design, data collection, data analysis, and manuscript composition, with oversight from Dr. Suzanne Tank. Within this chapter, co-authors Alireza Saidi-Mehrabad and Dr. Brian Lanoil provided methodological assistance and guidance on data analysis.

MacDonald, E., Tank, S., Saidi-Mehrabad, A. and B. Lanoil. Varying DOM Composition and Biolability Throughout Thermokarst-affected Permafrost Stratigraphy. In preparation for submission to *Journal of Geophysical Research: Biogeosciences*.

To my Dziadzio,

you'll always be jumping.

"Then I might know like water how to balance

The weight of hope against the light of patience"

— *A Short Story of Falling* by Alice Oswald

ACKNOWLEDGMENTS

First and foremost, I would like to thank my supervisor, Dr. Suzanne Tank, for her unwavering support throughout this thesis. This experience has been overwhelmingly positive, and I attribute that mostly to Suzanne. As a driven mentor, I am grateful to her for leading me towards a high level of scientific rigour, while exemplifying compassionate leadership and fostering my professional growth. I would like to thank the members of my committee, Dr. Duane Froese, Dr. Steve Kokelj, and Dr. Brian Lanoil, for providing invaluable samples, immense insight and guidance. I would also like to thank my arms-length examiner, Dr. Alberto Reyes, for sharing his time and expertise. Thank you to both Dr. Ryan Hutchins and Alireza Saidi-Mehrabad for their methodological assistance, which elevated the caliber of this research.

An immense thank you to the communities of Inuvik, Tuktoyaktuk, and Fort McPherson (Tetl'it Zheh), for sharing your land and welcoming me into your community. Thank you to the Gwich'in Renewable Resources Council, and to wildlife monitors Billy Wilson and Peter Snowshoe for their extensive knowledge of the land. A special thanks to Gabriela Lech and Casey Buchanan for their assistance in the field, and to my row-housemates for transforming the cold, wet summer into an amazing experience. I am grateful for financial support from the University of Alberta, National Science and Engineering Research Council, UAlberta North, Aurora Research Institute, and Northern Scientific Training Program.

Thank to you my entire support network. I am endlessly grateful for the academic advice and friendship I found in my Tank labmates, CSA members, and colleagues at the Centre for Writers. Thank you to my friends and family around the world, for lending me your ear, your heart, and sometimes even your couch. To my mom and dad: it seems incomprehensible to thank you for everything that you have done for me. So, thank you for always supporting me, and for letting me see Lucy when we videocall. To Kevin, I haven't figured out how, as the younger sibling, you became wiser than me, but I am so thankful for your kindness, your honesty, and your friendship. Thank you to my Babcia and Dziadzio for your interest in my research, for encouraging me to pursue science, and for your unquestioning support. To my partner, Spencer, thank you for brining me home-made meals when I was working late in the lab, for listening to my practice presentation and still coming to the public one, for offering feedback on my random rants, and for showing me how wonderful love can be(an).

TABLE OF CONTENTS

LIST OF TABLES

LIST OF FIGURES

CH. 1: Introduction

1.1 Climate Change, Carbon, and the Arctic

Since substantial atmospheric release of greenhouse gases, such as carbon dioxide, in the last century has led to climate change, there has been increasing effort to understand the processes within ecosystems that both sequester and release carbon (Heimann and Reichstein 2008). Due to profound changes in Earth system processes, the ability for an ecosystem to act as a sink may decline over time, and some ecosystems may transition to becoming a source of carbon (Le Quéré et al. 2009). This shift is expected to occur in permafrost regions, where warming temperatures enhance permafrost thaw and cause previously sequestered carbon to be released into the atmosphere, creating a positive feedback loop with climate change (Schuur et al. 2015).

Concern about the permafrost carbon feedback has prompted estimates of the amount of carbon stored in northern regions, and predictions for the amount of carbon that may be released following thaw. A recent estimate suggests that approximately 1460-1600 Gt of organic carbon may be stored in Arctic and boreal permafrost regions, of which between 10-240 Gt of carbon may be released into the atmosphere by 2100 (Meredith et al. 2019); but uncertainty regarding the mechanistic pathways that affect storage and release of carbon in different regions hampers predictions. While there are different mechanistic pathways for release and uptake of carbon, one of the key natural pathways for release of atmospheric carbon is through microbial decomposition (biodegradation; Battin et al. 2008). Importantly, not all organic matter is equally susceptible to degradation, due in part to differences in the composition of the substrate (Marschner and Kalbitz 2003) and activity of the microbial community (Graham et al. 2012). Since the rate and extent of biodegradation will partly dictate the subsequent release of carbon dioxide, there has been a surge in studies in the last decade that aim to quantify biodegradability of permafrost-derived organic carbon.

1.1.1 The Emerging Consensus of Biolabile Permafrost-DOM

Carbon stored in organic matter can become available to biodegradation following dissolution into the aqueous state as dissolved organic matter (DOM), and can undergo biodegradation in situ, along transport pathways, and within aquatic systems (Abbott et al. 2016). There are strong interactions between terrestrial and aquatic environments in permafrost

landscapes, which enable multiple different pathways for transport and processing of carbon (Vonk, Tank, and Walvoord 2019). Porewaters leach DOM from soils, which can then travel through sub-surface channels or interact with various types of surface waters including streams, rivers, ponds, or lakes, and can eventually reach the Arctic ocean.

There have been numerous investigations of DOM biodegradation within aquatic systems, and more recently for permafrost soil leachates, which have identified that compositional differences in permafrost-DOM make it more readily biodegraded than contemporary sources of DOM. In aquatic systems, DOM from permafrost thaw streams has demonstrated relatively high biodegradability compared to modern river DOM sources (Vonk et al. 2013), with decomposition occurring most rapidly in first-order watersheds, allowing the permafrost 'signal' to quickly disappear within stream networks (Spencer et al. 2015; Drake et al. 2015). In situ, mineralization can occur immediately upon thaw within soil pore waters (Vonk, Tank, and Walvoord 2019), where biodegradation rates of permafrost-derived DOM can not only exceed active layer-derived DOM (Ward and Cory 2015; Panneer Selvam et al. 2017, but see Wickland et al. 2018), but can further increase with depth (Heslop et al. 2019).

The differences in susceptibility to biodegradation, or biolability, have been linked to DOM compositional differences, because permafrost generally contains relatively high proportions of protein-like, microbially-produced, and aliphatic compounds that are preferentially consumed over humic-like, terrestrially-derived, aromatic compounds (Wickland et al. 2012; Abbott et al. 2014; Drake et al. 2015; Ward and Cory 2015; Spencer et al. 2015; Mann et al. 2016; Wickland et al. 2018; Textor et al. 2019). This has led to an emerging consensus that permafrost-derived DOM is universally highly biolabile, even though few studies consider how the composition of permafrost-origin DOM may vary according to its formation and modification processes.

1.1.2 Uncertainties Remain for Permafrost-DOM Variability

The circumpolar Arctic is heterogeneous at regional, landscape, and stratigraphic scales, highlighting the need to consider how variability across these scales may influence the biogeochemistry of DOM that is liberated to aquatic flowpaths following permafrost thaw. At a regional scale, numerous biodegradation and compositional studies have been completed for areas such as Siberia (Vonk et al. 2013; Spencer et al. 2015; Mann et al. 2016), and Alaska

(Drake et al. 2015; Ewing et al. 2015; Ward and Cory 2015; Wickland et al. 2018; Heslop et al. 2019; Textor et al. 2019), but are somewhat sparse for China (Wang et al. 2018) and Canada (Littlefair and Tank 2018). These regions differ in their geological history, where factors such as glaciation, extent of permafrost, and parent material can all contribute to the chemical composition of permafrost (Lacelle et al. 2019; Tank et al. 2020), and therefore may also impact the biogeochemical cycling of permafrost-derived DOM. At a landscape scale, biodegradability has been assessed in permafrost peatlands (Panneer Selvam et al. 2017; Burd et al. 2020), but other landscape types, such as forested areas, riparian zones, or hills and valleys, are either consolidated (e.g., Wickland et al. 2018) or have been excluded from studies to date. At a stratigraphic scale, most biogeochemical studies do not consider variation with depth, and focus on a single type of permafrost "end-member", even though stratigraphic units that have undergone subsequent modification can display geochemical characteristics (Burn 1997; Lacelle et al. 2019). Here, the term "end-member" refers to permafrost that formed under varying environmental conditions, which is influenced by geological setting, climate, and ecosystem history that act together over time to shape distinct types of permafrost material.

1.1.3 Microbes in Permafrost are Influenced by Thaw and DOM Composition

In recent decades, a surprising consensus has developed that even at low temperatures within permafrost, microbes can be active by growing, dividing, and performing metabolic functions (e.g., Mackelprang et al. 2017). These active microbial communities can be highly diverse across permafrost regions (Malard and Pearce 2018 and references within). The heterogeneity of permafrost landscapes may contribute to spatial variation in local microbes, influencing both the taxonomic structure and the functional capabilities of the microbial community (Jansson and Taş 2014). In addition to differing between the active layer and permafrost, the microbial community composition can be highly variable within permafrost stratigraphies, varying at scales as fine as 3 cm (Müller et al. 2018). Microbial diversity is also reflected in surface water environments, such that the taxonomic structure can vary not only between thaw ponds and rock-basin lakes, but also demonstrate immense diversity among thaw ponds within the same valley (Comte et al. 2016).

Despite the diversity of permafrost microbes, they can be vulnerable to impacts from permafrost thaw (Blaud et al. 2015). Following thaw, the permafrost microbial community structure can rapidly converge to become more similar to the active layer (Mackelprang et al.

2011). Permafrost thaw can induce structural changes by decreasing the representation of *Proteobacteria*, *Acidobacteria* and *Actinobacteria*, while increasing representation of *Firmicutes* and *Bacteriodetes* (Coolen and Orsi 2015). In situ sustained thaw (ten years of experimental warming) linked microbial community structural changes to differences in respiration rates, suggesting thaw-induced structural shifts may have important implications for carbon cycling (Monteux et al. 2018).

Permafrost thaw can also indirectly affect microbes by changing the types of substrate, such as through differing DOM compositions, that are readily available for microbes to utilize. The source of DOM can strongly shape microbial community structure (Ward et al. 2017), such that microbes from different inocula sources can converge based on the source of DOM (Judd, Crump, and Kling 2006). Less oxygenated compounds found in permafrost-derived DOM were associated with higher bacterial production rates and growth efficiencies when compared to the more oxygenated DOM derived from the active layer (Ward and Cory 2015). In contrast, while there were no significant differences in production or growth efficiencies, there were higher bacterial respiration and carbon consumption rates when microbes were exposed to more biolabile DOM derived from thawed permafrost relative to the active layer (Panneer Selvam et al. 2017).

It is important to consider not only how permafrost thaw may affect microbes, but also if there are implications for DOM biodegradation rates. Retrogressive thaw slumps, a dramatic form of permafrost thaw (Lacelle et al. 2015; Kokelj, Tunnicliffe, and Lacelle 2017), can mobilize substantial thaw material and alter the composition of DOM in recipient streams (Littlefair, Tank, and Kokelj 2017). However, a gap of knowledge remains on how the composition of microbial communities may be affected by thaw slumps, or if changes in the microbial community may subsequently affect biodegradation rates of DOM derived from thawing permafrost.

1.1.4 Study Region Description

The western Canadian Arctic is a highly diverse region, where permafrost stratigraphies can contain multiple permafrost end-members that have undergone various formation and modification processes (Rampton 1988). We included samples from three general areas that represent varying permafrost extent, glacial legacy, and thermokarst influence. The northernmost

area is along the Inuvik-Tuktoyaktuk Highway (ITH), NT, which spans a forest to tundra transition (south to north; Kokelj et al. 2017a), and includes plains with gently sloping topography, as well as the coastlands that have hummocky topography (Rampton 1988) with abundant lakes (Burn and Kokelj 2009). To the southwest is the Peel Plateau, NT, a fluvially-incised moraine landscape, with abundant ice-rich tills and a patchy distribution of glacifluvial and glacilacustrine sediments (Kokelj, Tunnicliffe, and Lacelle 2017; Kokelj et al. 2017b). These two areas (the ITH and Peel Plateau) are in the continuous permafrost zone within a region that was previously glaciated, and have been strongly shaped by the glacial legacy (Burn and Kokelj 2009; Mackay 1963; Rampton 1988). Extensive permafrost thaw, thermokarst development, and lake drainage through the Holocene has significantly modified these glacially conditioned landscapes.

The Peel Plateau has abundant valleys and streams that incise the landscape, where recent warming has intensified thermokarst activity (Kokelj et al. 2017b). Thermokarst can manifest as multiple geomorphic formations, but retrogressive thaw slumps are the dominant mode of slope failure in the Peel Plateau (Lacelle et al. 2015; Kokelj, Tunnicliffe, and Lacelle 2017). The headwalls of these thaw slumps expose a striking permafrost stratigraphy, typically revealing an active layer overlying permafrost above a thaw unconformity demarcating the extent of deeper thaw during the early Holocene, and underlying ice-rich tills (Burn 1997; Zolkos, Tank, and Kokelj 2018; Lacelle et al. 2019). The relict active layer formed during a warming period in the early Holocene, when an increase in active layer thickness facilitated soil development. Upward aggradation of permafrost followed in association with cooling during the middle and late Holocene (Burn 1997; Kokelj et al. 2017b; Lacelle et al. 2019).

The southernmost area is in the Klondike region of central Yukon, which is in the discontinuous permafrost zone and was not previously glaciated (Froese et al. 2009). Here, loessal sediments and a variety of ground ice bodies formed, creating ice-rich syngenetic permafrost, locally known as ‘muck’, and otherwise referred to as ‘Yedoma’ (terminology varies by country and discipline; French and Pollard 1985; Schirrmeister et al. 2013). While this region has undergone significant aggradation of loessal silts, variation in temperature through the Pleistocene caused marked shifts in vegetation, productivity, and the rapidity of permafrost aggradation, and thus also the organic matter content of these Yedoma soils (Mahony 2015).

1.2 Project Goals and Research Objectives

The variation in permafrost characteristics across the western Canadian Arctic provides an opportunity to test how permafrost-origin DOM may vary according to differing formation processes. This project aims to investigate how the composition of DOM leached from permafrost may vary across diverse permafrost end-members, how compositional differences may relate to biodegradation rates, and if these biodegradation rates are affected by the addition of microbial communities sourced from areas with contrasting degrees of impact from permafrost thaw.

This thesis is formatted as two manuscript-style chapters with appendices. Details for the objectives and hypotheses for each data chapter are described below. The final chapter provides a summary of general conclusions, including a brief discussion of some limitations for the results presented. I also provide recommendations for future research that could build upon the findings described in this thesis.

The first component of my thesis undertakes a highly detailed DOM compositional analysis for multiple end-member types, using permafrost cores that were previously collected by Dr. Duane Froese, Dr. Steve Kokelj, and colleagues, augmented by a series of near-surface samples that I collected in summer 2018. The research objectives for Chapter 2 are: to assess (1) how DOM composition may vary across end-members that have contrasting histories of formation and modification; and (2) how the composition of DOM leached from contemporary active layer samples from multiple landscape types (peatland, riparian and hilltop) compares to the composition of DOM leached from permafrost end-members.

I hypothesize that (1) DOM composition will differ among end-member types, such that the proportion of aliphatic compounds will be highest in Yedoma and till samples due to reduced processing, and lower in diamicton, lacustrine and peat samples due to partial processing; and (2) active layer samples will have similar DOM composition across landscape type, but that the active layer leachates will contain a higher proportion of aromatic compounds and more oxygenated compounds relative to permafrost leachates.

The second component of the project includes a biodegradation experiment for DOM derived from the contemporary active layer, the Holocene-associated relict active layer, and Pleistocene-associated tills, linking both compositional characterization and microbial

community structure analyses. The research objectives for Chapter 3 are: to assess (1) if the DOM composition of permafrost leachates varies across stratigraphic units, and how this variation may tie to differences in biodegradation rates; and (2) whether microbial communities from different sources within this disturbed landscape (e.g., unimpacted streams, relative to thaw slump runoff) differ in their composition, or enable differences in biodegradation rates.

I hypothesize that (1) DOM composition will differ across strata, such that Holocene-associated permafrost will release more biolabile DOM with higher biodegradation rates than Pleistocene-associated sources, which will both exceed active layer leachates; and (2) the initial structure of microbial communities will be different due to contrasting sources of the inoculum, but that the structure will converge based on the DOM composition, and that biodegradation rates will be similar regardless of inocula source.

CH. 2: DOM Composition Varies with Permafrost Type across the Western Canadian Arctic

2.1 Introduction

There has been increasing effort to characterize organic matter that may be released from permafrost, since decomposition of the large stocks of carbon stored in permafrost soils may perpetuate a permafrost carbon feedback (Hugelius et al. 2014; Schuur et al. 2015). Decomposition of organic matter can occur via different mechanistic pathways, and upon dissolution into the aqueous state as dissolved organic matter (DOM), it can undergo mineralization by microbial organisms (biodegradation; Battin et al. 2008). DOM released from permafrost has been shown to be highly susceptible to biodegradation, and is therefore generally considered to be biolabile (Vonk et al. 2015; Drake et al. 2015; Ewing et al. 2015; Ward and Cory 2016; Heslop et al. 2019). The susceptibility of DOM to biodegradation is strongly related to its composition (Kalbitz et al. 2003), but characterizing the complex, heterogenous mixture that comprises the bulk DOM pool requires highly-detailed techniques, such as Fourier transform ion cyclotron resonance mass spectrometry (FT-ICR MS; Koch and Dittmar 2006; Dittmar et al. 2008).

There has been a surge in studies utilizing FT-ICR MS to characterize DOM composition over the past decade, which has provided insight into DOM composition in peatlands (Hodgkins et al. 2014), fluvial systems (Spencer et al. 2015), and lakes (Johnston et al. 2019) affected by permafrost thaw. To assess DOM that is directly available to be leached from permafrost soils, the water-extractable fraction of organic matter (WEOM) has been employed to assess the composition and biolability of permafrost in Alaska (Ward and Cory 2015; Heslop et al. 2019; Textor et al. 2019) and China (Wang et al. 2018). These studies have often concluded that DOM derived from permafrost soils is comprised of highly saturated, aliphatic compounds (e.g., lipids, proteins and carbohydrates), which tend to be more biolabile than less saturated (e.g., lignins and tannins), or aromatic compounds (e.g., phenolics or combustion-derived black carbon; Hodgkins et al. 2014; Spencer et al. 2014; Wang et al. 2018). Importantly, most studies to date that examine DOM composition have compared permafrost-derived DOM extracts to those from the active layer (e.g., Ward and Cory 2015; Wang et al. 2018; Textor et al. 2019), or have focused on a single type of permafrost “end-member” (e.g., Yedoma deposit in Heslop et al. 2019), but have

not yet accounted for how variation in permafrost history of formation and modification may influence DOM composition.

In this study, the term "end-member" refers to different permafrost material that formed under varying environmental conditions, as a result of geologic context, climate, and ecosystem history. Differentiating permafrost into end-member types enables consideration of differences in formation and modification, which can vary substantially across regional (e.g., outside of vs within past glacial limits), local (e.g., locations of organic matter accumulation), and sub-local (i.e., within permafrost stratigraphies) scales. In addition to differing permafrost formation, such as through syngenetic (deposits are immediately incorporated through upwards aggradation) or epigenetic (downward aggradation of previously deposited material; French and Shur 2010) formation, differences in thaw-driven modification can vary substantially. For example, glacial-origin unconsolidated deposits (tills) that thaw can be reworked to form diamicton deposits; formation of waterbodies create thermal disturbances, thawing underlying permafrost and maintaining sediments in an unfrozen state to form a talik; following the drainage of thermokarst lakes, permafrost can aggrade into exposed lake bottom sediments (lacustrine); these flat, poorly drained environments also typically facilitated peat formation, which becomes preserved in a frozen state through upward aggradation of the permafrost (Rampton 1988; Morris et al. 2018; Burn and Kokelj 2009; Meyers and Lallier-Vergès 1999). The diversity of formation and modification highlights the need to consider how DOM derived from differing permafrost end-members may vary in its composition.

To examine if spatial and stratigraphic variation may lead to differences in DOM composition, we sampled diverse end-member types from a broad latitudinal and permafrost gradient across the western Canadian Arctic. We obtained samples from sites with contrasting geomorphic, climate, and ecosystem histories. A majority of sites are from previously glaciated landscapes within the continuous permafrost zone that span the treeline transition in the Northwest Territories (Burn and Kokelj 2009). This region has dynamic depositional environments, where variation in Holocene climate and post-glacial terrain modification have produced a high degree of landscape heterogeneity suggesting variable sensitivities to impacts from climate change (Lantz, Gergel, and Kokelj 2010; Kokelj et al. 2017b). Additionally, a small portion of samples were collected from the extensive-discontinuous permafrost zone in the unglaciated region of

central Yukon, which is characterized by substantial aggradation of loessal silts (Froese et al. 2009).

Here, we assess (1) how DOM composition may vary across end-members from permafrost terrain that have contrasting geological origins and have been subject to varying degree of thaw modification, and (2) how contemporary active layer samples from multiple terrain types (peatland, riparian and hilltop) compares to those from permafrost end-members. We used FTICR-MS to characterize DOM composition for the WEOM fraction leached from diverse permafrost end-member types, including tills, diamicton, lacustrine, peat, and Yedoma deposits, as well as from contemporary active layer samples from multiple landscape types.

2.2 Study Region Description

The broad study area spans ca. six degrees of latitude in the western Canadian Arctic, from the northern Northwest Territories (NT) to the Klondike region in central Yukon. Sites in the NT are in a glaciated terrain within the zone of continuous permafrost spanning the forest to tundra transition zone (south to north; Kokelj et al. 2017a; Burn and Kokelj 2009). As a result, material in this region is associated with glacial origins, while post-glacial modification by thaw and ecological succession contribute to permafrost variability. This region is divided into two physiographic subdivisions. The southern sites (BH1–6; Figure 2-1) are located in the Anderson Plains, which is characterized by gently sloping topography with some basins and valleys, where imperfect drainage can facilitate formation of peatlands (Rampton 1988; Vardy, Warner, and Aravena 1998). The northern sites (BH7–10) are in the Tuktoyaktuk Coastlands, which is characterized by rolling hummocky topography with intervening valleys (Rampton 1988) and abundant depressions where lakes form (Burn and Kokelj 2009).

While the glacial legacy has strongly shaped the NT region, dynamic depositional environments and variation in Holocene climate have enabled thaw-drive modification, creating multiple permafrost end-member types that can be found throughout this region. The Laurentide Ice Sheet glaciated this area during the late Wisconsinan (Murton 2009), which deposited abundant till sediments derived from carbonate- and sulfide-rich shale bedrock (Norris 1973; Zolkos, Tank, and Kokelj 2018). While deep tills have likely remained frozen since deposition, more shallow deposits thawed during a warming period in the early Holocene, and were reworked as diamicton (we distinguish diamicton from tills when it has undergone some degree of thaw or processing) before re-

incorporation into permafrost during a subsequent cooling period (Burn 1997). Driven by the transition from warmer to cooler temperatures in the Holocene, a similar pattern of thaw, processing, and re-freezing affected other types of ecosystem soils and sediments. Warming enhanced plant productivity and increased production of organic matter, and in areas with poor drainage, saturated soils led to incomplete decomposition, allowing accumulation of peat that gradually aggraded into permafrost in cooler temperatures (Morris et al. 2018). During warm or wet conditions, thaw lakes commonly formed in depressions (Burn and Kokelj 2009) where lacustrine sediments, which typically contain a mixture of terrigenous and autochthonous (within-lake) organic matter (Meyers and Lallier-Vergès 1999) accumulated in lake basins. Thermal disturbance of the lake would have resulted in talik formation so the lacustrine sediments would have been completely thawed for a significant amount of time. Drainage or drying of lake basins was followed by permafrost aggradation, followed by gradual peat accumulation and concurrent upward aggradation of the permafrost table. In addition to these permafrost end-member types, we also sampled contemporary active layer soils from multiple landscapes (peatland, riparian and hilltop) to understand how variation between divergent sources of surficial soils compares to that between our permafrost end-members.

In contrast to site in the NT, the Klondike region is unglaciated terrain within the extensive-discontinuous permafrost zone (Froese et al. 2009). Because it was too dry to support extensive glaciation during the last glacial interval, loessal sediments and syngenetic permafrost aggraded during the late Wisconsinan (Fraser and Burn 1997; Froese et al. 2009). In addition to aggrading clastic sediments, a variety of ground ice bodies formed, creating ice-rich syngenetic permafrost, locally known as ‘muck’ (terminology varies by country, and is also described as ‘ice complex’ or ‘Yedoma’ in the Russian literature; French and Pollard 1985; Schirrmeister et al. 2013). While this region is characterized by substantial aggradation of loessal silts during the last glacial period, variation in temperature through the Pleistocene caused marked shifts in vegetation, productivity, and the rapidity of permafrost aggradation, and thus also the organic matter content of these Yedoma soils (Mahony 2015). Yedoma from the Klondike region has been shown to range from relatively organic-rich sediments (~5.2% carbon) associated with spruce and shrub macrofossils representative of a warmer and wetter environment (ca. 50,000–36,000 calibrated years before present; cal ybp), to organic-poor grey silts (~1.5% carbon) that are associated with graminoids and reduced shrub vegetation, representative of a colder, drier period (ca. 27,000-13,150 cal ybp; Mahony 2015).

Samples from the Klondike region thus provide the opportunity to compare Yedoma permafrost from western Canada to that from other regions that have been previously characterized (e.g., Spencer et al. 2015; Ewing et al. 2015).

2.3 Methods

2.3.1 Sample Collection

To better understand the importance of variation in geomorphic and ecological history, we selected a series of distinct end-members that represent varying formation and modification processes. Till, diamicton, peat, lacustrine, and active layer samples were each obtained from varying depths within cores collected from the NT region, while Yedoma was collected from the Klondike region. We collected bulk active layer soil and permafrost samples from clusters of hilltops, riparian, and peatland sites across a latitudinal gradient through the forest-tundra transition zone (Figure 2-1). Borehole samples below two meters (2–15 m depths; Table 2-1.) were collected in February 2017 using a LECO corer or an auger with diamond teeth, as part of a larger geotechnical program to characterize permafrost conditions along the Inuvik-Tuktoyaktuk Highway (ITH; Ensom et al. 2020). Samples from above two meters (0.2–2 m depths; Table 2-1.) were collected from the same sites in July 2018, using either a gas or electric drill with diamond teeth. Samples from the Mint Gulch site in the Klondike region were collected horizontally from a mining exposure using an electric drill with diamond teeth, from Yedoma deposits approximately 6-7 m below the surface. In all cases, samples were transported from the field to the laboratory in a frozen state, then were stored in a dark freezer (-20°C) until processing.

2.3.2 Leaching and Processing Procedure

To remove contamination, the surface (~2 mm) of all samples were scraped clean using a sterile razor blade. A tooth saw was then used to isolate the target end-member depth, and a chisel and hammer were used to separate the subsample. Subsamples were kept frozen (-20°C) in the dark until lyophilization (freeze-drying). Large rocks and debris were removed by hand following lyophylization, then material was homogenized using a mortar grinder with a natural agate mortar and pestle. Approximately 4 g of homogenized material was placed into pre-cleaned (acid-washed, MilliQ rinsed, then combusted at 475°C for four hours) glass 50 mL centrifuge

tubes. Sample tubes were sealed with PTFE-lined caps and stored overnight in a dark fridge (4°C) until leaching.

To characterize the organic matter relevant for the soil-water interface, we chose to use MilliQ water as the solvent to capture the WEOM fraction (following e.g., Ward and Cory 2015; Drake et al. 2015; Wickland et al. 2018; Heslop et al. 2019). We added 40 mL of MilliQ (1:10 soil weight to water volume), shook the samples in the dark for two hours, centrifuged at 1200 g for 10 minutes, then collected the supernatant using a glass pipette (Tfaily et al. 2017). The WEOM was filtered through 0.45 μm PES syringe filters, then the filtrate was collected into pre-cleaned glass beakers and stored in a dark fridge (4°C) until sample analysis. We completed a sequential extraction on the remaining sediment using methanol and chloroform, then used the methanol fraction for further analysis since it is able to capture a different range of compounds than the WEOM fraction (Tfaily et al. 2017). We briefly compare the relative abundance of compound classes when using these different solvents (Figure A1-1), but focus on the WEOM fraction for most of our analyses.

2.3.3 FT-ICR MS and Ancillary Chemical Analyses

Following common methodology, WEOM leachates were acidified with trace metal grade hydrochloric acid to pH 2, then passed through 100 mg Bond Elut PPL cartridges (Agilent Technologies; Dittmar et al. 2008). The solid-phase concentrated samples were eluted with 1 mL methanol into pre-cleaned 2 mL glass amber vials, then were stored in a dark freezer (-20°C) until they were injected into the FT ICR MS. We used a 9.4T Bruker Apex-QE mass spectrometer (Bruker Daltonics) with an Apollo II electrospray ionization source in negative mode. Samples were injected at a flow rate of 120 μL hr^{-1} to acquire 300 spectra scans. We assigned formulae based on quality-inspected masses, following published protocol (Merder et al. 2020). The formulae were used to calculate a corresponding oxygen to carbon ratio (O/C), hydrogen to carbon ratio (H/C), and modified aromatic index (AI; Koch and Dittmar 2006). The O/C, H/C and AI were then used to sort the compounds into five broad classes: ‘aliphatic’ (H/C >=1.5), ‘low O unsaturated’ (H/C <1.5, O/C <=0.5, AI <0.5), ‘high O unsaturated’ (H/C <1.5, O/C >0.5, AI <0.5), ‘aromatic’ (0.5<=AI<0.67), ‘condensed aromatic’ (AI>=0.67; Hawkes et al. 2020; Figure A1-2). For each sample, compounds were expressed in relative abundance using sum-normalized intensity.

WEOM leachate subsamples were collected for analysis of soil organic matter (SOM) concentration, dissolved organic carbon (DOC) concentration, DOM composition using absorbance (i.e., the slope ratio; Helms et al. 2008), dissolved trace metals, and total dissolved phosphorus (TDP). Analyses followed standard techniques as described in the supplement.

2.3.4 Statistical Analyses

All statistical analyses were completed using R version 3.6.3, including frequently used packages *ggplot2*, *dplyr*, and *tidyr*. Linear regression was used to determine relationships between SOM and leachate DOC, TDP, and S_r. We used *vegan* to determine Bray-Curtis Dissimilarity of FT-ICR MS compounds, visualized using non-metric multidimensional scaling (NMDS). This was coupled with Spearman's rank correlation to determine which compounds were most strongly associated with the first NMDS axis (MDS1).

2.4 Results

2.4.1 Bulk Leachate Properties

Across all end-member samples, DOC and TDP were positively correlated to SOM ($p<0.001$, $R^2=0.506$ and $p=0.004$, $R^2=0.532$, respectively), which generally declined with depth. Comparing samples among end-member types, both DOC and TDP were relatively high for peat and active layer samples, but relatively low for till, lacustrine, and Yedoma samples (Figure 2-2). Conversely, S_r (a DOM compositional metric that declines with increasing molecular weight) was negatively correlated to SOM ($p=0.002$, $R^2=0.591$) and increased with depth, suggesting a transition from higher molecular weight compounds in active layer sources and peat samples towards lower molecular weight compounds in other leachate types (Helms et al. 2008). While trace metal concentrations showed no clear trends with depth, there were differences among end-member types (see also Lacelle et al. 2019). Lacustrine leachates had markedly higher concentrations of magnesium, calcium and strontium than all other end-members (Figure A1-3). Sodium was higher in diamicton and Yedoma leachates, but slightly lower in till samples. Peat leachates were distinguished by higher zinc and arsenic concentrations than all other end-members.

2.4.2 FT-ICRMS Reveals Clear Differences among Permafrost End-member Types

While active layer leachates were clearly distinct in their DOM composition compared to those from permafrost, we also found substantial differences in compound class proportions

among permafrost end-member types (Figure 2-3). The proportion of compound classes broadly indicates the relative abundance of compounds that are present in DOM, where aliphatic compounds include lipids, proteins and carbohydrates, unsaturated compounds include lignins and tannins, and aromatic compounds include phenolics and combustion-derived black carbon (Hodgkins et al. 2014; Spencer et al. 2014; Wang et al. 2018). Active layer leachates had a higher proportion of both aromatic and condensed aromatic compounds, and a lower proportion of aliphatic compounds, compared to all permafrost end-members. Within the permafrost end-members, the proportion of aliphatic compounds generally increased, while aromatics decreased, moving from diamicton, to lacustrine, to Yedoma, to peat, to till leachates. Diamicton and till leachates had relatively high proportions of low-oxygen unsaturated compounds, while till also had relatively low proportions of high-oxygen unsaturated compounds. Notably, these trends changed when using chloroform-methanol (instead of MilliQ) as the solvent (Figure A1-1). Here, methanol fractions captured a higher proportion of aliphatics in all but till leachates, and slightly reduced overall proportions of aromatic and condensed aromatic classes. Compared to WEOM leachates, methanol extractions had fewer high-oxygen unsaturated compounds, but more low-oxygen unsaturated compounds.

The NMDS reinforced the findings of the compound class assessment, and further showed that active layer leachates were compositionally similar to each other regardless of landscape type. Similarly, permafrost leachates showed little to no variation among landscapes within end-member types, but demonstrated a clear demarcation among end-member types (Figure 2-4a). Along MDS1, diamicton leachates were most compositionally similar to active layer leachates, and were relatively similar to peat, lacustrine, and Yedoma leachates. Till leachates were most dissimilar from other end-member types, and also display more compositional variation within this end-member type. There was muted divergence along MDS2, which separated single hilltop diamicton and till samples from all other leachates, showing a marginal effect from landscape type. A van Krevelen plot of the correlation between individual compounds and MDS1 demonstrates that leachates positively associated with MDS1 (particularly tills) were predominantly associated with low-oxygen compounds, mostly in the unsaturated and aromatic classes (Figure 2-4b). In contrast, leachates negatively associated with MDS1 (active layer) were predominantly associated with moderate-oxygen unsaturated and

aromatic classes. Leachates located more centrally along MDS1 (peat, lacustrine, Yedoma, diamicton) displayed a range of unique compounds across O/C, H/C, and compound classes.

Across all samples, FTICR-MS detected 6,450 compounds. Interestingly, the number of compounds detected within end-member types ranged substantially, from 4155 ± 48.7 (mean ± standard deviation; n=2) in lacustrine leachates to 1961 ± 1310 (n=2) in diamicton leachates (Table 2-1.). While ~31% of the compounds detected were present in all six end-member types, ~12% were found to be unique to one end-member type alone (Table 2-1.; Figure 2-5). Compounds unique to active layer leachates covered a broad range of classes, but were mostly high-oxygen aromatics and low-oxygen condensed aromatics (Figure 2-5a). Diamicton, lacustrine, and peat leachates all had fewer unique compounds which spanned the oxygenation gradient, but were primarily aliphatic, with some unsaturated and aromatic compounds (Figure 2-5b). Till leachates had unique compounds that were predominantly low-oxygen and spanned a range of saturation (H/C) from aromatic to aliphatic (Figure 2-5c). Compounds unique to Yedoma were in the low-to moderate-oxygen aliphatic class, with sparse compounds in aromatics and high-oxygen aliphatic classes (Figure 2-5d).

2.5 Discussion

Active layer leachates showed strong compositional similarity across a ~100 km latitudinal gradient, demonstrating little to no variation by landscape type (peatlands, riparian zones, and hilltops). Similar to previous studies (Mann et al. 2014; Spencer et al. 2015; Ward and Cory 2015; Wang et al. 2018; Heslop et al. 2019), active layer leachates had higher molecular weight (low S_r), more aromatic (low H/C) compounds, and were more oxygenated (high O/C) than permafrost end-members. Although leachable DOC, TDP, molecular weight, and proportion of aromatic compounds generally declined with depth, there was marked variation observed among permafrost end-member types. This likely reflects differences in permafrost formation processes, such that unmodified tills were substantially dissimilar from all other end-member types. While Yedoma composition was relatively more similar to diamicton, peat, and lacustrine, the presence of unique compounds among these end-members suggests that differences in thaw-driven modification can lead to distinct permafrost-derived DOM composition.

2.5.1 Permafrost End-members Display Unique DOM Compositions

While compounds unique to the active layer span oxygenation and saturation, compounds unique to the permafrost end-members were predominantly low- and moderate-oxygenated compounds, with sparse highly-oxygenated compounds in the aliphatic class. We observed an increasing proportion of aliphatic compounds, coupled with decreasing aromatic compounds, moving from diamicton, to lacustrine, to peat, to till leachates. Although some of these end-members were collected from the same permafrost core (Table 2-1.), their formation and modification processes have been substantially different. Tills represent bedrock-derived sediment deposited by the Laurentide Ice Sheet (Murton 2009; Kokelj, Tunnicliffe, and Lacelle 2017), and since these were sampled at depths greater than 10 m, it is unlikely they have been affected by modification associated with permafrost thaw (Burn 1997; Lacelle et al. 2019). Warmer temperatures during the early Holocene enabled thaw of shallow till deposits, re-working this material through various modification processes before re-incorporation into permafrost as diamicton. Soils and sediments that remained unfrozen for centuries to millennia accumulated in lake basins as lacustrine deposits, or in areas with increased plant productivity as peat deposits, which then aggraded more gradually (Rampton 1988; Burn 1997; Morris et al. 2018). The diamicton, lacustrine, and peat leachates demonstrate compositional similarity to each other, and are more similar to active layer leachates than they are to tills. This indicates that thaw-driven modification plays a key role in shaping DOM composition, and appears to enable compositions that are distinct from both contemporary active layer soils and ancient, unmodified till deposits.

Although Yedoma appeared similar to lacustrine and peat leachates in MDS space, the unique compounds from Yedoma leachates are well constrained to low oxygen, aliphatic species, while compounds unique to lacustrine and peat have more variation in oxygenation and saturation. The high proportion of aliphatic compounds in peat was surprising, because peat porewaters have previously demonstrated low proportions of aliphatic compounds (Hodgkins et al. 2016). In contrast, abundant aliphatic compounds in Yedoma are congruent with studies of Yedoma from other regions of the Arctic (Spencer et al. 2015; Stubbins et al. 2017; Drake et al. 2018). The organic matter content (SOM and DOC) in our Yedoma samples were comparable to our lacustrine and till samples, and were similar to organic carbon content for Yedoma from the North Slope of Alaska (radiocarbon dated to between 37,000–9,000 cal ybp; Gaglioti et al. 2018). Interestingly, our DOC concentrations were orders of magnitude lower than those reported for

Yedoma leachates from Alaska (Ewing et al. 2015; Drake et al. 2015; Heslop et al. 2019) and from streams draining thaw features in Siberia (Vonk et al. 2013; Spencer et al. 2015). The differences in DOC concentrations could result from regional variability, or may reflect differences in the age of the material. The higher DOC reported in other studies has been associated with more ancient material (~134,000–21,000 ybp), while our Klondike Yedoma samples are considerably younger (radiocarbon dates from soil samples below and above the Yedoma samples range between ca. 16,060–13,280 cal ybp). The younger material is representative of a time with lower plant productivity and reduced incorporation of organic matter due to a cooler, drier period that was beginning to transition to a relatively warmer, wetter period in the late Pleistocene (Mahony 2015).

While some permafrost end-member types were more compositionally similar to one another than others, the presence of unique compounds for all end-member types emphasizes the heterogeneity in permafrost carbon biogeochemistry, and its relationship to mode of permafrost formation and past thaw modification processes (see also Tank et al. 2020). Compositional differences among end-member types were independent of latitude (across the ~six degree span reported here). These clear compositional differences indicate varying susceptibility to decomposition across permafrost types of differing origin, with subsequent implications for organic carbon fate.

2.5.2 Linking DOM Composition with Biolability

Although we did not measure susceptibility to decomposition here, other studies have established strong links between DOM composition and biodegradation, providing a basis to assess how the differences that we quantify may affect biolability. The aliphatic class that we demarcate here can be further distinguished by the degree of oxygenation, including lipids (low O:C), proteins and peptides (moderate O:C; Hodgkins et al. 2014), as well as carbohydrates (high O:C; Spencer et al. 2015). Because this class is highly saturated and energy-rich, it is generally preferentially consumed and considered to be the most biolabile class of compounds (Textor et al. 2019). The unsaturated class is associated with lignins (moderate O:C), and tannins (high O:C), which are considered to be more recalcitrant (Hodgkins et al. 2014), although highly-oxygenated unsaturated compounds can be somewhat biolabile under anoxic conditions (Heslop et al. 2019). Aromatics are associated with phenolic compounds derived from vascular plants, though may also represent microbial biomass, while the more condensed aromatics can include combustion-derived black carbon (Spencer et al. 2014; Wang et al. 2018). Both of these

aromatic classes are considered to be recalcitrant, where some compounds may actually inhibit microbial activity (Ward and Cory 2015).

Based on the increased biolability of aliphatic compounds, the relative proportion of compounds in this class can be used to predict potential susceptibility to biodegradation (Textor et al. 2019). Relating this to the DOM composition in our samples, till leachates had the highest proportion of aliphatic compounds overall, although the aliphatic class contributes only a small portion of the compounds unique to this end-member. The abundant aliphatic compounds in tills may be a consequence of more mineral-rich particles that facilitate strong adsorption of organic matter (Ward and Cory 2015), potentially coupled with high desorption that allows this aliphatic DOM to be leached with water (Kothawala, Moore, and Hendershot 2009). Lacustrine, peat, and Yedoma contained fairly high proportions of both the aliphatic class and highly-oxygenated unsaturated compounds, suggesting these may be more biolabile than active layer-derived DOM, but less so than till-derived DOM. Interestingly, studies quantifying biodegradation rates for some of these end-members display mixed results, where peat has demonstrated relatively low biodegradation rates (Shirokova et al. 2019; Burd et al. 2020), Yedoma has demonstrated high biodegradation rates (Vonk et al. 2013; Drake et al. 2015; Heslop et al. 2019), and lacustrine biolability has yet to be studied.

2.6 Implications of Key Findings

The DOM compositional differences among end-members observed here appear to be strongly influenced by permafrost history, and in particular how past thaw can modify organic matter which later becomes incorporated into permafrost. These differences may also have implications for biolability, and thus how the substantial DOM that is lost to aquatic flowpaths following permafrost thaw (Plaza et al. 2019) impact the permafrost carbon feedback (Schuur et al. 2015). Our findings serve as a reminder that the WEOM fraction most easily leached to aquatic flow paths is representative of only a portion of the organic matter pool (Figure A1-1). This may help to explain differences between soil-based measurements of permafrost biolability (e.g., Kuhry et al. 2020) and those that focus on DOM, while also reinforcing the need for a more thorough integration of organic matter characterization across terrestrial-aquatic continua (Vonk, Tank, and Walvoord 2019). Most importantly, these results act as a call for other studies to include geological/geomorphic context and permafrost history as an underpinning to understand the fate of permafrost-origin DOM, and incorporate this variation into projections of future

change. Constraining DOM composition, lability, and assessing its stratigraphic variability will become more pressing as the spatial and stratigraphic extent of thaw increases with future warming.

Table 2-1. Coring sites and their associated landscape with various end-members, where listed depths (m) denote mid-depth of the subsample. The compounds refer to those identified using FT-ICR MS, where unique compounds are those that occur only in the specified end-member type.

Site	Latitude (DMS)	Longitude (DMS)	Land-scape	Active Layer (m)	Peat (m)	Till (m)	Lacus-trine (m)	Diamic-ton (m)	Yedoma (m)
BH1	68° 32' 19.54"	133° 46' 22.73"	Peatland	0.32	0.82	—	—	—	—
BH2	68° 32' 17.95"	133° 45' 46.15"	Hilltop	0.32	—	11.25	—	—	—
BH3	68° 32' 2.94"	133° 45' 52.24"	Riparian	0.32	—	—	—	—	—
BH4	68° 44' 57.73"	133° 32' 29.51"	Peatland	—	3.7	—	5.86	—	—
BH5	68° 45' 7.7"	133° 32' 28.25"	Hilltop	—	—	14.25	—	—	—
BH6	68° 45' 32.98"	133° 32' 42.72"	Riparian	—	—	—	—	1.12	—
BH7	69° 1' 7.79"	133° 16' 31.19"	Hilltop	0.32	—	4.75	—	—	—
BH8	69° 0' 45.25"	133° 16' 13.4"	Peatland	0.32	1.52	—	10.22	—	—
BH9	69° 0' 46.4"	133° 18' 23.36"	Riparian	0.32	—	9.25	—	—	—
BH10	69° 16' 13.84"	132° 56' 4.45"	Hilltop	—	—	—	—	9.5	—
KL	63° 56' 15.94"	138° 53' 23.06"	Yedoma	—	—	—	—	—	6.0, 7.0
Total compounds				2747	3573	2499	4155	1961	3449
Mean (SD)				(484)	(325)	(1010)	(48.7)	(1310)	(18.3)
Unique compounds				136	14	151	11	3.5	38
Mean (SD)				(14)	(3)	(92)	(2)	(3)	(40)

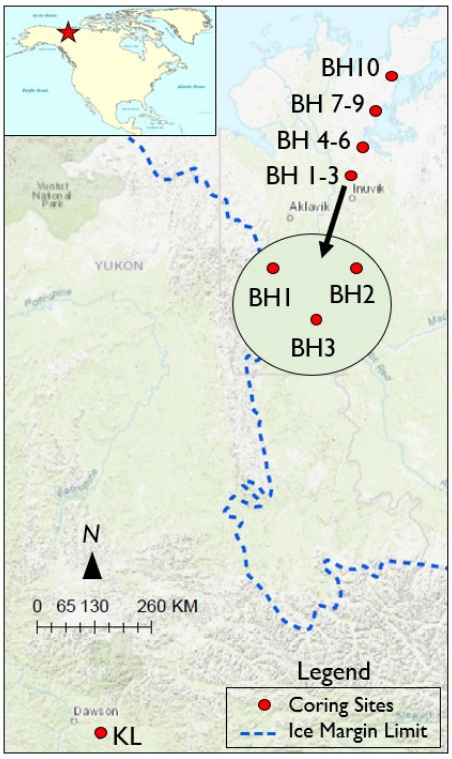

Figure 2-1. A map to show the location of permafrost core sites used for this study. For sites BH1-BH9, site clusters (e.g., BH1, 2, and 3) typically include one hilltop, riparian, and polygonal peatland site. Site KL reflects unglaciated loess (Yedoma) from the Klondike region of the Yukon. End-member types reflect ancient bedrock-derived glacial deposits (tills), re-worked mixed material (diamicton), partially decomposed material (peat), and thermokarst lake basin material (lacustrine), collected from depths described in Table 2-1. The ice margin limit denotes the previous expanse of the Laurentide Ice Sheet, which covered most sites except for KL.

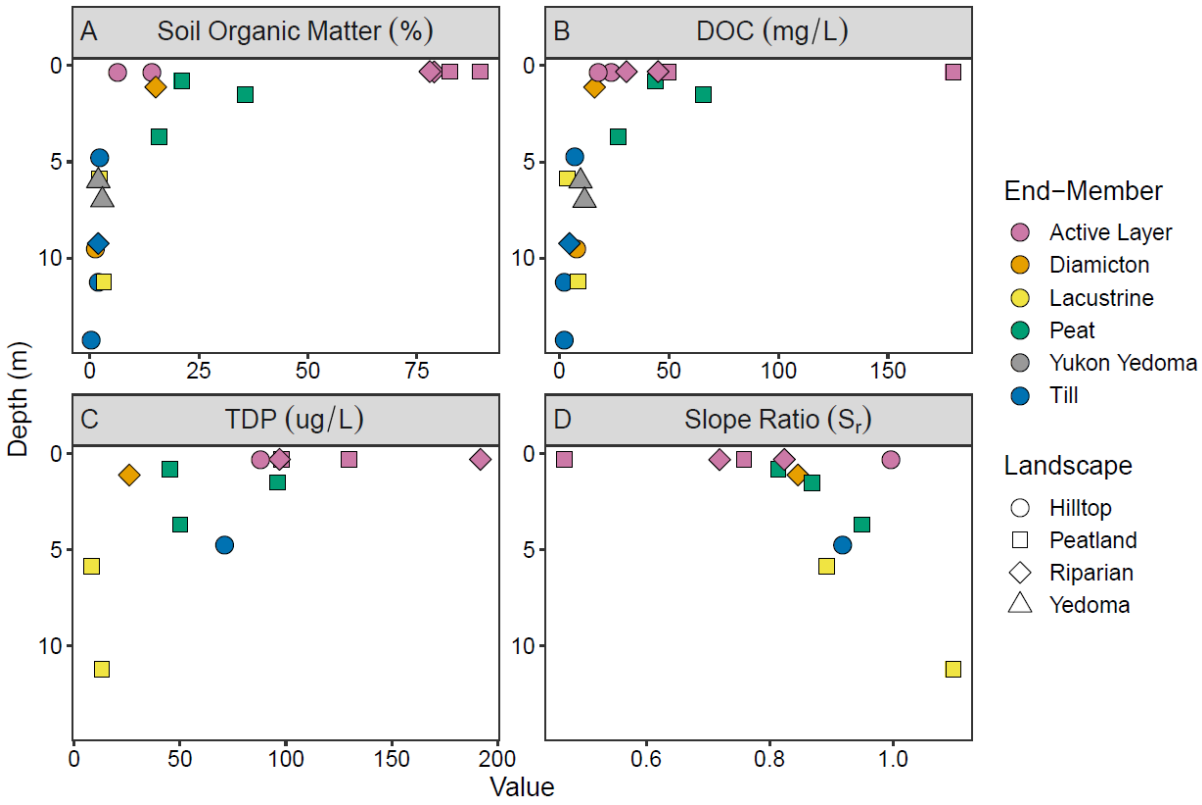

Figure 2-2. Soil and DOM characteristics along subsample depth showing a) soil organic matter content; b) dissolved organic carbon concentration; c) total dissolved phosphorus concentration; and d) absorbance slope ratio, a metric of DOM composition which increases with decreasing molecular weight. Sample sizes are n=19 for both a and b; n=12 for both c and d due to some missing Yedoma, till and diamicton samples.

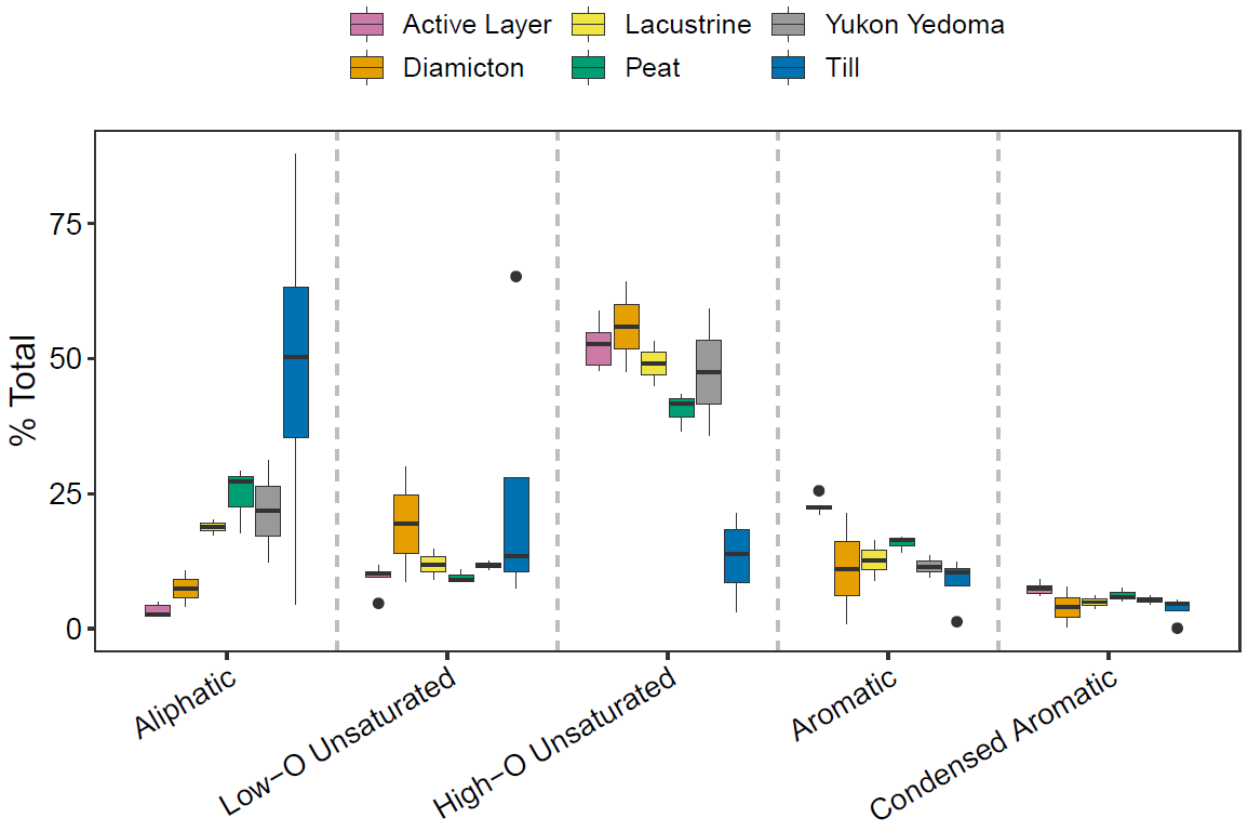

Figure 2-3. Boxplots to illustrate the proportional abundance (normalized to total intensity) of compounds identified by FTICR-MS, sorted into broad class groups. Boxes show median, 25th, and 75th percentiles, whiskers span 1.5 times the interquartile range, and points are outliers.

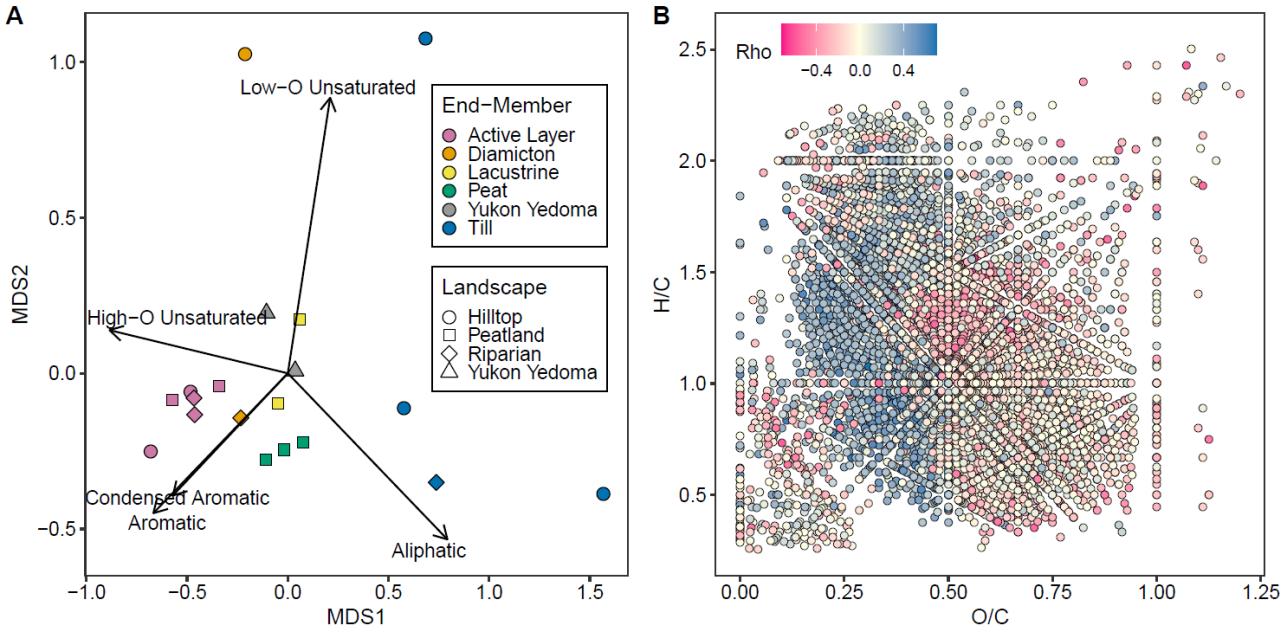

Figure 2-4. Leachate DOM composition displayed as a) non-metric multidimensional scaling (k=2, stress=0.102) showing Bray-Curtis dissimilarity of the relative abundance of compounds (normalized to total intensity) detected by FTICR-MS. Sites that are further apart are less compositionally similar. Panel b) shows a van Krevelen plot showing the oxygen:carbon (O/C) and hydrogen:carbon (H/C) ratio of the compounds detected by FTICR-MS, where rho is the correlation between individual compounds and MDS1 (pink points are associated with more negative MDS1 values, while blue points are associated with more positive MDS1 values).

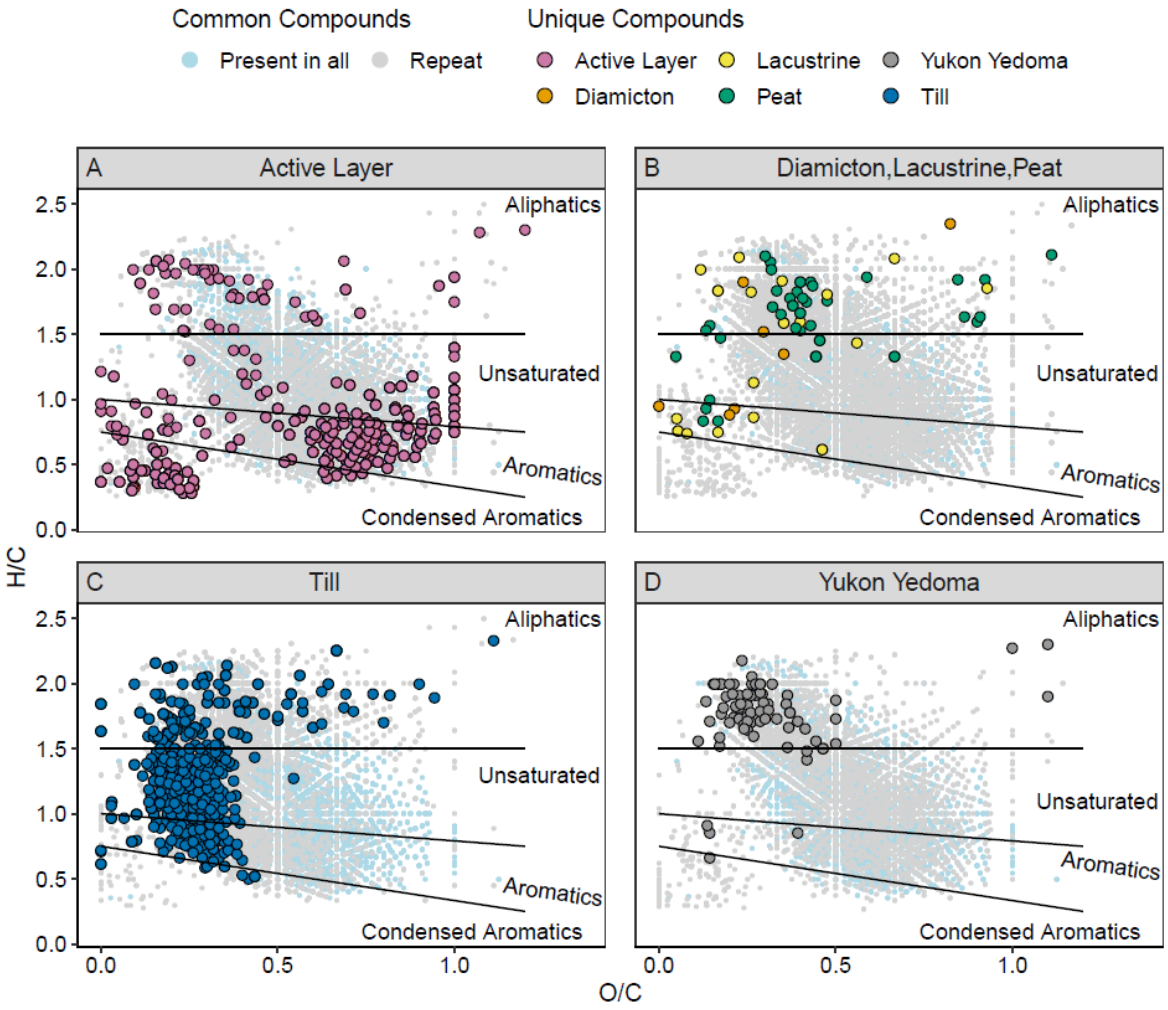

Figure 2-5. Van Krevelen plots showing the oxygen:carbon (O/C) and hydrogen:carbon (H/C) ratio for the compounds detected by FTICR-MS (n=6,450). Unique compounds (n=759) are those found to only exist in one end-member type, which are denoted using the same colour scheme as in Figure 2-2. Conversely, compounds that were present in all end-member types are shown in light blue (n=2,020), while compounds that were present in more than one, but not all end-member types, are shown in light grey (n=3,671).

3.1 Introduction

Northern permafrost soils store a vast amount of carbon (Hugelius et al. 2014), but warming temperatures are enhancing permafrost thaw (Schuur and Abbott 2011). Following permafrost thaw, carbon within organic matter can become available to contemporary biogeochemical cycling, because after dissolution into the aqueous state as dissolved organic matter (DOM), it can be decomposed by microbes (biodegradation; Battin et al. 2008). This process can occur along the soil-aquatic continuum in situ, as DOM is transported along hydrologic flow paths, and within surface waters (Graham et al. 2012; Abbott et al. 2016; Vonk, Tank, and Walvoord 2019). Biodegradation mineralizes DOM to carbon dioxide and methane, enabling a feedback to climate change known as the permafrost carbon feedback (Schuur et al. 2015). Importantly, not all DOM is equally susceptible to biodegradation, due to differences in the composition of the substrate (Abbott et al. 2014; Tanski et al. 2017; Schädel et al. 2014) and activity of the microbial community (Graham et al. 2012; Judd, Crump, and Kling 2006). Therefore, the extent to which permafrost regions will be affected by climate change—and also contribute to it—partly depends on the biodegradation rate of DOM released following permafrost thaw.

The large and vulnerable stores of permafrost carbon (Schuur and Abbott 2011; Hugelius et al. 2014) have prompted recent investigations to quantify biodegradability of DOM derived from permafrost. Numerous studies in Siberia and Alaska have found that Yedoma (syngenetic aeolian-origin permafrost) deposits release DOM dominated by simple molecules that undergo rapid biodegradation (Ewing et al. 2015; Drake et al. 2015; Spencer et al. 2015; Heslop et al. 2019), creating an emerging consensus that permafrost-derived DOM is highly bioavailable (but see, for example, Wickland et al. 2018). However, given that DOM composition is strongly influenced by the surrounding environment from which it is derived (Knoblauch et al. 2013), the provenance of permafrost likely affects DOM composition and biolability. Therefore, DOM derived from different terrain types or along depths within a variable stratigraphy may be variable in its composition and biolability. Within the western Canadian Arctic, past work on the Peel Plateau, NT, has found that biodegradation rates for rill-water draining from thermokarst features were elevated compared to unimpacted stream sites, but were generally lower than rates

from Yedoma regions (Littlefair and Tank 2018). Differences in biodegradation rates between thermokarst features were postulated to reflect the relative proportion of distinct stratigraphic materials being thawed, prompting our investigation to test whether biolability differs across variable permafrost stratigraphies (Burn 1997; Lacelle et al. 2019).

The Peel Plateau, NT, was previously glaciated and consists of ice-rich tills and glaciofluvial materials deposited at the margins of the Laurentide Ice Sheet (Kokelj, Tunnicliffe, and Lacelle 2017). This area is characterized by a high density of retrogressive thaw slumps—a dramatic form of thermokarst—which grow as exposures of ice-rich permafrost (up to tens of meters in thickness) thaw along slopes (Lacelle et al. 2015; Kokelj, Tunnicliffe, and Lacelle 2017). Thaw slumps can mobilize thick stratigraphic sequences including the contemporary active layer, a relict active layer that thawed during the early Holocene and then re-froze with subsequent cooling conditions, and underlying Pleistocene-origin glacial tills that have been unaffected by past thaw (Burn 1997; Kokelj et al. 2017b). These units have demonstrated variation in their biogeochemical characteristics (Lacelle et al. 2019), pointing to potential differences in DOM composition, and thus, biolability.

Microbial communities also play an important role in DOM biodegradation (Graham et al. 2012), but areas with extensive permafrost thaw, such as the Peel Plateau, can create rapidly-changing environments that may impact the structure of local microbial communities. Permafrost thaw can directly affect the structure of microbial communities, enabling rapid shifts from a frozen to thawed state (Mackelprang et al. 2011). Additionally, permafrost thaw may not only increase the amount of organic matter that becomes available to microbial communities (Schuur and Abbott 2011), but may also lead to changes in the composition of DOM released, indirectly affecting microbial communities because DOM composition can strongly shape microbial community structure (Ward et al. 2017). For example, thaw slumps have been shown to alter DOM release into impacted streams (Littlefair, Tank, and Kokelj 2017), but it is not well known how microbial community structure may be affected by exposure to material released from these thaw slumps, or whether changes in the microbial community structure may also affect DOM biodegradation.

While Quaternary legacies and varying climate conditions have created distinct permafrost stratigraphy on the Peel Plateau, the landscape continues to evolve at a rapid pace

(Lacelle et al. 2015; Segal, Lantz, and Kokelj 2016; Kokelj, Tunnicliffe, and Lacelle 2017; Van der Sluijs et al. 2018). As increasing permafrost thaw continues to expose distinct stratigraphic units, organic matter will become susceptible to leaching; but little is known about how DOM leached from different stratigraphic units might vary in its composition and biolability, or how microbial communities differ across the land-to-water continuum in thaw-affected areas. This prompted us to investigate (1) if the composition of permafrost leachates varies across stratigraphic units on the Peel Plateau, and how this variation may be linked to differences in biodegradation rates, and (2) whether microbial communities from different sources within this disturbed landscape (e.g.,, unimpacted streams, relative to thaw slump runoff) differ in their composition, or enable differences in biodegradation.

3.2 Methods

3.2.1 Study Area

Our study was conducted on the Peel Plateau, a fluvially-incised moraine landscape situated between the Richardson Mountains (to the southeast) and the Mackenzie Delta (to the northwest). This area has been strongly shaped by its glacial legacy, falling within the western margin of the Laurentide Ice Sheet that covered the area until approximately 18,500 years before present (ybp; Kokelj, Tunnicliffe, and Lacelle 2017). Ice-rich tills were deposited with the advance and retreat of the Laurentide Ice Sheet, along with a patchy distribution of glaciofluvial and glaciolacustrine sediments (Kokelj, Tunnicliffe, and Lacelle 2017; Kokelj et al. 2017b). Although permafrost is continuous throughout these deposits, a thaw unconformity demarcates a relict active layer that formed during a warm interval in the early Holocene (Burn 1997). This warming locally increased thermokarst activity, where active layer deepening facilitated soil development, which then stabilized as permafrost aggraded with subsequent cooling during the middle and late Holocene (Burn 1997; Kokelj et al. 2017b; Lacelle et al. 2019). The contemporary active layer thaws seasonally during the summer (Kane, Hinzman, and Zarling 1991), and is geochemically distinct from both the relict active layer and the deeper, unaffected till deposits (Lacelle et al. 2019).

The Peel Plateau has abundant valleys and streams that incise the landscape, where recent warming has accelerated ongoing thermokarst activity (Kokelj et al. 2017b). Thermokarst can manifest as multiple geomorphic formations, but retrogressive thaw slumps are the most

prevalent form on the Peel Plateau, often developing on ice-rich slopes (Lacelle et al. 2015; Kokelj, Tunnicliffe, and Lacelle 2017). Following thaw of massive ice, the ground subsides and mobilizes large quantities of material into recipient streams, increasing solute and sediment concentrations by multiple orders of magnitude (Malone et al. 2013; Kokelj and Jorgenson 2013; Lacelle et al. 2019). The headwalls of these thaw slumps expose the underlying permafrost stratigraphy, providing the opportunity to study the composition and biolability of DOM derived from these distinct stratigraphic units.

3.2.2 Sample Collection

To investigate the biodegradability of organic matter from thaw slump headwalls, we collected samples from slumps HB, HD, and FM3 (Figure 3-1). All slumps were active at the time of sampling in summer 2018, and occur along an east-west gradient that spans recessional positions of the Laurentide Ice Sheet (Kokelj, Tunnicliffe, and Lacelle 2017). The western HB lies closer to the maximum limit of ice extent (~18,000 cal ybp), while HD and FM3 are more closely situated with a relatively more recent recessional position of the retreating ice sheet (~16,000–14,000 cal ybp; Kokelj, Tunnicliffe, and Lacelle 2017; Dalton et al. 2020 and references within). FM3 is considered a 'mega-slump' with a large headwall (~6–12 m) and well-developed debris tongue (Malone et al. 2013; Kokelj et al. 2013), while HD and HB have slightly shallower headwalls (~6–10 m) and less extensive debris tongues (Littlefair, Tank, and Kokelj 2017). Thaw slump headwall heights reflect the relative proportion of contemporary active layer soils versus ice-rich, Pleistocene tills versus Holocene-derived relict active layer, where larger headwalls can decrease downstream dissolved organic carbon (DOC) concentrations (Littlefair, Tank, and Kokelj 2017) and facilitate sulfuric acid-driven carbonate weathering (Zolkos, Tank, and Kokelj 2018).

To include the three stratigraphic units representative of this area, we collected material from the contemporary active layer (all three sites), the early-Holocene relict active layer (HD and FM3), and the undisturbed Pleistocene layer (all three sites). At each site, a chisel was used to collect approximately 4 kg of soil or permafrost into sterile whirlpak bags, which were transported chilled to a field lab in Inuvik, NT, and stored in a dark freezer (-20°C) overnight. We also collected water samples from adjacent streams at each slump site to provide representative inocula for the biodegradation experiment. These samples were collected from an unimpacted (upstream) site, as well as from the slump-impacted rillwater draining from the

slump headwall. Water samples were collected in pre-cleaned (soaked overnight in 10% HCl, then rinsed seven times with MilliQ water) 1 L HDPE bottles, and kept cool during transport from the field to the laboratory. Stream water samples were immediately filtered through pre-combusted glass fibre filters (475°C for 4 hours; 0.7 μm nominal pore size; Whatman GF/F) upon return to the lab, and the filtrate was stored chilled (4°C) and in the dark until experimental processing, which was completed within 2 days (Vonk et al. 2015; Littlefair, Tank, and Kokelj 2017).

3.2.3 Leachate Preparation

To leach the soil and permafrost samples, collected material was transferred into pre-cleaned 4 L HDPE containers, to which MilliQ water was added at a 1:1 (soil weight to water volume) ratio (Carter 1993). Samples were vigorously shaken and allowed to thaw in the dark at 4°C for 24 hours. The resulting leachate was decanted using a peristaltic pump to separate the liquid from the residual soil slurry. Turbid leachates were centrifuged (Primo R, Thermo Scientific Hereaus) at 8000 rpm for 2 to 5 minutes at 4°C, then filtered through pre-combusted glass fibre filters (Whatman GF/F) before homogenization in a pre-cleaned 4 L HDPE container. The soil/permafrost material weight to extractant volume ranged from 0.5 to 1.4, which is well above the recommended lower limit of 0.25 for representative DOC (i.e., the carbon fraction of DOM) in soil extractions (Jones and Willett 2006). Prior to inoculating and incubating this leachate (see below), the absorbance was measured at 254 nm to ensure that leachate DOC concentrations (based on known concentration-absorbance relationships; Weishaar et al. 2003) were not so high that anoxia might be a concern (since substantial DOC concentrations could lead to rapid degradation) within the intended 28-day incubation period. To normalize absorbance, active layer samples from FM3 and HD, as well as Pleistocene samples from HD, were further diluted to an absorbance of 1.0 using 18.3 MΩ MilliQ water. The pre-filter system for the input MilliQ water feed (town of Inuvik water supply) malfunctioned during sample dilutions for FM3 active layer, necessitating the use of 13 MΩ MilliQ water instead of 18.3 MΩ MilliQ water, which may have contributed organic contamination (elevated TDP and TOC) in the sample. Based on this consideration, we have included this sample in our presentation of oxygen depletion over time (see below) but removed it from all other analyses.

3.2.4 Experimental Procedure

Filtered leachates were distributed into three pre-cleaned 2 L HDPE bottles. These bottles received a 10% v/v addition of either: upstream inoculum (U), within-slump inoculum (W), or additional leachate to enable a native inocula (N). An inoculated and killed (K) treatment was completed for a subset of sites; these received upstream inoculum, but then were killed using a 0.1% v/v addition of concentrated trace metal grade hydrochloric acid (Vonk et al. 2015). All four treatments (U, W, N, K) were applied to leachates from the active layer (A), Holocene (H), and Pleistocene (P) from FM3, as well as the active layer and Pleistocene from HD. Due to limited leachate volume, only upstream and within inoculum treatments (no native) were added to Holocene leachates from HD. Throughout, samples are referred to using abbreviations that reference site (HB, HD, and FM3), stratigraphic layer (A, H, P) and, where appropriate, inoculum type (U, W, N, or K). Full collection and incubation details are provided in Table 3-1.

Inoculated leachates were aerated with compressed air for 10 minutes to enable a similar oxygen status at the onset of the incubation, then 120 mL aliquots were poured into triplicate glass bottles pre-fitted with an oxygen SPOT sensor on the interior wall (PreSens, Germany). Oxygen concentrations were used to track bacterial respiration and were coupled with initial and final carbon concentrations to quantify biodegradation (Berggren, Lapierre, and del Giorgio 2012). In addition to the K samples described above, triplicate 18.3 MΩ MilliQ bottles were established as negative controls for our microbial work (see below). All bottles were filled without headspace, capped with chlorobutyl isopropene stoppers (Niemann et al. 2015), and sealed with an aluminum crimp top. Experiment bottles were stored in a dark incubator at room temperature for 28 days (Vonk et al. 2015).

3.2.5 Leachate Chemistry

Prior to filling bottles, but after adding inocula, filtered leachates were subsampled for initial (time=0): DOC concentration, DOM absorbance and fluorescence, total dissolved nitrogen (TDN), nitrate and nitrite, total dissolved phosphorus (TDP), and particulate organic carbon (POC). Oxygen concentrations were measured immediately following experimental setup, and every 1-3 days thereafter to ensure oxic conditions persisted throughout the experiment. Final oxygen measurements were taken immediately before terminating the experiment (time=28 days), at which time all experimental bottles were shaken, opened and subsampled for: DOC

concentration, DOM absorbance and fluorescence, trace metals, nitrate and nitrite. Final samples were re-filtered to remove any biomass or flocculation prior to sub-sampling. Despite filtering, some particles (<0.7 μm) were visible in the experimental subsample bottles. This filtrate was measured for its POC content as described below.

Subsamples for DOC concentration were collected into borosilicate vials, immediately preserved with 0.1% v/v HCl, and stored at 4°C in the dark (Vonk et al. 2015). DOC subsamples were analyzed on a TOC-5000A (Shimadzu), using the mean concentration of three to five injections (to satisfy coefficient of variance <2%) from each sample vial. The settled particles from the acidified DOC bottles were used to determine POC concentrations following filtration through pre-combusted (180°C for 30 minutes) silver filters (0.1 μm pore size; Sterlitech). Filters were immediately placed into pre-combusted (500°C for five hours) glass petri dishes, dried at 60°C overnight, and packed into tin capsules for analysis of POC concentration at the UC Davis Stable Isotope Facility (Micro Cube elemental analyzer; Elementar Analysensysteme GmbH). Blank filters were also processed to ensure that they were carbon free. The initial POC and DOC concentrations were summed to determine the initial total organic carbon (TOC) concentration. Absorbance and fluorescence samples were collected into amber glass bottles and stored at 4°C until analysis using a spectrofluorometer (Aqualog, Horiba Scientific) within 7 days of collection. Absorbance was measured using a 1-cm quartz cell at 1-nm increments between 250 and 800 nm. Absorbance slopes were calculated for 275–295 nm ($S_{275\text{-}295}$) and 350-400 ($S_{350\text{-}400}$) nm, then we used the ratio of these slopes ($S_{275\text{-}295}/S_{350\text{-}400}$) to determine slope ratio (S_r; Helms et al. 2008). Fluorescence excitation ranged from 240-450 nm, at 5 nm intervals, while emission was measured between 300 and 600 nm at 2 nm intervals. Fluorescence data were processed using the R package *eemR*. To correct raw EEMs, we removed the blank, corrected for inner filter effects, and normalized to raman units. We calculated the Fluorescence Index (FI), Biological Index (BIX), and Humification Index (HIX), as well as peaks A, B, C, M, and T (Table A2-1). Peaks are expressed as the proportion contributing to the total fluorescence signal (sum of all peaks).

Nutrients and trace metals analyses were submitted to the Canadian Association for Laboratory Accreditation (CALA) ISO/IEC 17025-accredited Biogeochemical Analytical Services Lab (BASL) at the University of Alberta. Subsamples for TDN and TDP were collected into 50 mL polypropylene centrifuge tubes, and stored in the dark at 4°C. Samples for nitrate and

nitrite were collected into 15 mL polypropylene centrifuge tubes, acidified with HNO_3 to pH<2, and stored in the dark at -20°C. TDN, TDP, nitrate and nitrite subsamples were analyzed using a QuickChem QC8500 FIA Automated Ion Analyzer (Lachat Instruments). Subsamples for trace metals (Al, Ca, Fe, K, Mg, Na, Ag, As, Ba, Be, Cd, Co, Cr, Cu, Mn, Mo, Ni, Pb, Sb, Se, Sr, Tl, V, Zn) were collected into 15 mL polypropylene centrifuge tubes, acidified with HNO_3 to pH<2, and stored in the dark at 4°C until analysis using a Thermo ICAP-6300 Inductively Coupled Argon Plasma - Optical Emission Spectrometer (Thermo Fisher Scientific).

In addition to these experimental samples, separate headwall samples were collected from Holocene and Pleistocene permafrost from site FM3 for $\delta^{18}O$ analysis to aid in identifying approximate origin of the material. The FM3 headwall sample bags were gently inverted to homogenize the material, and water was collected using a 60 mL syringe. The syringes were inverted to allow particles to settle, then the supernatant water was filtered through a syringe filter (0.45 μm pore size) into a 2 mL glass vial. Vials were tightly sealed to ensure there was no headspace or exposure to modern sources of water, and analyzed using a Water (H2O) Isotopes Analyzer L2130-i (Picarro) at BASL.

3.2.6 Microbial Community Composition

All equipment (e.g., filter towers, forceps, gloves, etc.) used for microbial subsampling was new (sterile) or was sterilized with 70% ethanol and rinsed seven times with deionized water. Subsamples for microbial community composition were collected at the onset and termination of the experiment by filtering leachate through pre-autoclaved (121°C for 1 hour) PES filters (0.2 μm pore size; Millipore Sigma). Filters were placed into 15 mL cryotubes, preserved with 1 mL RNALater, and were stored in the dark at -20°C until DNA extraction.

To extract DNA from filtered samples we used the DNA PowerSoil Pro Kit (Qiagen), with some modifications that had previously proven to increase extraction efficiency from permafrost samples (Saidi-Mehrabad et al. 2020). Briefly, we cut each sample filter in half using a sterile razor blade and processed each half separately for all extraction steps, then combined the two extractions into one final elution tube. We added an incubation time of five minutes following the addition of CD2, and an incubation time of ten minutes following the addition of CD3. We increased the centrifuge time to five minutes prior to adding CD6 (reduced volume to 20 uL), and immediately after its addition. DNA concentrations were measured using a Qubit

fluorometer (Invitrogen) with the high sensitivity DNA assay kit. Although DNA extraction was attempted for all initial leachate samples, only HB-A leachates produced DNA concentrations high enough for sequencing. Based on this limitation, the only final samples extracted were for the ones that paired with the initial HB-A samples, which include all three inocula sources (N, U, W).

To quantify changes in microbial community composition, we undertook amplicon sequencing (Illumina MiSeq) of the V4 region of the 16S rRNA gene, using primers 515F (5′-GTGYCAGCMGCCGCGGTAA-3′) and 806R (5′-GGACTACNVGGGTWTCTAAT-3′). Sequencing was conducted by Microbiome Insights (Vancouver, BC). Sequences were processed using the USEARCH (version 10.0.240) pipeline to merge the reads, and the MOTHUR (version 1.35.0) pipeline normalized merged reads to the lowest read count, where 96.6% of reads passed filtering (2> Qscore <20). The UPARSE greedy algorithm was used for operational taxonomic unit (OTU) picking, and also to remove chimeras and singletons. The OTUs were clustered at 97% similarity, and assigned taxonomy using the RDP classifier with the SILVA SEED database (version 132). Positive controls consisted of a known mixture of bacteria which were correctly identified. Negative controls were collected from both initial and final triplicate MilliQ incubation bottles, which were used to identify any contaminants via the R package *Decontam* (Davis et al. 2018). The OTU table was rarefied to 21,000 reads using random subsampling, where 4 OTUs were identified as contaminants and were removed, resulting in 1894 OTUs used for subsequent analyses.

3.2.7 Statistical Analyses

All statistical analyses were completed using R version 3.6.3, primarily using *ggplot2* to create figures. For all figures and text, error bars and confidence bounds represent standard error of the mean, unless otherwise stated. We used Spearman's Rank to assess correlations between various leachate chemistry parameters using *corrplot*. We used regression analysis to examine relationships between biogeochemical parameters (optical metrics, nutrients, and metal concentrations) and oxygen loss. Nutrient parameters were included as C:N and C:P, which were calculated as DOC:TDN and DOC:TDP. Because we wanted to include a wide range of variables, we chose to use least absolute shrinkage and selection operator (LASSO), which reduces coefficients to zero to provide an interpretable subset selection (Tibshirani 1996). Using *glmnet*, we applied a 10-fold cross validation to select the lambda that minimizes error. Input

variables were log-transformed to achieve normality, as assessed using the Shapiro-Wilk test, then were standardized (mean=0 and standard deviation=1) in order to directly compare the relative importance of each variable. To compare DOM composition among samples, we ran a principle components analysis (PCA) using *vegan* for parameters related to DOM (e.g., absorbance slope ratio, fluorescence indices and peaks). To compare the microbial community composition among treatments and across time, we used non-metric multidimensional scaling (NMDS) to visualize Bray-Curtis dissimilarity of the rarefied, decontaminated OTU table. *Simper* analysis identified the contribution of each class (sum of OTUs within a given class), and we tested the fit (α=0.05) of top class contributors (>1%) and DOM composition as vectors on the NMDS (based on 9999 permutations). We calculated various metrics including richness, Shannon's diversity, Inverse Simpson's diversity, and Simpson's evenness, and assessed differences in diversity among groups (α=0.05) using two-way ANOVA with fixed factors: time (T=0 and T=28) and inocula treatment (N, W, U), and if significant, used Tukey's HSD for pairwise comparisons.

3.3 Results

3.3.1 Leachate Chemistry

Leachate chemistry showed variation not only among active layer, Holocene and Pleistocene samples, but also among sites. TOC generally declined with depth (i.e., moving from active layer to Holocene to Pleistocene), except for HD samples which were similar for all layers (Figure 3-2). Nutrients (TDN and TDP) also declined with depth, where TDP showed a positive correlation with TOC (Figure A2-1). In contrast, pH was negatively correlated to TOC, with active layer leachates more acidic than their permafrost counterparts (Figure 3-2). This trend was coupled with moderate correlations between pH and various metals (Figure A2-1), where some metal concentrations (e.g., Al, Fe, Ba, Co, Cr, Cu, Ni, and Zn) tended to be higher in active layer leachates, while others (e.g., Ca, K, Mg, Na, Sr) tended to be higher in permafrost leachates. Stable water isotopes were more $\delta^{18}O$-enriched for Pleistocene samples ($\delta^{18}O$=-27.0 to -27.02 ‰) than Holocene samples ($\delta^{18}O$=-23.87 to -23.91 ‰), and were consistent with previously reported values in this region, confirming that the Pleistocene samples represent unthawed ground ice from the late Pleistocene, while Holocene samples represent the relict active layer (Michel 2011; Lacelle et al. 2013; Lacelle et al. 2019).

3.3.2 Oxygen Loss and its Key Drivers

On average, oxygen concentrations declined ~23.7% over the course of the 28-day incubations (Figure 3-3a). In contrast, both MilliQ and HCl-killed control treatments showed minimal O_2 loss (Figure A2-2). Absolute declines in oxygen were generally similar across inocula treatments, but varied among layers and sites (Figure 3-3a). The highest oxygen losses were in HD-H samples, while the lowest oxygen losses were in active layer leachates from FM3 and HD.

To assess oxygen loss relative to the TOC pool, we normalized oxygen loss to initial TOC concentration. Similar to results for absolute oxygen loss, there were clear differences in normalized oxygen consumption between layers and sites (Figure 3-3b). Within HD and FM3, normalized oxygen loss was highest for Holocene leachates (mean ± SE; 47.1 ± 6.64%) and lowest for active layer leachates (8.56 ± 3.42%). Though Holocene samples were not collected from HB, Pleistocene leachates from this site showed the greatest overall normalized oxygen loss (58.5 ± 8.63%). Across treatments, normalized oxygen loss was fairly similar, though was slightly higher in upstream-and within slump-innoculated treatments, relative to native inocula.

LASSO regression produced a model with eleven variables correlated to oxygen loss, and this model effectively predicted the measured oxygen loss values (R^2=98.8; Figure A2-3). Key predictors of O_2 loss included metrics related to DOM composition (Peak C, BIX), nutrients (C:N, C:P), metal concentrations (Mg, K, Ba), and pH (Table 3-2). Normalized oxygen loss was greatest in samples where DOM composition was less humic-like (low %Peak C), had higher nutrient concentrations (low C:N and C:P), higher Mg concentrations, and higher pH.

3.3.3 DOM Compositional Changes

A PCA to assess differences in DOM composition across all initial and final incubation samples showed high variability along the two axes (Figure 3-4). PCA axis 1 (PC1), which accounted for 71% of the variation explained in DOM composition, separated samples with a high degree of humification (positive HIX; Ohno 2002) and high relative proportion of humic-like components (proportion of peaks A, C, and M) from those with a high relative proportion of protein-like components (peaks B and T; Coble 1996; Figure 4). Along this gradient, FM3-P and HD-H leachates were more humic-like, while HD-P, FM3-H, HD-A and HB-A were somewhat neutral, and HB-P were more protein-like. PCA axis 2 (PC2), which explained 15% of the

variance in our dataset, was positively related to samples with DOM characteristic of microbial sources (greater BIX and FI; McKnight et al. 2001; Huguet et al. 2009), and with lower molecular weight (greater S_R; Helms et al. 2008). Along PC2, most active layer samples were closely associated with terrestrial-derived components (lower FI and BIX), except for HB-A, which had a negative association. Within sites, final samples tended to shift towards more humic-like relative to initial samples.

The relative change in individual metrics of DOM composition over the 28-day incubation demonstrate a clear shift away from microbial-like DOM (decreasing BIX), but preservation of humified components (increasing HIX; Figure 3-5) across all incubated samples. Declines in BIX were coupled with decreases in protein-like components (peaks B and T), while increases in HIX were accompanied by higher molecular weight (lower S_r) and an increase in the relative proportion of humic-like components (peaks A, M, and C). Increasing humification was inversely related to depth, where the percent change in HIX was amplified in active layer leachates and more modest in Pleistocene leachates, except for a greater loss of protein-like components in Holocene leachates.

3.3.4 Microbial Community Composition and Diversity

Although microbial community composition was only assessed in initial and final samples from HB-A, we use differences in the N, W, and U innocula treatments to consider how inocula source affected variation in microbial community composition over time. Simper analysis identified that classes *Verrucomicrobiae*, *Gammaproteobacteria*, *Bacteroidia*, *Saccharimonadia*, *Actinobacteria, Parcubacteria, Planctomycetacia*, and *Deltaproteobacteria* contributed >1% to dissimilarity, and were fit as significant vectors ($p<0.05$) for the NMDS. There was no statistical significance ($p>0.05$) for using vectors based on DOM composition (Sr, BIX, FI, HIX and proportion of fluorescent peaks) for the NMDS. Contrary to our expectations, the microbial community composition from initial samples was very similar across all three treatments (Figure 3-6a). Initial samples were positively associated with *Gammaproteobacteria*, *Parcubacteria*, and *Saccharimonadia*, whose proportions declined in most final samples (Figure 3-6b).

The microbial community compositional response over time was quite variable by treatment and by NMDS axes. Final samples from U-inoculated treatments were dissimilar from

initial samples and other treatments across both the primary axis (MDS1), associated with greater increases in *Planctomycetacia* and decreases in *Actinobacteria* relative to other treatment groups, and the secondary axis (MDS2), associated with greater increases in *Verrucomicrobiae* and decreases in *Gammaproteobacteria* relative to other treatment groups. In contrast, final samples from N- and W-inoculated treatments were similar to initial samples along MDS1, but showed divergence along MDS2, where W-inoculated treatments, associated with an increase in *Deltaproteobacteria*, were also dissimilar from N-inoculated treatments.

Diversity metrics identified a significant decline in number of taxa (two-way ANOVA: $p<0.001$ for richness) and an increased evenness across taxonomic groups (two-way ANOVA: $p<0.001$ for evenness) over the course of the 28-day experiment (Figure A2-4). Pairwise comparisons found significantly higher richness (Post-hoc Tukey's HSD: $p=0.01$) and lower evenness (Post-hoc Tukey's HSD: $p=0.03$) in N-inoculated treatments relative to W-inoculated treatments, while U-inoculated treatments had significantly higher Shannon diversity compared to W-inoculated treatments (Post-hoc Tukey's HSD: $p=0.02$).

3.4 Discussion

Multiple studies to date indicate that DOC released from permafrost is highly biolabile (Vonk et al. 2013; Mann et al. 2014; Drake et al. 2015; Ewing et al. 2015; Spencer et al. 2015; Heslop et al. 2019; but see Wickland et al. 2019). However, studies that leach DOM directly from permafrost have been limited to areas with geomorphic characteristics that differ from that on the Peel Plateau, and tend to either focus on deep, Pleistocene Yedoma (Ewing et al. 2015; Drake et al. 2015; Heslop et al. 2019) or relatively shallow permafrost (Ward and Cory 2015; Panneer Selvam et al. 2017; Wickland et al. 2018). Here, we present the first evidence (to our knowledge) of varying DOM composition and biodegradation across distinct stratigraphic units within sites subject to thawing permafrost. Permafrost leachates had higher carbon-normalized biodegradation than active layer leachates, and variability within permafrost leachates was well-predicted by leachate characteristics. Biodegradation resulted in a relative depletion in microbial/protein-like DOM components, and a relative enrichment in humic-like components (see also Wickland et al. 2012; Abbott et al. 2014; Drake et al. 2015; Mann et al. 2016; Wickland et al. 2018), while nutrients and metal concentrations were also correlated with biodegradation rates. Although the different inocula treatments did not lead to large differences in

biodegradation rates, there were shifts over time in microbial community composition, where the source of the inocula influenced the direction of divergence.

3.4.1 Varying DOM Biolability in Permafrost Stratigraphic Units

On the Peel Plateau, permafrost leachates almost universally experienced higher carbon-normalized biodegradation rates compared to active layer leachates. This finding is congruent with other studies (Ward and Cory 2015; Panneer Selvam et al. 2017), but we further identify that stratigraphic units within the permafrost column vary in their biolability. Generally, DOM leached from Holocene permafrost was more biolabile than DOM leached from Pleistocene permafrost. This is consistent with increased biodegradation for within-slump rill water that had a more Holocene-aged signature (via $\delta^{18}O$) compared to a more Pleistocene-aged signature (Littlefair and Tank 2018). Notably, the extent and consistency of this trend depended on the site; decomposition rates for HD-H leachates were markedly higher than for HD-P leachates, while FM3 displayed similar rates for both Holocene and Pleistocene-origin leachates. Since the provenance of permafrost reflects not only sediment deposition, but also formational processes, past thaw, and exposure to modification, these factors act together through time to shape permafrost characteristics, thereby also shaping the composition of DOM leached from this permafrost. Because the Peel Plateau is a heterogenous landscape with a complex geological history, site-specific compositional attributes may play a key role in determining the biolability of permafrost throughout the stratigraphic column.

Comparing biodegradation rates to studies from other regions provides insight into how the regional setting may influence biolability. For example, carbon-normalized biodegradation rates in our Holocene leachates are higher than those reported for Holocene-origin leachates from interior Alaska (Wickland et al. 2018), but this region has a glacial legacy that contrasts with the Peel Plateau. Sites in interior Alaska included a peatland and forested areas (Wickland et al. 2018), which have not undergone extensive glaciation, and primarily formed as syngenetic permafrost (Péwé 1975). In contrast, our thaw slump sites are in mostly epigenetic permafrost, where Holocene leachates reflect the relict active layer that has been modified from past thaw (Kokelj, Tunnicliffe, and Lacelle 2017). While regional differences in the type of parent material, mode of permafrost formation, or glacial legacy may contribute to the discrepancy in biodegradation rates, thaw-driven modification in our Holocene samples would have enabled soil

development and increased incorporation of organic matter, and therefore may enhance biolability of DOM leached from this modified material.

While some Pleistocene leachate rates were comparable to rates in other regions, we observed high variation among sites on the Peel Plateau. The higher biodegradation rates from HB were similar to rates reported for Pleistocene-origin Yedoma from various locations (Ewing et al. 2015; Drake et al. 2015), while degradation rates from FM3 and HD were generally lower. Samples in HB were compositionally more microbial/protein-like than FM3 and HD, which likely contributed to its increased biolability. Importantly, these sites span different recessional fronts of the Laurentide Ice Sheet that may have influenced permafrost composition (Kokelj, Tunnicliffe, and Lacelle 2017). HB lies furthest west and is closer to the maximum westward extent of the ice sheet (~18,000 cal ypb) that may have allowed more time for microbial re-working, while FM3 and HD lie closer to a relatively more recent recessional front (~16,000–14,000 cal ybp; Kokelj, Tunnicliffe, and Lacelle 2017; Dalton et al. 2020 and references within). The clear compositional differences in these sites reinforces that glacial legacy and geologic setting have a strong influence on shaping DOM composition derived from permafrost with differing origins.

3.4.2 Drivers of DOM Biodegradation

Similar to other studies (e.g., Mann et al. 2016; Drake et al. 2015; Wickland et al. 2018), initial DOM composition was the primary indicator of biolability, where the relative proportion of humic-like versus protein-like components led to predictable differences in degradation rates across stratigraphic units and among sites. While we observed a general compositional shift over the 28-day experiment to less fresh/protein-like and higher molecular weight DOM, nutrient ratios and metal concentrations were also important predictors of biodegradation. Biodegradation rates were inversely related to C:N and C:P, reinforcing that nutrient status is an important driver of DOM biolability (Marschner and Kalbitz 2003; Wickland et al. 2012; Littlefair and Tank 2018). The DOC:TDN ratio can also provide information on DOM composition, because low C:N can indicate less degraded, microbially-produced DOM (Brookshire et al. 2005; Fellman, Hood, and Spencer 2010). Trace metal concentrations, and to a lesser extent pH, were also important predictors for biodegradation rates. The precise role of how metals identified in our LASSO regression affect biodegradation is not well known, and studies have found mixed results for metals both enhancing and inhibiting biodegradability (Marschner and Kalbitz 2003). There

was also a moderate to strong correlation for most metals with pH, and both of these factors can influence the activity and structure of the microbial community (Ward and Cory 2015; Jiang et al. 2019), which may have subsequently affected biodegradation rates.

3.4.3 Shifts in Microbial Community Composition

Analysis of pre-and post-incubation microbial community composition from HB-A samples amended with U, W, and N inocula demonstrate clear shifts by treatment over time, which appeared to be at least partly driven by initial source of the inocula. The classes that were identified as top contributors to the community composition shifts have been previously reported across permafrost regions (Jansson and Taş 2014), including in Alaska (Taş et al. 2014), in Siberia (Gittel et al. 2014), the Tibetan Plateau (Zhang et al. 2014) and in Greenland (Gittel et al. 2014). The microbial community compositional shifts were coupled with a reduced number of taxonomic groupings in incubated samples, but increased evenness of taxa, over time. This suggests that the microbial community underwent selection, where a small subset became more uniformly abundant, but the class selection varied by treatment.

Upstream-inoculated treatments showed a clear divergence from those amended with inocula from within-slump rillwater and native leachate. This may reflect the greater tendency of microbes leached from active layer soils (the N inocula) and particle-rich slump runoff (the W inocula) to have been associated with particles compared to those from upstream sites (Littlefair, Tank, and Kokelj 2017). Although microbial community compositional shifts were not significantly associated with metrics for DOM composition, the U-inoculated leachates had lower C:N and higher Mg concentrations (both important predictors for biodegradation rates) compared to both N- and W-amended HB-A leachates. Since all inocula treatments were applied to the same leachate, changes in the microbial community response likely reflect differences based on the initial source of the inocula, despite the similarity of initial microbial communities. Surprisingly, U-inoculated and W-inoculated treatments displayed slightly higher biodegradation rates than the N-inoculated treatments, suggesting that microbial communities from aqueous environments (streams and rill-water) may be more effective at degrading DOM than their soil-associated counterparts (active layer soils).

3.5 Conclusion

Sampling thaw slumps across the Peel Plateau, we observed high variability in both DOM composition and biodegradation across sites and stratigraphies. In sites with all three strata, Holocene leachates were generally more biolabile than Pleistocene leachates, which both exceeded the active layer leachates. Differences in DOM composition appear to be strongly influenced by glacial legacy and past thaw, which combine to act over time and differentiate biolability across sites and within permafrost stratigraphies. We also observed clear shifts in the microbial community composition over the incubation period, where the direction of divergence depended on the source of the inocula treatment. Inocula from aqueous sources demonstrated stronger compositional shifts, and also showed slightly higher biodegradation rates than inocula from soil. Therefore, material released from thaw slumps may lead to microbial community compositional shifts, and biodegradation rates could increase when DOM enters into recipient aqueous environments. These results emphasize the need to account for variation in DOM composition and biolability at a stratigraphic scale, while considering changes to microbial community composition, which will likely impact the fate of carbon following permafrost thaw.

Table 3-1. Site and sample processing information, where ID represents the Site-Layer format (A=active layer, H=Holocene, P=Pleistocene). Depth refers to the depth of sample collection from the ground surface (0 m). Mass refers to the mass of soil or permafrost material, to which the volume of MilliQ was added, and Vol is the approximate volume of total leachate. The Soil:Extract ratio is the Mass/Vol, while Leach:DI ratio indicates further dilution. Treatments refer to the inocula treatments used for each sample.

Site Lat, Long	ID	Depth (m)	Mass (g)	MilliQ (mL)	Vol (L)	Soil: Extract Ratio	Leach: DI Ratio*	Treatments
67°14'23.89", -135°49'7.03"	HB-A	0.3	4012.1	4020.3	2.85	1.40	1.00	U,W,N
	HB-P	7.0	2479.9	2488.1	4.50	0.55	1.00	U,W,N
67°15'12.06", -135°16'22.12"	FM3-A	0.3	6228.8	6249.1	4.80	1.30	0.10	U,W,N,K
	FM3-H	2.0	4786.4	4843.0	3.80	1.20	0.99	U,W,N,K
	FM3-P	3.0	4791.7	4828.6	5.10	0.94	0.99	U,W,N,K
67°24'0.00", -135°20'2.40"	HD-A	0.3	4169.0	4177.5	3.10	1.30	0.83	U,W,N,K
	HD-H	2.0	1608.2	1608.2	1.75	0.92	1.00	U,W
	HD-P	3.0	3417.5	3431.7	3.40	1.00	0.88	U,W,N,K

*Dilution applied to leachate in order to achieve absorbance at 254 nm <1, so that high concentrations of organic carbon would not lead to anoxia within the 28-day experiment.

Table 3-2. Results for LASSO regression of predictor variables for normalized oxygen consumption. Timepoint references when the sample was collected, and coefficient represents the slope for the variable. Input variables were standardized to enable direct comparison of the coefficients for each variable.

Variable	Timepoint	Coefficient
Peak C (%)	0	-1.2933
Mg	28	1.1532
C:N	0	-0.5743
Bix	0	-0.5407
K	28	-0.4051
C:P	0	-0.3385
Ba	28	0.3157
pH	0	0.2482
Ni	28	0.1934
S_R	0	-0.0872
Cu	28	-0.0733

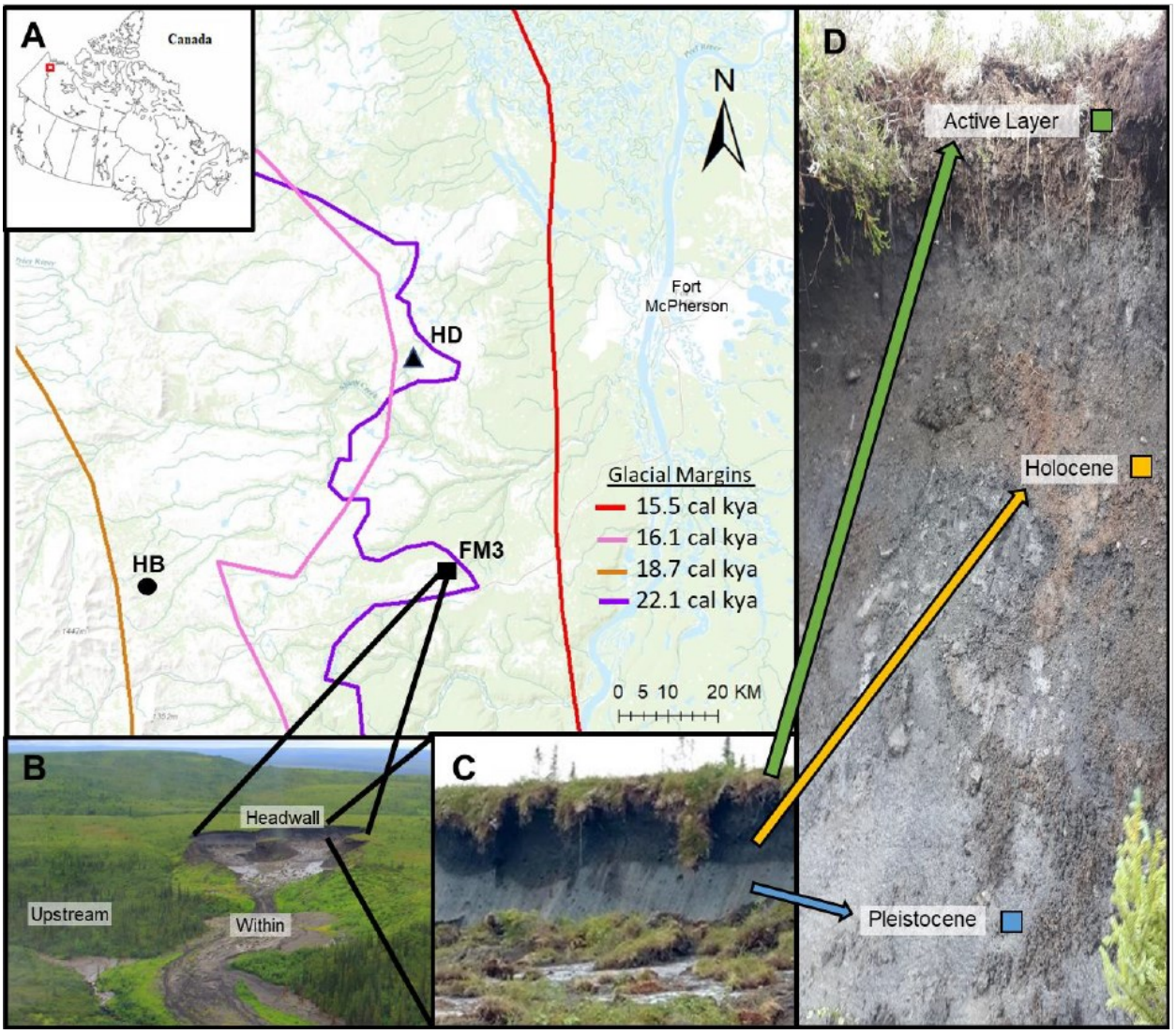

Figure 3-1. Site sampling map showing A) all three slump locations; B) FM3 with the stream sampling locations, where upstream is unaffected by the thaw slump, and within is sampled from the rillwater draining the slump headwall (photo credit: Dr. Scott Zolkos); C) the thaw unconformity at FM3 demarcates the darker, relatively organic-rich relict active layer above the light, ice-rich undisturbed permafrost; and D) headwall sampling references from FM3, including active layer (0.3 m), Holocene (2 m), and Pleistocene (3 m) sampling locations. Glacial margin shapefiles were retrieved from supplementary data in Dalton et al. 2020.

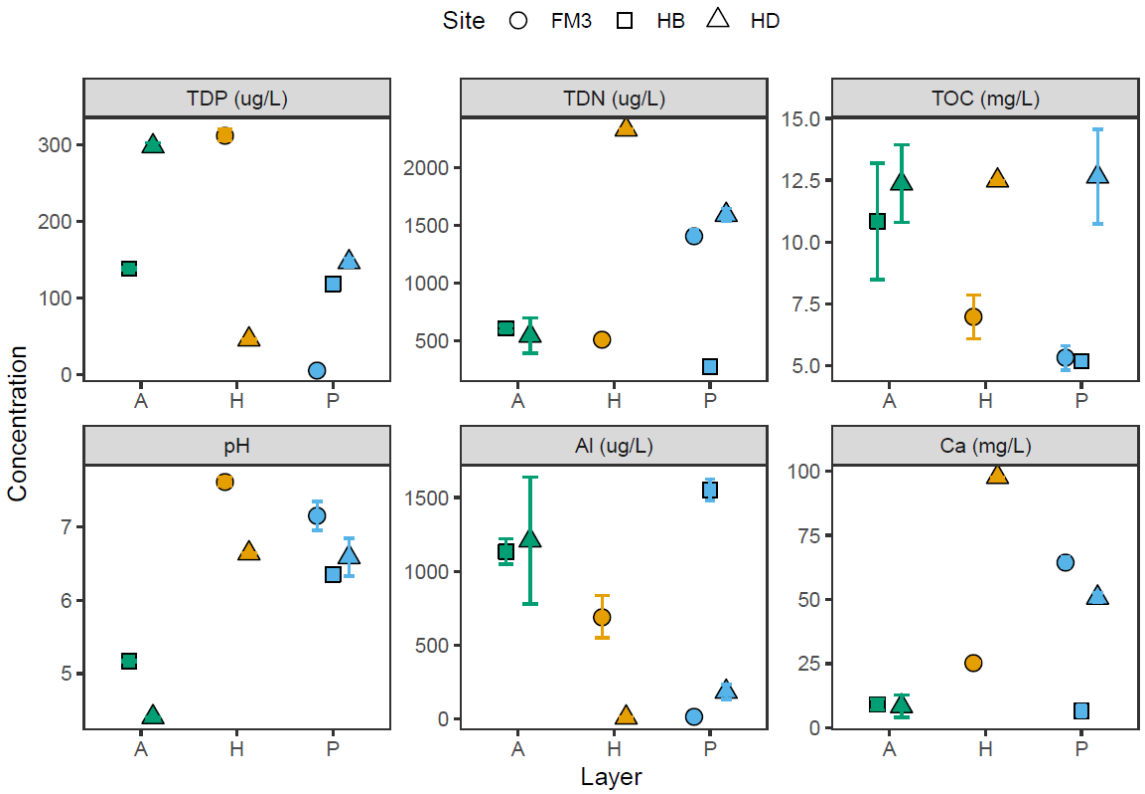

Figure 3-2. Pre-incubation concentrations of TDN, TDP, TOC, and pH, and post-incubation concentrations of aluminum and calcium. Data points represent the mean and standard error of all treatments (N, U, W, as applicable) for each site (denoted by shape) and layer (denoted by colour, where A=active layer, H=Holocene, and P=Pleistocene). Units of measurement and parameter name is provided in the header of each plot, with “free” y-axes to capture the appropriate range for each parameter.

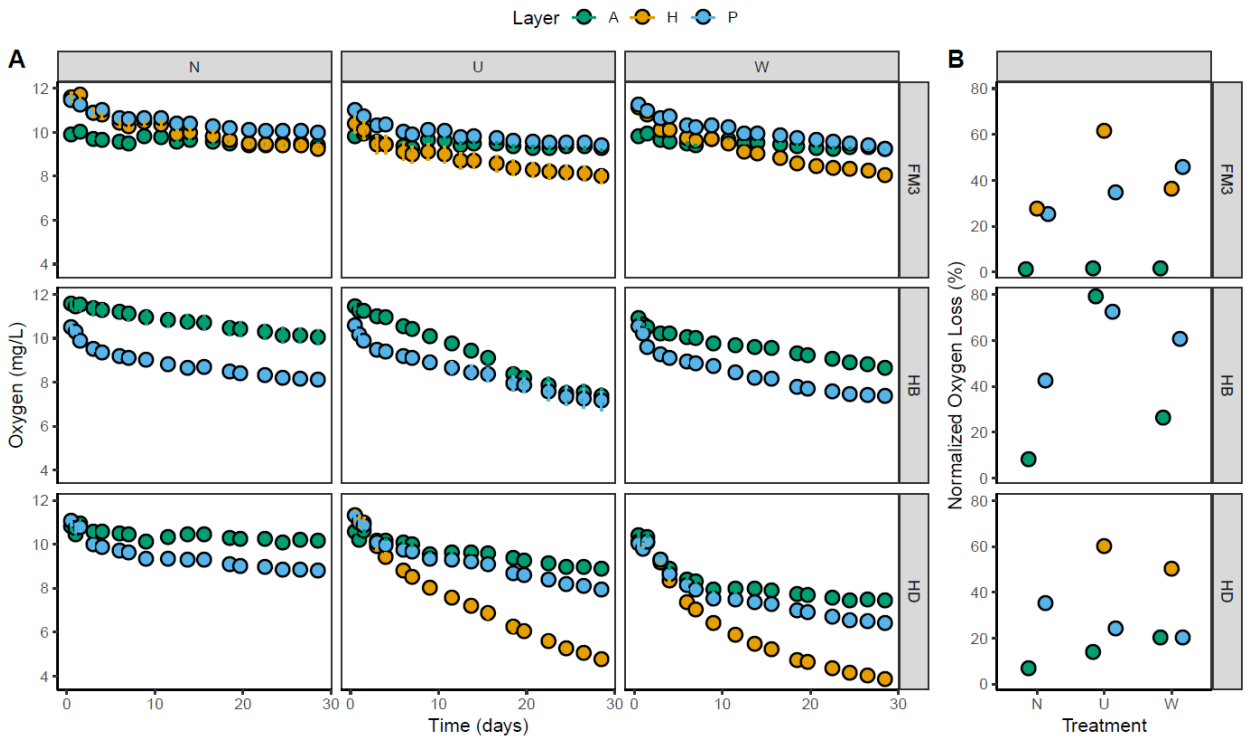

Figure 3-3. Oxygen loss for sample leachates during the experiment, where horizontal sections represent sites, vertical sections represent the inoculate treatments (N=native, U=upstream, W=within-slump), and colour denotes layer (A=active layer, H=Holocene, and P=Pleistocene). Panel A) shows absolute change in oxygen concentrations over time, measured every 2-3 days during the 28-day experiment. Error bars represent standard error about the mean from triplicate bottles, but are sometimes hidden by the symbol (due to small error range). Panel B) shows oxygen loss normalized to initial TOC concentration (Initial [O_2] – Final [O_2] / Initial [TOC] x 100) to indicate oxygen consumption relative to the available TOC pool.

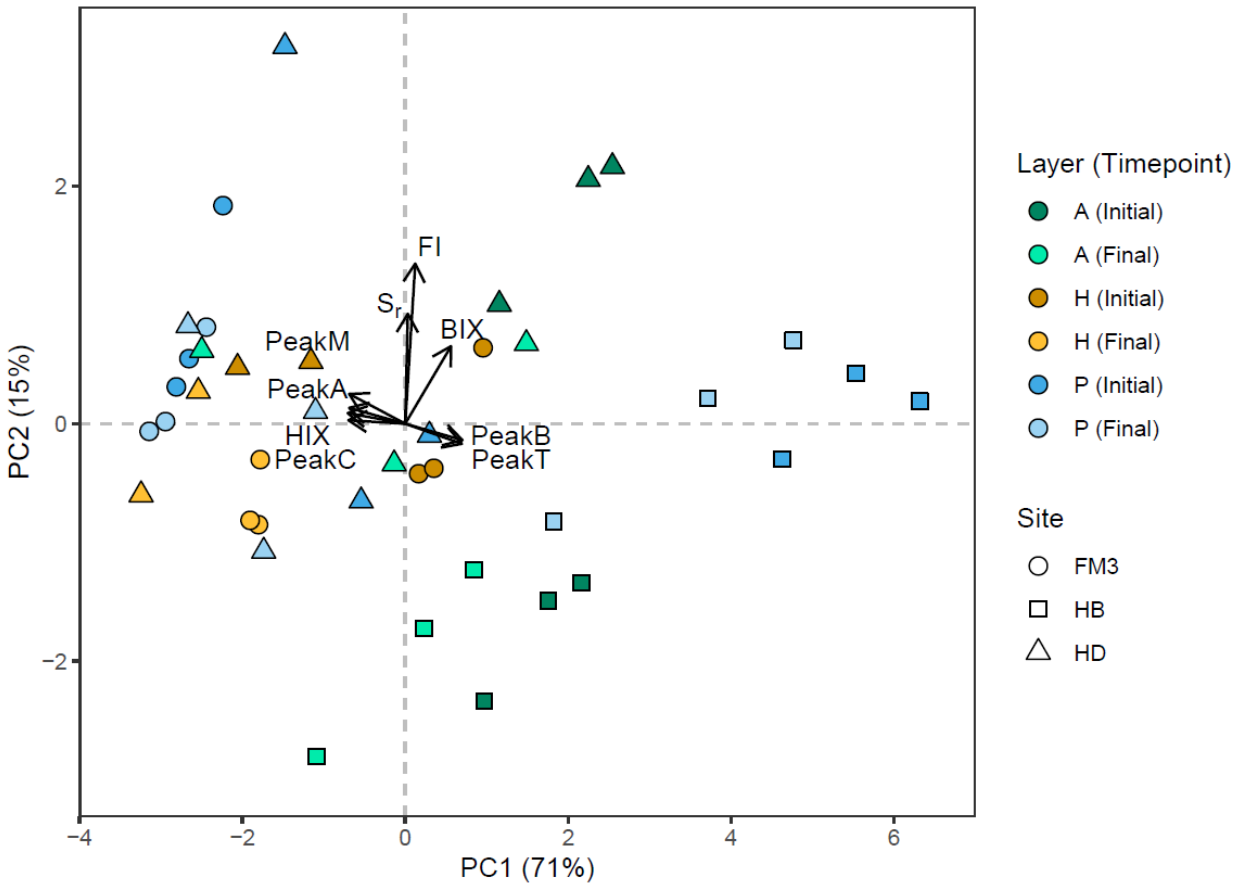

Figure 3-4. Principal Components Analysis for initial and final DOM composition metrics, where arrows represent eigenvectors for FI=fluorescence index, BIX=biological index, HIX=humification index, Sr=slope ratio, as well as for the proportion of fluorescent peak A, B, C, M, and T relative to the total fluorescent signal.

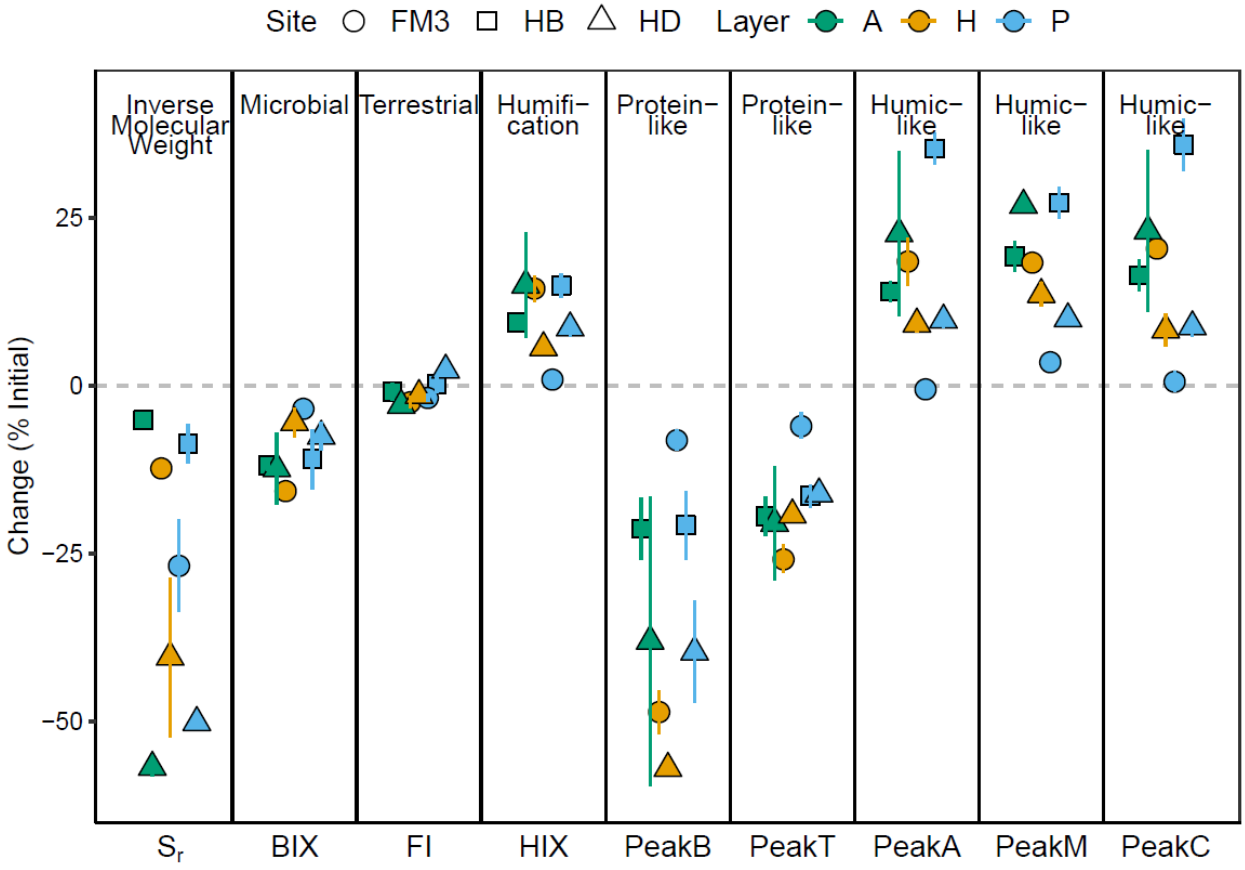

Figure 3-5. The change in DOM composition (characterized by fluorescence peaks, indices, and slope ratio), calculated as percent change from initial (Initial – Final / Initial x 100). Data points represent the mean and standard error of all treatments (N, U, W, as applicable) for each site (denoted by shape) and layer (denoted by colour, where A=active layer, H=Holocene, and P=Pleistocene). Negative values indicate a loss over time, while positive values indicate a gain. Input values of Sr, BIX, FI, and HIX represent the absolute value for these parameters, while input values of fluorescent peaks represent the contribution of each peak to the total fluorescent pool.

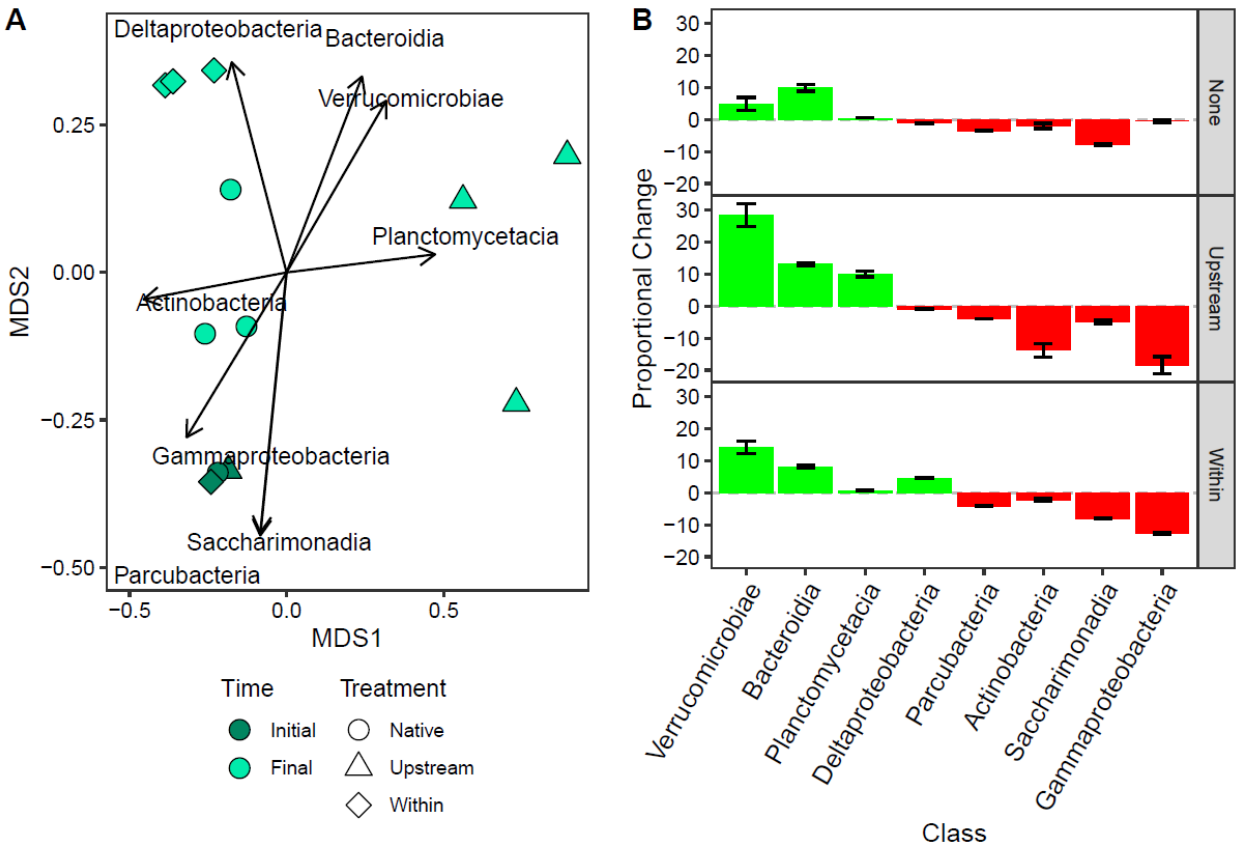

Figure 3-6. Microbial community composition at t=0 and t=28 for HB-A leachates amended with N, U, and W inocula. Panel A) shows non-metric multidimensional scaling (k=2, stress=0.047) of Bray-Curtis dissimilarity for relative abundance of rarefied OTUs. Simper analysis identified the classes that contributed >1% to dissimilarity, which were significant vectors for the NMDS based on 9999 permutations. Panel B) shows the change (positive=green, negative=red) in the proportion of these classes (contributed >1% to dissimilarity) over the course of the 28-day experiment. Rows denote the treatment, bars represent the mean, and error bars show the standard error for triplicates.

CH. 4: General Conclusions

4.1 Summary of General Conclusions

Through the detailed DOM compositional analyses in Chapter 2, we found that permafrost end-members were highly diverse across samples collected in the western Canadian Arctic. We found that the proportion of aliphatic compounds generally reflected the degree of processing, congruent with my hypothesis, though were lower in Yedoma than expected based on studies of Yedoma from other regions. Active layer leachates displayed compositionally similarity across landscape type, but were dissimilar from all permafrost end-members due to a higher proportion of aromatic compounds and more oxygenated compounds, as expected based on my hypothesis. Exposure to modification processes such as past thaw led to some compositional overlap among peat, lacustrine, and Yedoma leachates, which were compositionally distinct from glacial-origin till deposit leachates. Differences in the proportion of aliphatic versus aromatic compound classes suggest permafrost end-members will also vary in their biolability, as was similarly demonstrated in Chapter 3, which found contrasting DOM composition and biolability across stratigraphic units. Permafrost leachates were more biolabile than active layer leachates, with slightly more biolabile DOM in Holocene leachates than Pleistocene leachates. While these results generally agreed with my hypothesis, there was more variation among permafrost leachates by site than expected. Corroborating that past thaw can influence DOM composition, the increased biolability of Holocene leachates was tied to higher proportions of protein-like, microbially-produced components, which were preferentially consumed over humic-like, terrestrially-derived components. DOM compositional metrics were among the top predictors for biolability, and biodegradation rates were not strongly impacted by adding inocula from different sources, consistent with my hypothesis. The microbial community structure results did not agree with my hypothesis, since we found that the structure was initially similar and actually diverged over time; the source of the inocula appeared to influence the direction and extent of structural shifts, potentially due to the sediment and particle abundance present at each of the sources from which the inocula were sampled.

4.1.1 Research Limitations and Improvements

For the compositional analyses in Chapter 2, although FT-ICR MS produces high-resolution results, as with most analyses, it is subject to some limitations. One of the main

challenges associated with FT-ICR MS is charge competition between ions, where the negative ion mode used in this study preferentially selects for acidic analytes (such as carboxylic acids) over less acidic ions (such as alcohols or nitrogen-containing compounds; Koch et al. 2008; Tfaily et al. 2017). Choice of solvent and other experimental conditions can influence analyte abundance, which prompted us to attempt sequential extraction using MilliQ water, followed by methanol and chloroform, which together capture a greater range of compounds than one solvent alone (Tfaily et al. 2017). Unfortunately, upon injecting the chloroform leachates into the FT-ICR MS, these samples were found to be highly contaminated and therefore were not analyzed. The contamination could result from multiple, potentially co-occurring causes, including exposure to plastic during the sample collection phase (Tfaily et al. 2017), from using HPLC-grade chloroform that may have been either contaminated during production or too low-quality, or due to infrequent use of hydrophobic solvents in the FT-ICR MS instrument that led to contamination following injection (Randy Whittal, University of Alberta Mass Spectrometry Laboratory, pers. comm.). Including the hydrophobic fraction extracted with chloroform would have contributed to a broader, more complete characterization for permafrost-derived DOM.

For the biodegradation experiment completed in Chapter 3, some logistical complications and methodological choices contributed to limitations in the observed results. As with all experiments conducted in a laboratory setting, these experiments do not mimic the natural setting found in the in situ environment. Although we attempted to control temperature throughout the 28-day experiment, the incubator in our field laboratory malfunctioned a few days prior to setting up the experiment. In conjunction with this, local temperatures increased significantly one week, which led to the incubation bottle temperatures fluctuating from ~18°C to 28°C. These fall closely within the range of temperatures commonly used in biodegradation experiments (from 3.5°C to 25°C; Vonk et al. 2015), but the changing temperatures may have affected the biodegradation rates. Since all experimental bottles, including the controls, experienced the same fluctuation, our interpretation of the relative rates should still accurately reflect changes in biodegradation among leachates. Future biodegradation experiments should be conducted using an incubator that can maintain a constant temperature to alleviate this as a potentially confounding factor.

We initially chose to focus on the dissolved fraction of organic matter, which is functionally defined as the DOM passed through 0.45 to 0.7 μm (nominal pore size) filters.

While inocula used in other biodegradation experiments is occasionally filtered through 1.2 μm, filtering through 0.7 μm was previously determined to contain sufficient bacteria to serve as inocula (Vonk et al. 2015). Although filtering introduces size-based selection for the bacterial community, this has been shown to not impact DOM degradation dynamics (Dean et al. 2018). However, filtering through 0.7 μm may alter predatory dynamics by excluding bacteriovores (Dean et al. 2018), and therefore may have had an effect on the structure of the bacterial communities that were characterized in a subset of our experimental bottles.

Contrary to our expectations, the microbial community composition from initial samples was similar across treatments that included inocula from unimpacted stream water, thaw-slump rill water, and leachate-specific samples. While this could indicate that microbial community composition is similar across all three sources, it is possible that the storage required for our initial community samples led to a deviation from the in situ community composition. While we did still observe differences in the response of the microbial community structure among inocula sources, the degree or direction of divergence may have been different if the inocula was added immediately after collection. If logistically feasible, inocula should be collected and added to experimental leachates as soon as possible, ideally within a few hours to prevent rapid shifts in the microbial community.

Our microbial community structure analyses were limited by low concentrations of DNA extracted from the samples, such that active layer leachates from one site were the only samples sent for sequencing. Since we had to partition the 120 mL experimental volume into multiple analyses, we were only able to filter ~15-50 mL for the DNA extraction samples, which may have contributed to the low concentrations of DNA. While incubation bottle size is a trade-off between sample volume and potential "bottle effects" (Vonk et al. 2015), larger incubation bottles may be necessary for characterizing microbial community structure from permafrost leachates.

4.2 Future Research

The compositional differences and varying biolability presented in this study highlight that DOM is shaped by its genesis and provenance, creating a need for future research to investigate how permafrost-derived DOM may further vary in other regions that have contrasting geologic, geomorphic, temperature, or ecosystem history than the terrain types described here.

Comparing composition and biodegradability of end-members types similar to the ones used in this study will help to illuminate how regional differences may or may not affect DOM characteristics. This future research may lend itself to including additional end-members that were not addressed here, if there are other relevant permafrost end-members in different areas or regions. Since we observed differences in the proportion of compounds extracted using MilliQ water and chloroform:methanol, additional research that uses multiple, contrasting solvents will help to create a more complete assessment of the divergence between permafrost composition and the WEOM fraction that is available to aquatic systems. While we observed increased biolability of Holocene-associated DOM compared to Pleistocene-associated DOM in our incubation work, this assessment used samples collected from the headwalls of thaw slumps, so it would be interesting to investigate whether these patterns hold for other manifestations of permafrost thaw, such as active layer thickening, active layer detachment slides, etc. In the case of reduced or absent permafrost thaw, the near-surface sediments may be of a greater concern than the deeper deposits, while detachment slides or other mass wasting may mix material from multiple deposit depths, potentially altering the effective biolability of otherwise distinct units. In addition to the stable water isotope ($\delta^{18}O$) analysis performed on a subset of samples in Chapter 3, analyzing radiocarbon ($\delta^{14}C$) would better constrain how age of the sample material may be related to permafrost-derived DOM composition and biodegradability. Furthermore, analysis of stable isotopes of DOC and/or soil organic carbon ($\delta^{13}C$), which is useful for determining the sources of organic carbon, would provide additional insight to complement optical-based metrics.

BIBLIOGRAPHY

Abbott, Benjamin W., Jeremy B. Jones, Edward A. G. Schuur, F. Stuart Chapin III, William B. Bowden, M. Syndonia Bret-Harte, Howard E. Epstein, et al. 2016. "Biomass Offsets Little or None of Permafrost Carbon Release from Soils, Streams, and Wildfire: An Expert Assessment." *Environmental Research Letters* 11 (3): 034014. https://doi.org/10.1088/1748-9326/11/3/034014.

Abbott, Benjamin W., Julia R. Larouche, Jeremy B. Jones, William B. Bowden, and Andrew W. Balser. 2014. "Elevated Dissolved Organic Carbon Biodegradability from Thawing and Collapsing Permafrost." *Journal of Geophysical Research: Biogeosciences* 119 (10): 2014JG002678. https://doi.org/10.1002/2014JG002678.

Battin, Tom J., Louis A. Kaplan, Stuart Findlay, Charles S. Hopkinson, Eugenia Marti, Aaron I. Packman, J. Denis Newbold, and Francesc Sabater. 2008. "Biophysical Controls on Organic Carbon Fluxes in Fluvial Networks." *Nature Geoscience* 1 (2): 95–100. https://doi.org/10.1038/ngeo101.

Berggren, Martin, Jean-François Lapierre, and Paul A. del Giorgio. 2012. "Magnitude and Regulation of Bacterioplankton Respiratory Quotient across Freshwater Environmental Gradients." *The ISME Journal* 6 (5): 984–93. https://doi.org/10.1038/ismej.2011.157.

Blaud, Aimeric, Thomas Z. Lerch, Gareth K. Phoenix, and A. Mark Osborn. 2015. "Arctic Soil Microbial Diversity in a Changing World." *Research in Microbiology*, Special issue on Microbial diversity, adaptation and evolution, 166 (10): 796–813. https://doi.org/10.1016/j.resmic.2015.07.013.

Brookshire, E. N. Jack, H. Maurice Valett, Steven A. Thomas, and Jackson R. Webster. 2005. "Coupled Cycling of Dissolved Organic Nitrogen and Carbon in a Forest Stream." *Ecology* 86 (9): 2487–96. https://doi.org/10.1890/04-1184.

Burd, Katheryn, Cristian Estop-Aragonés, Suzanne E. Tank, and David Olefeldt. 2020. "Lability of Dissolved Organic Carbon from Boreal Peatlands: Interactions between Permafrost Thaw, Wildfire, and Season." *Canadian Journal of Soil Science*, February, CJSS-2019-0154. https://doi.org/10.1139/CJSS-2019-0154.

Burn, Chris R. 1997. "Cryostratigraphy, Paleogeography, and Climate Change during the Early Holocene Warm Interval, Western Arctic Coast, Canada." *Canadian Journal of Earth Sciences* 34 (7): 912–25. https://doi.org/10.1139/e17-076.

Burn, Chris R., and Steven V. Kokelj. 2009. "The Environment and Permafrost of the Mackenzie Delta Area." *Permafrost and Periglacial Processes* 20 (2): 83–105. https://doi.org/10.1002/ppp.655.

Burn, Chris R., Steven V. Kokelj, and J Ross Mackay. 2009. "The Thermal Regime of Permafrost and Its Susceptibility to Degradation in Upland Terrain near Inuvik, N.W.T." *Permafrost and Periglacial Processes* 20 (2): 221–27. https://doi.org/10.1002/ppp.649.

Carter, Martin R. 1993. *Soil Sampling and Methods of Analysis*. Boca Raton: Lewis Publishers.

Coble, Paula G. 1996. "Characterization of Marine and Terrestrial DOM in Seawater Using Excitation-Emission Matrix Spectroscopy." *Marine Chemistry* 51 (4): 325–46. https://doi.org/10.1016/0304-4203(95)00062-3.

Comte, Jerome, C. Lovejoy, S. Crevecoeur, and W. F. Vincent. 2016. "Co-Occurrence Patterns in Aquatic Bacterial Communities across Changing Permafrost Landscapes." *Biogeosciences* 13 (1): 175–90. https://doi.org/10.5194/bg-13-175-2016

Coolen, Marco J. L., and William D. Orsi. 2015. "The Transcriptional Response of Microbial

Communities in Thawing Alaskan Permafrost Soils." *Frontiers in Microbiology* 6. https://doi.org/10.3389/fmicb.2015.00197

Davis, Nicole M., Diana M. Proctor, Susan P. Holmes, David A. Relman, and Benjamin J. Callahan. 2018. "Simple Statistical Identification and Removal of Contaminant Sequences in Marker-Gene and Metagenomics Data." *Microbiome* 6 (1): 1–14. https://doi.org/10.1186/s40168-018-0605-2.

Dean, Joshua F., Jurgen R. van Hal, Han Dolman, Rien Aerts, and James T. Weedon. 2018. "Filtering Artefacts in Bacterial Community Composition Can Affect the Outcome of Dissolved Organic Matter Biolability Assays." *Biogeosciences Discussions*, July, 1–19. https://doi.org/10.5194/bg-2018-282.

Dittmar, Thorsten, Boris Koch, Norbert Hertkorn, and Gerhard Kattner. 2008. "A Simple and Efficient Method for the Solid-Phase Extraction of Dissolved Organic Matter (SPE-DOM) from Seawater." *Limnology and Oceanography: Methods* 6 (6): 230–35. https://doi.org/10.4319/lom.2008.6.230.

Drake, Travis W., François Guillemette, Jordon D. Hemingway, Jeffery P. Chanton, David C. Podgorski, Nikita S. Zimov, and Robert G. M. Spencer. 2018. "The Ephemeral Signature of Permafrost Carbon in an Arctic Fluvial Network." *Journal of Geophysical Research: Biogeosciences*, May. https://doi.org/10.1029/2017JG004311.

Drake, Travis W., Kimberly P. Wickland, Robert G. M. Spencer, Diane M. McKnight, and Robert G. Striegl. 2015. "Ancient Low–Molecular-Weight Organic Acids in Permafrost Fuel Rapid Carbon Dioxide Production upon Thaw." *Proceedings of the National Academy of Sciences* 112 (45): 13946–51. https://doi.org/10.1073/pnas.1511705112.

Ensom, Tim, Morse, Peter, Kokelj, Steven V., MacDonald, Erin N., Young, Joe, Tank, Suzanne E., Subedi, Rupesh, Grozic, Edward, and Ariane Castagner. 2020. "Permafrost Geotechnical Borehole Data Synthesis: 2013-2017 Inuvik-Tuktoyaktuk Region, Northwest Territories." Open File 8652, 78 pages, geotechnical data, and appendices. https://doi.org/10.4095/321869.

Ewing, Stephanie A., Jonathan A. O'Donnell, George R. Aiken, Kenna Butler, David Butman, Lisamarie Windham-Myers, and Mikhail Z. Kanevskiy. 2015. "Long-Term Anoxia and Release of Ancient, Labile Carbon upon Thaw of Pleistocene Permafrost." *Geophysical Research Letters* 42 (24): 2015GL066296. https://doi.org/10.1002/2015GL066296.

Fellman, Jason B., Eran Hood, and Robert G. M. Spencer. 2010. "Fluorescence Spectroscopy Opens New Windows into Dissolved Organic Matter Dynamics in Freshwater Ecosystems: A Review." *Limnology and Oceanography* 55 (6): 2452–62. https://doi.org/10.4319/lo.2010.55.6.2452.

Fraser, Taylor A., and Chris R. Burn. 1997. "On the Nature and Origin of 'Muck' Deposits in the Klondike Area, Yukon Territory." *Canadian Journal of Earth Sciences* 34 (10): 1333–44. https://doi.org/10.1139/e17-106.

French, Hugh M, and Wayne H Pollard. 1985. "Ground-Ice Investigations, Klondike District, Yukon Territory," 11.

French, Hugh, and Yuri Shur. 2010. "The Principles of Cryostratigraphy." *Earth-Science Reviews* 101 (3–4): 190–206. https://doi.org/10.1016/j.earscirev.2010.04.002.

Froese, Duane G., Grant D. Zazula, John A. Westgate, Shari J. Preece, Paul T. Sanborn, Alberto V. Reyes, and Nicholas J.G. Pearce. 2009. "The Klondike Goldfields and Pleistocene Environments of Beringia." *GSA Today* 19 (8): 4. https://doi.org/10.1130/GSATG54A.1.

Gaglioti, Benjamin V., Daniel H. Mann, Pamela Groves, Michael L. Kunz, Louise M.

Farquharson, Richard E.Reanier, Benjamin M. Jones and Matthew J. Wooller. 2018. "Aeolian stratigraphy describes ice-age paleoenvironments in unglaciated Arctic Alaska." *Quaternary Science Reviews* 182: 175–190. https://doi.org/10.1016/j.quascirev.2018.01.002.

Gittel, Antje, Jiří Bárta, Iva Kohoutová, Robert Mikutta, Sarah Owens, Jack Gilbert, Jörg Schnecker, et al. 2014. "Distinct Microbial Communities Associated with Buried Soils in the Siberian Tundra." *The ISME Journal* 8 (4): 841–53. https://doi.org/10.1038/ismej.2013.219.

Gittel, Antje, Jiří Bárta, Iva Kohoutová, Jörg Schnecker, Birgit Wild, Petr Čapek, Christina Kaiser, et al. 2014. "Site- and Horizon-Specific Patterns of Microbial Community Structure and Enzyme Activities in Permafrost-Affected Soils of Greenland." *Frontiers in Microbiology* 5. https://doi.org/10.3389/fmicb.2014.00541.

Graham, David E, Matthew D Wallenstein, Tatiana A Vishnivetskaya, Mark P Waldrop, Tommy J Phelps, Susan M Pfiffner, Tullis C Onstott, et al. 2012. "Microbes in Thawing Permafrost: The Unknown Variable in the Climate Change Equation." *The ISME Journal* 6 (4): 709–12. https://doi.org/10.1038/ismej.2011.163.

Hawkes, Jeffrey A, D'Andrilli, Juliana, Sleighter, Rachel L, Chen, Henglong, Hatcher, Patrick G, Ijaz, Amna, Khaksari, Maryam et al. 2020. "Limnology and oceanography methods an international laboratory comparison of dissolved organic matter composition by high resolution mass spectrometry". *Limnology and Oceanography: Methods*, 1-24, https://doi.org/10.1002/lom3.10364.

Heimann, Martin, and Markus Reichstein. 2008. "Terrestrial Ecosystem Carbon Dynamics and Climate Feedbacks." *Nature* 451 (7176): 289–92. https://doi.org/10.1038/nature06591.

Helms, John R., Aron Stubbins, Jason D. Ritchie, Elizabeth C. Minor, David J. Kieber, and Kenneth Mopper. 2008. "Absorption Spectral Slopes and Slope Ratios as Indicators of Molecular Weight, Source, and Photobleaching of Chromophoric Dissolved Organic Matter." *Limnology and Oceanography* 53 (3): 955–69. https://doi.org/10.4319/lo.2008.53.3.0955.

Heslop, Joanne K., Winkel, Matthias, Walter Anthony, Katey, M, Spencer, Rob G. M., Podgorski, David C., P. Zito, A. Kholodov, M. Zhang, and Susanne Liebner. 2019. "Increasing Organic Carbon Biolability With Depth in Yedoma Permafrost: Ramifications for Future Climate Change." *Journal of Geophysical Research: Biogeosciences* 124 (7): 2021–38. https://doi.org/10.1029/2018JG004712.

Hodgkins, Suzanne B., Malak M. Tfaily, Carmody K. McCalley, Tyler A. Logan, Patrick M. Crill, Scott R. Saleska, Virginia I. Rich, and Jeffrey P. Chanton. 2014. "Changes in Peat Chemistry Associated with Permafrost Thaw Increase Greenhouse Gas Production." *Proceedings of the National Academy of Sciences* 111 (16): 5819–24. https://doi.org/10.1073/pnas.1314641111.

Hodgkins, Suzanne B., Malak M. Tfaily, David C. Podgorski, Carmody K. McCalley, Scott R. Saleska, Patrick M. Crill, Virginia I. Rich, Jeffrey P. Chanton, and William T. Cooper. 2016. "Elemental Composition and Optical Properties Reveal Changes in Dissolved Organic Matter along a Permafrost Thaw Chronosequence in a Subarctic Peatland." *Geochimica et Cosmochimica Acta* 187 (August): 123–40. https://doi.org/10.1016/j.gca.2016.05.015.

Hugelius, Gustaf, Strauss, Jens, S. Zubrzycki, J. W. Harden, E. A. G. Schuur, C.-L. Ping, L. Schirrmeister, et al. 2014. "Estimated Stocks of Circumpolar Permafrost Carbon with

Quantified Uncertainty Ranges and Identified Data Gaps." *Biogeosciences* 11 (23): 6573–93. https://doi.org/10.5194/bg-11-6573-2014.
Huguet, Arnaud, L. Vacher, S. Relexans, S. Saubusse, J. M. Froidefond, and E. Parlanti. 2009. "Properties of Fluorescent Dissolved Organic Matter in the Gironde Estuary." *Organic Geochemistry* 40 (6): 706–19. https://doi.org/10.1016/j.orggeochem.2009.03.002.
Jansson, Janet K., and Neslihan Taş. 2014. "The Microbial Ecology of Permafrost." *Nature Reviews Microbiology* 12 (6): 414–25. https://doi.org/10.1038/nrmicro3262.
Jiang, Zhiwei, Yanyu Lu, Jiaqi Xu, Mingqi Li, Guangchun Shan, and Qunliang Li. 2019. "Exploring the Characteristics of Dissolved Organic Matter and Succession of Bacterial Community during Composting." *Bioresource Technology* 292 (November): 121942. https://doi.org/10.1016/j.biortech.2019.121942.
Johnston, Sarah Ellen, Matthew J. Bogard, Jennifer A. Rogers, David Butman, Robert G. Striegl, Mark Dornblaser, and Robert G. M. Spencer. 2019. "Constraining Dissolved Organic Matter Sources and Temporal Variability in a Model Sub-Arctic Lake." *Biogeochemistry* 146 (3): 271–92. https://doi.org/10.1007/s10533-019-00619-9.
Judd, Kristin E., Byron C. Crump, and George W. Kling. 2006. "Variation in Dissolved Organic Matter Controls Bacterial Production and Community Composition." *Ecology* 87 (8): 2068–79. https://doi.org/10.1890/0012-9658(2006)87[2068:VIDOMC]2.0.CO;2.
Kalbitz, Karsten., J. Schmerwitz, D. Schwesig, and E. Matzner. 2003. "Biodegradation of Soil-Derived Dissolved Organic Matter as Related to Its Properties." *Geoderma*, Ecological aspects of dissolved organic matter in soils, 113 (3): 273–91. https://doi.org/10.1016/S0016-7061(02)00365-8.
Kane, Douglas L., Larry D. Hinzman, and John P. Zarling. 1991. "Thermal Response of the Active Layer to Climatic Warming in a Permafrost Environment." *Cold Regions Science and Technology* 19 (2): 111–22. https://doi.org/10.1016/0165-232X(91)90002-X.
Knoblauch, Christian, Christian Beer, Alexander Sosnin, Dirk Wagner, and Eva-Maria Pfeiffer. 2013. "Predicting Long-Term Carbon Mineralization and Trace Gas Production from Thawing Permafrost of Northeast Siberia." *Global Change Biology* 19 (4): 1160–72. https://doi.org/10.1111/gcb.12116.
Koch, Boris P., and T. Dittmar. 2006. "From Mass to Structure: An Aromaticity Index for High-Resolution Mass Data of Natural Organic Matter." *Rapid Communications in Mass Spectrometry* 20 (5): 926–32. https://doi.org/10.1002/rcm.2386.
Koch, Boris P., Kai-Uwe Ludwichowski, Gerhard Kattner, Thorsten Dittmar, and Matthias Witt. 2008. "Advanced Characterization of Marine Dissolved Organic Matter by Combining Reversed-Phase Liquid Chromatography and FT-ICR-MS." *Marine Chemistry* 111 (3): 233–41. https://doi.org/10.1016/j.marchem.2008.05.008.
Kokelj, Steven V., and M. T. Jorgenson. 2013. "Advances in Thermokarst Research." *Permafrost and Periglacial Processes* 24 (2): 108–19. https://doi.org/10.1002/ppp.1779.
Kokelj, Steven V., D. Lacelle, T. C. Lantz, J. Tunnicliffe, L. Malone, I. D. Clark, and K. S. Chin. 2013. "Thawing of Massive Ground Ice in Mega Slumps Drives Increases in Stream Sediment and Solute Flux across a Range of Watershed Scales." *Journal of Geophysical Research: Earth Surface* 118 (2): 681–92. https://doi.org/10.1002/jgrf.20063.
Kokelj Steven V., Palmer M. J., Lantz T. C., and Burn C. R. 2017a. "Ground Temperatures and Permafrost Warming from Forest to Tundra, Tuktoyaktuk Coastlands and Anderson Plain, NWT, Canada." *Permafrost and Periglacial Processes* 28 (3): 543–51. https://doi.org/10.1002/ppp.1934.

Kokelj, Steven V., Trevor C. Lantz, Jon Tunnicliffe, Rebecca Segal, and Denis Lacelle. 2017b. "Climate-Driven Thaw of Permafrost Preserved Glacial Landscapes, Northwestern Canada." *Geology* 45 (4): 371–74. https://doi.org/10.1130/G38626.1.

Kokelj, Steven V., Jon F. Tunnicliffe, and Denis Lacelle. 2017. "The Peel Plateau of Northwestern Canada: An Ice-Rich Hummocky Moraine Landscape in Transition." In *Landscapes and Landforms of Western Canada*, 109–22. World Geomorphological Landscapes. Springer, Cham. https://doi.org/10.1007/978-3-319-44595-3_7.

Kuhry, Peter, Jiří Bárta, Daan Blok, Bo Elberling, Samuel Faucherre, Gustaf Hugelius, Christian J. Jørgensen, Andreas Richter, Hana Šantrůčková, and Niels Weiss. 2020. "Lability Classification of Soil Organic Matter in the Northern Permafrost Region." *Biogeosciences* 17 (2): 361–79. https://doi.org/10.5194/bg-17-361-2020.

Lacelle, Denis, Alex Brooker, Robert H. Fraser, and Steve V. Kokelj. 2015. "Distribution and Growth of Thaw Slumps in the Richardson Mountains–Peel Plateau Region, Northwestern Canada." *Geomorphology* 235 (April): 40–51. https://doi.org/10.1016/j.geomorph.2015.01.024.

Lacelle, Denis, Marielle Fontaine, André Pellerin, Steve V. Kokelj, and Ian D. Clark. 2019. "Legacy of Holocene Landscape Changes on Soil Biogeochemistry: A Perspective From Paleo-Active Layers in Northwestern Canada." *Journal of Geophysical Research: Biogeosciences* 124 (9): 2662–79. https://doi.org/10.1029/2018JG004916.

Lacelle, Denis, Bernard Lauriol, Grant Zazula, Bassam Ghaleb, Nicholas Utting, and Ian D. Clark. 2013. "Timing of Advance and Basal Condition of the Laurentide Ice Sheet during the Last Glacial Maximum in the Richardson Mountains, NWT." *Quaternary Research* 80 (2): 274–83. https://doi.org/10.1016/j.yqres.2013.06.001.

Lantz, Trevor C., Sarah E. Gergel, and Steven V. Kokelj. 2010. "Spatial Heterogeneity in the Shrub Tundra Ecotone in the Mackenzie Delta Region, Northwest Territories: Implications for Arctic Environmental Change." *Ecosystems* 13 (2): 194–204. https://doi.org/10.1007/s10021-009-9310-0.

Le Quéré, Corinne, Michael R. Raupach, Josep G. Canadell, Gregg Marland, Laurent Bopp, Philippe Ciais, Thomas J. Conway, et al. 2009. "Trends in the Sources and Sinks of Carbon Dioxide." *Nature Geoscience* 2 (12): 831–36. https://doi.org/10.1038/ngeo689.

Littlefair, Cara A., and Suzanne E. Tank. 2018. "Biodegradability of Thermokarst Carbon in a Till-Associated, Glacial Margin Landscape: The Case of the Peel Plateau, NWT, Canada." *Journal of Geophysical Research: Biogeosciences* 123 (10): 3293–3307. https://doi.org/10.1029/2018JG004461.

Littlefair, Cara A., Suzanne E. Tank, and Steven V. Kokelj. 2017. "Retrogressive Thaw Slumps Temper Dissolved Organic Carbon Delivery to Streams of the Peel Plateau, NWT, Canada." *Biogeosciences* 14 (23): 5487–5505. https://doi.org/10.5194/bg-14-5487-2017.

Mackay, J Ross. 1963. "THE MACKENZIE DELTA AREA, N.W.T.," 212.

Mackelprang, Rachel, Mark P. Waldrop, Kristen M. DeAngelis, Maude M. David, Krystle L. Chavarria, Steven J. Blazewicz, Edward M. Rubin, and Janet K. Jansson. 2011. "Metagenomic Analysis of a Permafrost Microbial Community Reveals a Rapid Response to Thaw." *Nature; London* 480 (7377): 368–71.

Mackelprang, Rachel, Alexander Burkert, Monica Haw, Tara Mahendrarajah, Christopher H Conaway, Thomas A Douglas, and Mark P Waldrop. 2017. "Microbial Survival Strategies in Ancient Permafrost: Insights from Metagenomics." *The ISME Journal* 11 (10): 2305–18. https://doi.org/10.1038/ismej.2017.93.

Mahony, Matthew E. 2015. “Department of Earth and Atmospheric Sciences University of Alberta,” 207.
Malard, Lucie A., and David A. Pearce. 2018. “Microbial Diversity and Biogeography in Arctic Soils.” *Environmental Microbiology Reports* 10 (6): 611–25. https://doi.org/10.1111/1758-2229.12680.
Malone, Laura, Denis Lacelle, Steve Kokelj, and Ian D. Clark. 2013. “Impacts of Hillslope Thaw Slumps on the Geochemistry of Permafrost Catchments (Stony Creek Watershed, NWT, Canada).” *Chemical Geology* 356 (October): 38–49. https://doi.org/10.1016/j.chemgeo.2013.07.010.
Mann, Paul J., William V. Sobczak, Madeleine M. LaRue, Ekaterina Bulygina, Anna Davydova, Jorien E. Vonk, John Schade, et al. 2014. “Evidence for Key Enzymatic Controls on Metabolism of Arctic River Organic Matter.” *Global Change Biology* 20 (4): 1089–1100. https://doi.org/10.1111/gcb.12416.
Mann, Paul J., Robert G. M. Spencer, Peter J. Hernes, Johan Six, George R. Aiken, Suzanne E. Tank, James W. McClelland, Kenna D. Butler, Rachael Y. Dyda, and Robert M. Holmes. 2016. “Pan-Arctic Trends in Terrestrial Dissolved Organic Matter from Optical Measurements.” *Frontiers in Earth Science* 4. https://doi.org/10.3389/feart.2016.00025.
Marschner, Bernd, and Karsten Kalbitz. 2003. “Controls of Bioavailability and Biodegradability of Dissolved Organic Matter in Soils.” *Geoderma* 113 (3–4): 211–35. https://doi.org/10.1016/S0016-7061(02)00362-2.
McKnight, Diane M., Elizabeth W. Boyer, Paul K. Westerhoff, Peter T. Doran, Thomas Kulbe, and Dale T. Andersen. 2001. “Spectrofluorometric Characterization of Dissolved Organic Matter for Indication of Precursor Organic Material and Aromaticity.” *Limnology and Oceanography* 46 (1): 38–48. https://doi.org/10.4319/lo.2001.46.1.0038.
Merder, Julian, Jan A. Freund, Ulrike Feudel, Jutta Niggemann, Gabriel Singer, and Thorsten Dittmar. 2020. “Improved Mass Accuracy and Isotope Confirmation through Alignment of Ultrahigh-Resolution Mass Spectra of Complex Natural Mixtures.” *Analytical Chemistry* 92 (3): 2558–65. https://doi.org/10.1021/acs.analchem.9b04234.
Meredith, Michael, M. Sommerkorn, S. Cassotta, C. Derksen, A. Ekaykin, A. Hollowed, G. Kofinas, et al. 2019. “IPCC Special Report on the Ocean and Cryosphere in a Changing Climate”. https://www.ipcc.ch/srocc/chapter/chapter-3-2/.
Meyers, Philip A, and Elisabeth Lallier-Vergès. 1999. “Lacustrine Sedimentary Organic Matter Records of Late Quaternary Paleoclimates,” 28.
Michel, Fred. A. 2011. “Isotope Characterisation of Ground Ice in Northern Canada.” *Permafrost and Periglacial Processes* 22 (1): 3–12. https://doi.org/10.1002/ppp.721.
Morris, Paul J., Graeme T. Swindles, Paul J. Valdes, Ruza F. Ivanovic, Lauren J. Gregoire, Mark W. Smith, Lev Tarasov, Alan M. Haywood, and Karen L. Bacon. 2018. “Global Peatland Initiation Driven by Regionally Asynchronous Warming.” *Proceedings of the National Academy of Sciences* 115 (19): 4851–56. https://doi.org/10.1073/pnas.1717838115.
Monteux, Sylvain, James T. Weedon, Gesche Blume-Werry, Konstantin Gavazov, Vincent E. J. Jassey, Margareta Johansson, Frida Keuper, Carolina Olid, and Ellen Dorrepaal. 2018. “Long-Term in Situ Permafrost Thaw Effects on Bacterial Communities and Potential Aerobic Respiration.” *The ISME Journal* 12 (9): 2129–41. https://doi.org/10.1038/s41396-018-0176-z.
Müller, Oliver, Toke Bang-Andreasen, Richard Allen White, Bo Elberling, Neslihan Taş, Timothy Kneafsey, Janet K. Jansson, and Lise Øvreås. 2018. “Disentangling the

Complexity of Permafrost Soil by Using High Resolution Profiling of Microbial Community Composition, Key Functions and Respiration Rates." *Environmental Microbiology* 20 (12): 4328–42. https://doi.org/10.1111/1462-2920.14348.
Murton, Julian B. 2009. "Stratigraphy and Palaeoenvironments of Richards Island and the Eastern Beaufort Continental Shelf during the Last Glacial-Interglacial Cycle." *Permafrost and Periglacial Processes* 20 (2): 107–25. https://doi.org/10.1002/ppp.647.
Norris, D. K. 1973. "Tectonic Styles of Northern Yukon Territory and Northwestern District of Mackenzie, Canada: Regional Arctic Geology of Canada" 108: 23–40.
Panneer Selvam, Balathandayuthabani, Jean-François Lapierre, Francois Guillemette, Carolina Voigt, Richard E. Lamprecht, Christina Biasi, Torben R. Christensen, Pertti J. Martikainen, and Martin Berggren. 2017. "Degradation Potentials of Dissolved Organic Carbon (DOC) from Thawed Permafrost Peat." *Scientific Reports* 7 (April). https://doi.org/10.1038/srep45811.
Péwé, Troy Lewis. 1975. *Quaternary Geology of Alaska*. U.S. Government Printing Office.
Plaza, César, Elaine Pegoraro, Rosvel Bracho, Gerardo Celis, Kathryn G. Crummer, Jack A. Hutchings, Caitlin E. Hicks Pries, et al. 2019. "Direct Observation of Permafrost Degradation and Rapid Soil Carbon Loss in Tundra." *Nature Geoscience* 12 (8): 627–31. https://doi.org/10.1038/s41561-019-0387-6.
Rampton, V N. 1988. "Quaternary Geology of the Tuktoyaktuk Coastlands, Northwest Territories." 423. https://doi.org/10.4095/126937.
Saidi-Mehrabad, Alireza, Neuberger, Patrick, Cavaco, Maria, Froese, Duane, and Brian Lanoil. 2020. Optimization of subsampling, decontamination, and DNA extraction of difficult peat and silt permafrost samples. *BioRxiv.* https://doi.org/10.1101/2020.01.02.893438.
Salehi, M.H., O. Hashemi Beni, H. Beigi Harchegani, I. Esfandiarpour Borujeni, and H.R. Motaghian. 2011. "Refining Soil Organic Matter Determination by Loss-on-Ignition." *Pedosphere* 21 (4): 473–82. https://doi.org/10.1016/S1002-0160(11)60149-5.
Schädel, Christina, Edward A. G. Schuur, Rosvel Bracho, Bo Elberling, Christian Knoblauch, Hanna Lee, Yiqi Luo, Gaius R. Shaver, and Merritt R. Turetsky. 2014. "Circumpolar Assessment of Permafrost C Quality and Its Vulnerability over Time Using Long-Term Incubation Data." *Global Change Biology* 20 (2): 641–52. https://doi.org/10.1111/gcb.12417.
Schirrmeister, Lutz, D. Froese, V. Tumskoy, Guido Grosse, and Sebastian Wetterich. 2013. "Yedoma: Late Pleistocene Ice-Rich Syngenetic Permafrost of Beringia." Inbook. Encyclopedia of Quaternary Science. 2nd Edition. Amsterdam: Elsevier. April 2013. http://www.sciencedirect.com/science/article/pii/B9780444536433001060.
Schuur, Edward A. G., A. D. McGuire, C. Schädel, G. Grosse, J. W. Harden, D. J. Hayes, G. Hugelius, et al. 2015. "Climate Change and the Permafrost Carbon Feedback." *Nature* 520 (7546): 171–79. https://doi.org/10.1038/nature14338.
Schuur, Edward A. G., and Benjamin Abbott. 2011. "High Risk of Permafrost Thaw." *Nature* 480 (7375): 32–33. https://doi.org/10.1038/480032a.
Segal, Rebecca A, Trevor C Lantz, and Steven V Kokelj. 2016. "Acceleration of Thaw Slump Activity in Glaciated Landscapes of the Western Canadian Arctic." *Environmental Research Letters* 11 (3): 034025. https://doi.org/10.1088/1748-9326/11/3/034025.
Shirokova, Liudmila S., Artem V. Chupakov, Svetlana A. Zabelina, Natalia V. Neverova, Dahedrey Payandi-Rolland, Carole Causserand, Jan Karlsson, and Oleg S. Pokrovsky. 2019. "Humic Surface Waters of Frozen Peat Bogs (Permafrost Zone) Are Highly

Resistant to Bio- and Photodegradation." *Biogeosciences* 16 (12): 2511–26.
Spencer, Robert G. M., Weidong Guo, Peter A. Raymond, Thorsten Dittmar, Eran Hood, Jason Fellman, and Aron Stubbins. 2014. "Source and Biolability of Ancient Dissolved Organic Matter in Glacier and Lake Ecosystems on the Tibetan Plateau." *Geochimica et Cosmochimica Acta* 142 (October): 64–74. https://doi.org/10.1016/j.gca.2014.08.006.
Spencer, Robert G. M., Paul J. Mann, Thorsten Dittmar, Timothy I. Eglinton, Cameron McIntyre, R. Max Holmes, Nikita Zimov, and Aron Stubbins. 2015. "Detecting the Signature of Permafrost Thaw in Arctic Rivers." *Geophysical Research Letters* 42 (8): 2015GL063498. https://doi.org/10.1002/2015GL063498.
Stubbins, Aron, Paul J. Mann, Leanne Powers, Thais B. Bittar, Thorsten Dittmar, Cameron P. McIntyre, Timothy I. Eglinton, Nikita Zimov, and Robert G. M. Spencer. 2017. "Low Photolability of Yedoma Permafrost Dissolved Organic Carbon." *Journal of Geophysical Research: Biogeosciences* 122 (1): 2016JG003688. https://doi.org/10.1002/2016JG003688.
Tank, Suzanne E, Jorien, V. E., Walvoord, M. A., McClelland, J. W., Laurion, I., Abbot, B. W. 2020. "Landscape matters: Predicting the biogeochemical effects of permafrost thaw on aquatic networks with a state factor approach." *Permafrost and Periglacial Processes,* 1–13. https://doi.org/10.1002/ppp.2057.
Tanski, George, Hugues Lantuit, Saskia Ruttor, Christian Knoblauch, Boris Radosavljevic, Jens Strauss, Juliane Wolter, Anna M. Irrgang, Justine Ramage, and Michael Fritz. 2017. "Transformation of Terrestrial Organic Matter along Thermokarst-Affected Permafrost Coasts in the Arctic." *Science of The Total Environment* 581 (Supplement C): 434–47. https://doi.org/10.1016/j.scitotenv.2016.12.152.
Taş, Neslihan, Emmanuel Prestat, Jack W. McFarland, Kimberley P. Wickland, Rob Knight, Asmeret Asefaw Berhe, Torre Jorgenson, Mark P. Waldrop, and Janet K. Jansson. 2014. "Impact of Fire on Active Layer and Permafrost Microbial Communities and Metagenomes in an Upland Alaskan Boreal Forest." *The ISME Journal* 8 (9): 1904–19. https://doi.org/10.1038/ismej.2014.36.
Textor, Sadie R., Kimberly P. Wickland, David C. Podgorski, Sarah Ellen Johnston, and Robert G. M. Spencer. 2019. "Dissolved Organic Carbon Turnover in Permafrost-Influenced Watersheds of Interior Alaska: Molecular Insights and the Priming Effect." *Frontiers in Earth Science* 7. https://doi.org/10.3389/feart.2019.00275.
Tfaily, Malak M., Rosalie K. Chu, Jason Toyoda, Nikola Tolić, Errol W. Robinson, Ljiljana Paša-Tolić, and Nancy J. Hess. 2017. "Sequential Extraction Protocol for Organic Matter from Soils and Sediments Using High Resolution Mass Spectrometry." *Analytica Chimica Acta* 972 (June): 54–61. https://doi.org/10.1016/j.aca.2017.03.031.
Van der Sluijs, Jurjen, Steven V. Kokelj, Robert H. Fraser, Jon Tunnicliffe, and Denis Lacelle. 2018. "Permafrost Terrain Dynamics and Infrastructure Impacts Revealed by UAV Photogrammetry and Thermal Imaging." *Remote Sensing* 10 (11): 1734. https://doi.org/10.3390/rs10111734.
Vardy, Sheila R., Barry G. Warner, and Ramon Aravena. 1998. "Holocene Climate and the Development of a Subarctic Peatland near Inuvik, Northwest Territories, Canada." *Climatic Change* 40 (2): 285–313. https://doi.org/10.1023/A:1005473021115.
Vonk, Jorien E., S. E. Tank, and M. A. Walvoord. 2019. "Integrating Hydrology and Biogeochemistry across Frozen Landscapes." *Nature Communications* 10 (1): 5377. https://doi.org/10.1038/s41467-019-13361-5.

Vonk, Jorien E., Paul J. Mann, Sergey Davydov, Anna Davydova, Robert G. M. Spencer, John Schade, William V. Sobczak, et al. 2013. "High Biolability of Ancient Permafrost Carbon upon Thaw." *Geophysical Research Letters* 40 (11): 2689–93. https://doi.org/10.1002/grl.50348.

Vonk, Jorien, Suzanne Tank, Paul Mann, Robert Spencer, Claire Treat, Robert Striegl, Benjamin Abbott, and Kimberly Wickland. 2015. "Biodegradability of Dissolved Organic Carbon in Permafrost Soils and Aquatic Systems: A Meta-Analysis." *Biogeosciences (BG)* 12 (23): 6915–30.

Wang, Yinghui, Yunping Xu, Robert G. M. Spencer, Phoebe Zito, Anne Kellerman, David Podgorski, Wenjie Xiao, Dandan Wei, Harunur Rashid, and Yuanhe Yang. 2018. "Selective Leaching of Dissolved Organic Matter From Alpine Permafrost Soils on the Qinghai-Tibetan Plateau." *Journal of Geophysical Research: Biogeosciences* 123 (3): 1005–16. https://doi.org/10.1002/2017JG004343.

Ward, Collin P., and Rose M. Cory. 2015. "Chemical Composition of Dissolved Organic Matter Draining Permafrost Soils." *Geochimica et Cosmochimica Acta* 167 (October): 63–79. https://doi.org/10.1016/j.gca.2015.07.001.

Ward, Collin P., and Rose M. Cory.. 2016. "Complete and Partial Photo-Oxidation of Dissolved Organic Matter Draining Permafrost Soils." *Environmental Science & Technology* 50 (7): 3545–53. https://doi.org/10.1021/acs.est.5b05354.

Ward, Collin P., Sarah G. Nalven, Byron C. Crump, George W. Kling, and Rose M. Cory. 2017. "Photochemical Alteration of Organic Carbon Draining Permafrost Soils Shifts Microbial Metabolic Pathways and Stimulates Respiration." *Nature Communications* 8 (1). https://doi.org/10.1038/s41467-017-00759-2.

Weishaar, James L., George R. Aiken, Brian A. Bergamaschi, Miranda S. Fram, Roger Fujii, and Kenneth Mopper. 2003. "Evaluation of Specific Ultraviolet Absorbance as an Indicator of the Chemical Composition and Reactivity of Dissolved Organic Carbon." *Environmental Science & Technology* 37 (20): 4702–8. https://doi.org/10.1021/es030360x.

Wickland, Kim P., G. R. Aiken, K. Butler, M. M. Dornblaser, R. G. M. Spencer, and R. G. Striegl. 2012. "Biodegradability of Dissolved Organic Carbon in the Yukon River and Its Tributaries: Seasonality and Importance of Inorganic Nitrogen." *Global Biogeochemical Cycles* 26 (4). https://doi.org/10.1029/2012GB004342.

Wickland, Kimberly P, Mark P Waldrop, George R Aiken, Joshua C Koch, M Torre Jorgenson, and Robert G Striegl. 2018. "Dissolved Organic Carbon and Nitrogen Release from Boreal Holocene Permafrost and Seasonally Frozen Soils of Alaska." *Environmental Research Letters* 13 (6): 065011. https://doi.org/10.1088/1748-9326/aac4ad.

Zhang, Xinfang, Shijian Xu, Changming Li, Lin Zhao, Huyuan Feng, Guangyang Yue, Zhengwei Ren, and Guogdong Cheng. 2014. "The Soil Carbon/Nitrogen Ratio and Moisture Affect Microbial Community Structures in Alkaline Permafrost-Affected Soils with Different Vegetation Types on the Tibetan Plateau." *Research in Microbiology* 165 (2): 128–39. https://doi.org/10.1016/j.resmic.2014.01.002.

Zolkos, Scott, Suzanne E. Tank, and Steven V. Kokelj. 2018. "Mineral Weathering and the Permafrost Carbon-Climate Feedback." *Geophysical Research Letters* 45 (18): 9623–32. https://doi.org/10.1029/2018GL078748.

Appendix 1. Supporting information for Chapter 2

A1.1. Detailed Methods

To determine SOM content, we completed loss-on-ignition using ~5 g of freeze-dried sediments, which was aliquoted into a pre-cleaned glass petri dish, muffled at 360°C for 4 hours, placed in a dessicator to cool, then weighed to determine the difference in weight, expressed relative to initial weight (Salehi et al. 2011). To determine DOC, ~30 mL was aliquoted into pre-cleaned borosilicate vials, preserved with 30 µL concentrated hydrochloric acid, and stored in a dark fridge (4°C) until analysis (Vonk et al. 2015). Samples were analyzed on a Shimadzu TOC-5000A, which reports the mean concentration of three to five injections (to satisfy coefficient of variance <2%) from each sample vial. Subsamples for absorbance were aliquoted into pre-cleaned amber glass bottles, were stored in a dark fridge (4°C), then were analyzed using a Horiba Aqualog. Absorbance slopes from wavelengths 275-295 nm were divided by the slope from wavelengths 350-400 nm ($S_{275-295}/S_{350-400}$) to calculate slope ratio (S_r; Helms et al. 2008). Subsamples for TDP were aliquoted into 50 mL centrifuge tubes, then were submitted to the Biogeochemical Analytical Services Lab at the University of Alberta and analyzed using a Lachat QuickChem QC8500 FIA Automated Ion Analyzer. Subsamples for trace metal analysis were collected into 15 mL centrifuge tubes, preserved with 18% nitric acid, then were submitted to the ICPMS facility within the Canadian Center for Isotopic Microanalysis (CCIM) laboratory at the University of Alberta, and analyzed using a Thermo ICAP-6300 Inductively Coupled Argon Plasma - Optical Emission Spectrometer.

Table A1-1. Borehole (BH) sample depth, end-member (E-M) type (A.L.= active layer, lacust. = lascustrine, diamic. = diamicton, and Yed.= Yedoma), with geochemical parameters including soil organic matter (SOM), dissolved organic carbon (DOC), S_r (slope ratio is inversely related to molecular weight), and total dissolved phosphorus (TDP). DOM composition is presented using the proportional abundance (% is intensity sum normalized) of compounds detected using FTICR MS, grouped into broad classes aliphatic (aliphat.), low-oxygen unsaturated (low-O unsat.), high-oxygen unsaturated (high-O unsat.), aromatic (arom.) and condensed aromatics (cond. arom.).

BH	Depth (m)	E-M	SOM (%)	DOC (mg/ L)	S_r	TDP (µg/ L)	Ali-phat. (%)	Low-O Unsat. (%)	High-O Unsat. (%)	Arom. (%)	Cond. Arom. (%)
1	0.32	A.L.	89.54	179.9	0.47	98	2.5	9.5	48.8	25.5	6.5
1	0.82	Peat	21.14	43.73	0.81	45	17.8	10.9	43.4	17.0	7.6
2	0.32	A.L.	14.2	23.66	na	na	2.3	10.3	54.8	21.2	7.5
2	11.25	Till	1.94	2.15	na	na	4.5	65.1	10.4	12.4	5.3
3	0.32	A.L.	78.93	30.6	0.82	97	2.1	9.3	50.6	24.8	8.8
4	3.7	Peat	15.93	26.83	0.95	50	27.3	8.7	41.7	14.2	5.1
4	5.86	Lacust.	2.17	3.58	0.89	8	17.4	14.7	53.2	9.0	3.7
5	14.25	Till	0.34	2.21	na	na	87.9	7.5	3.1	1.2	0.0
6	1.12	Diamic.	15.13	16.05	0.85	26	10.8	8.7	47.6	21.3	7.6
7	0.32	A.L.	6.36	17.64	1	88	4.2	4.7	58.7	22.1	6.1
7	4.75	Till	2.25	6.92	0.92	71	45.8	15.5	21.4	10.8	4.8
8	0.32	A.L.	82.52	49.79	0.76	130	5.0	11.7	47.8	22.7	9.2
8	1.52	Peat	35.57	65.73	0.87	96	29.1	9.1	36.5	16.4	5.8
8	10.22	Lacust.	3.2	8.55	1.1	13	20.2	9.1	44.9	16.4	6.1
9	0.32	A.L.	77.94	45.03	0.72	192	2.5	10.4	52.7	22.5	7.8
9	9.25	Till	1.94	4.58	na	na	54.9	11.4	17.3	10.2	4.4
10	9.5	Diamic.	1.3	7.9	na	na	4.1	30.1	64.2	0.9	0.4
KL	6	Yed.	1.96	9.63	na	na	12.4	12.5	59.2	9.5	4.6
KL	7	Yed.	2.89	11.46	na	na	31.1	11.0	35.8	13.6	6.1

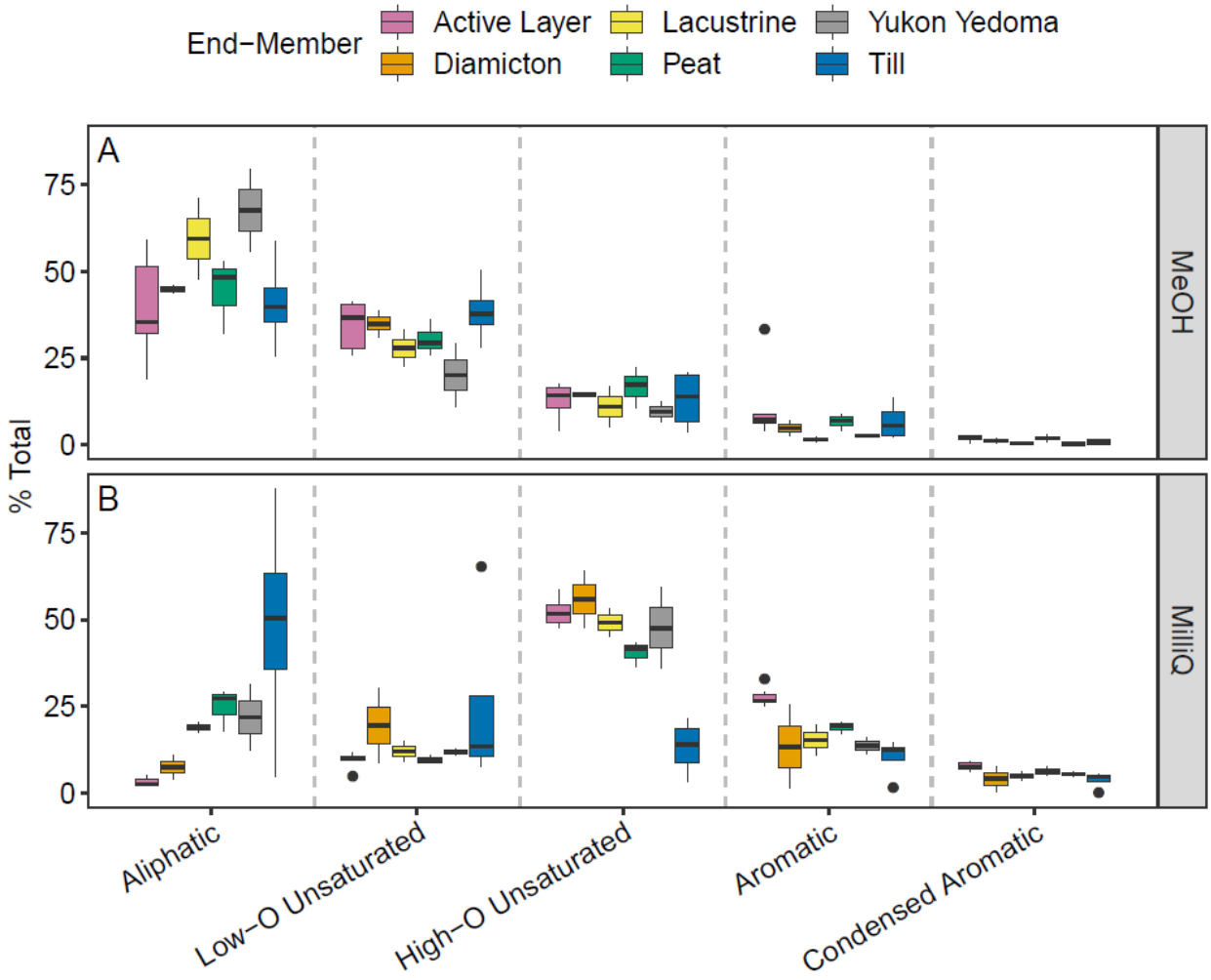

Figure A1-1. Boxplots to illustrate the proportional abundance of compound class groups for A) methanol and B) MilliQ. Panel B) is shown for comparison purposes here, and is identical to the plot in Figure 2-3; boxplot ranges follow those described in Figure 2-3.

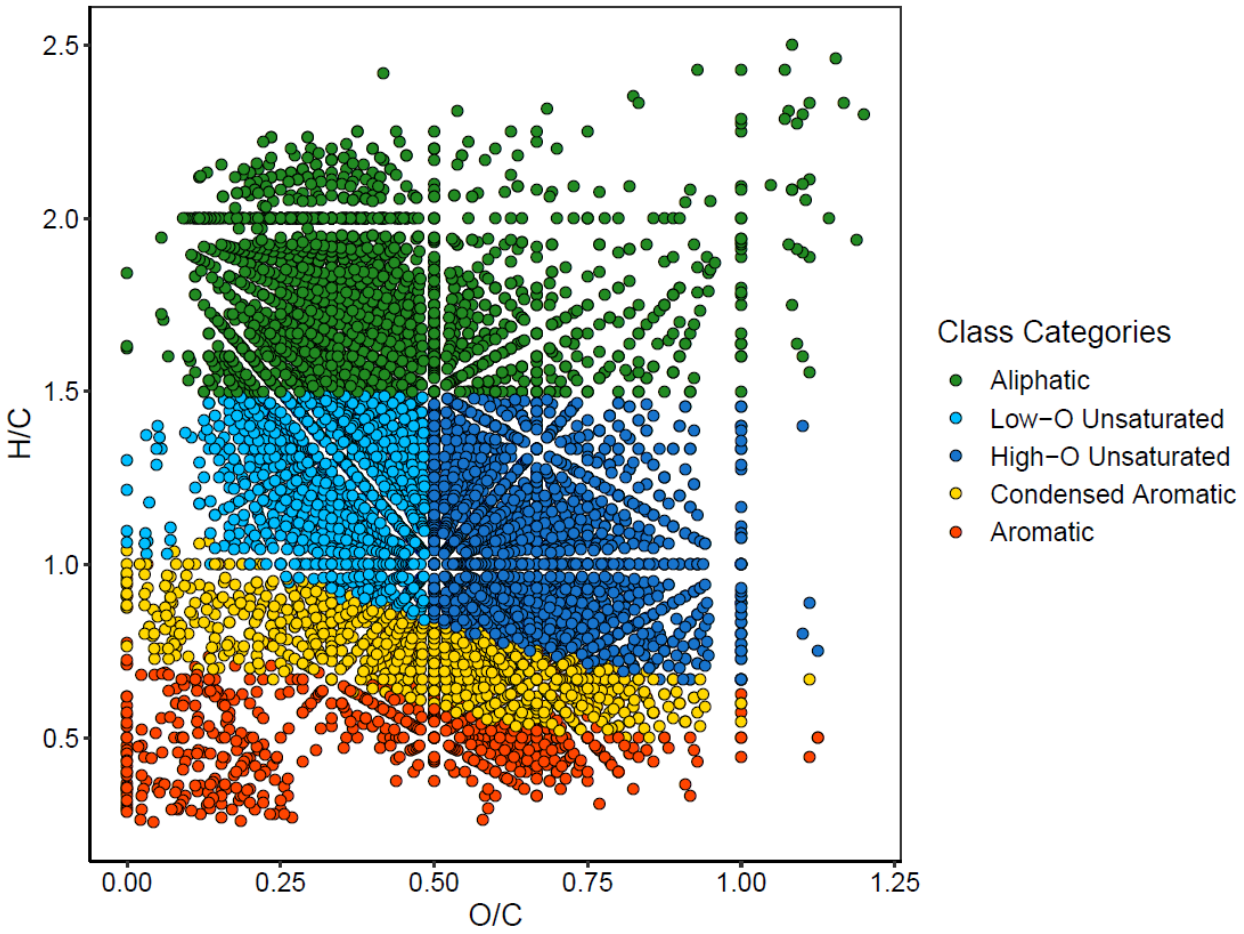

Figure A1-2. Van Krevelen plot showing the broad compound classes used in this study.

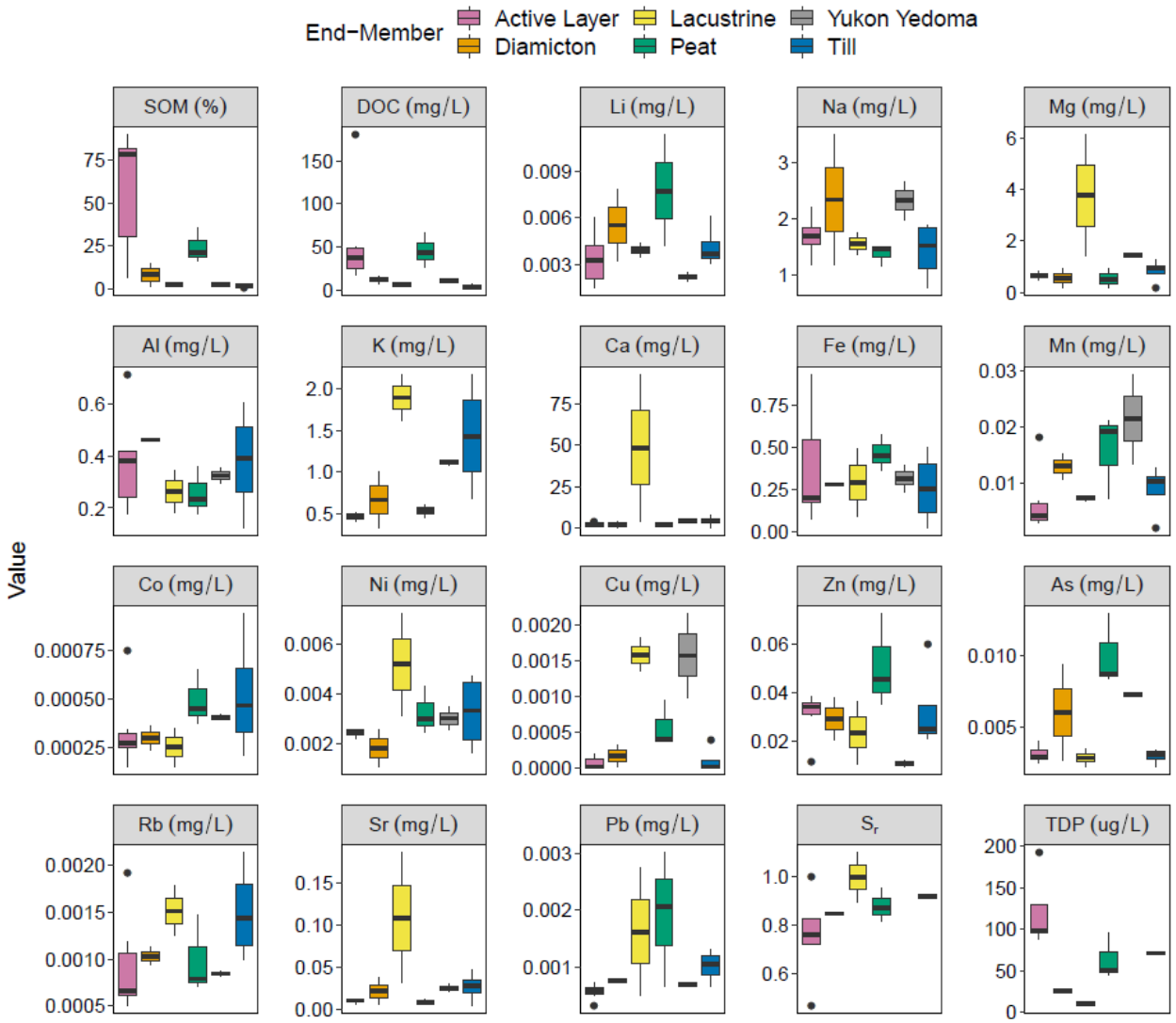

Figure A1-3. Boxplots for the nutrient concentrations, trace metal concentrations, and slope ratio for active layer and permafrost end-members. Headings denote the parameter and units, while colour denotes end-member type. Boxplot ranges follow those described in Figure 2-3.

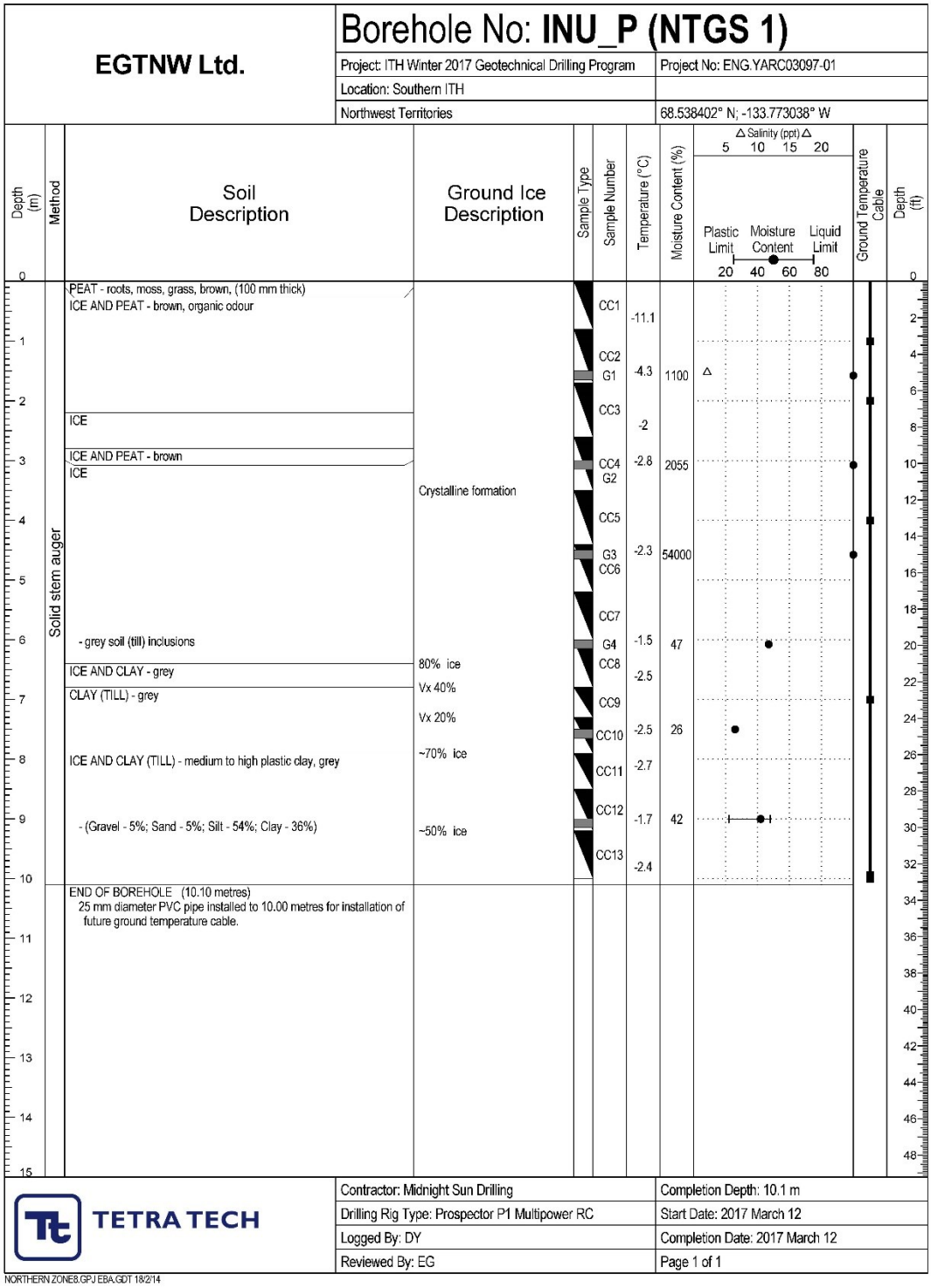

Figure A1-4. Sedimentological properties by depth for BH1 (NTGS1) collected in 2017, from appendix B in Ensom et al. 2020. Note that samples collected from less than 2 m were collected in 2018 from boreholes that were immediately adjacent to the boreholes depicted here.

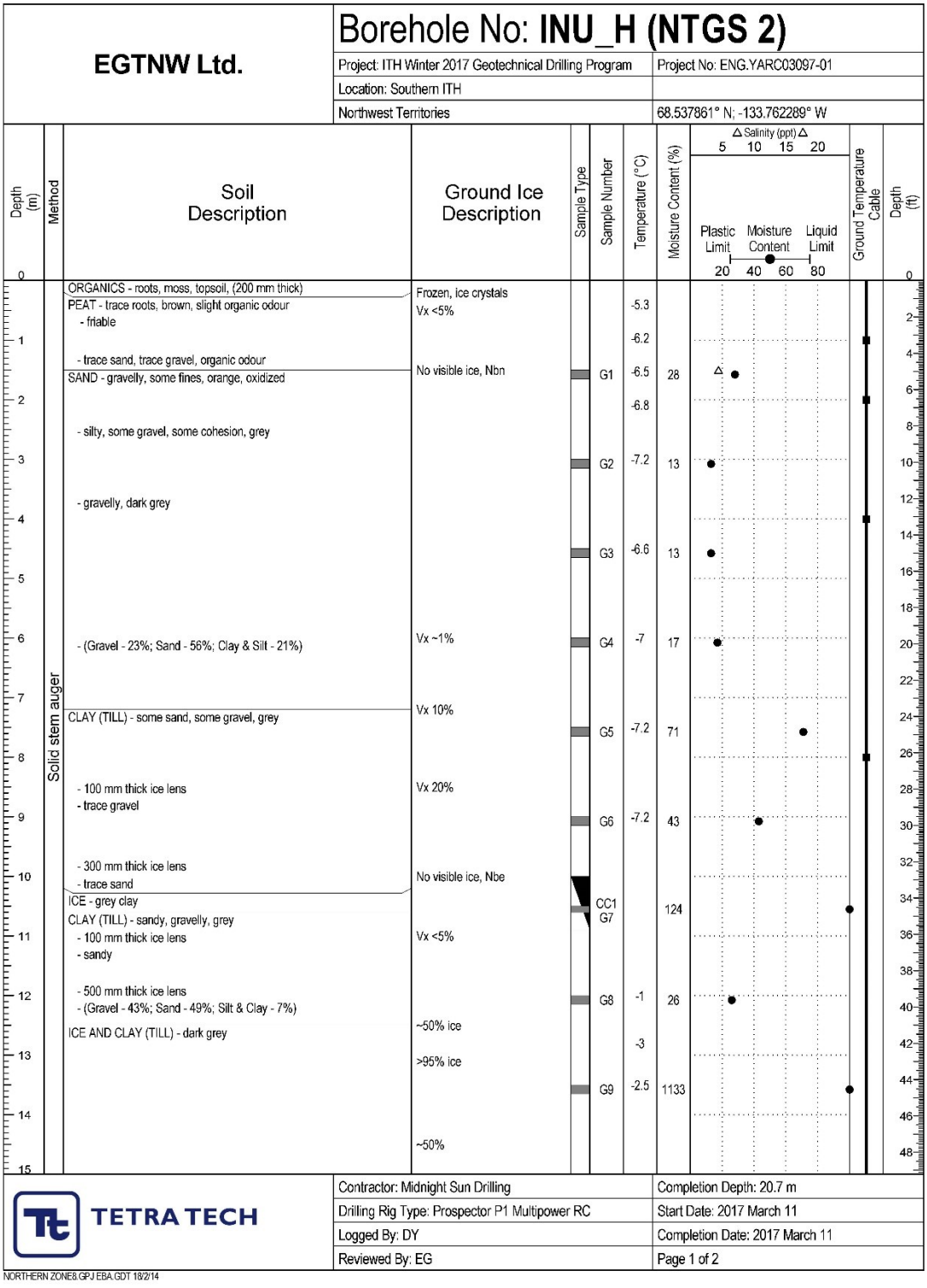

Figure A1-5. Sedimentological properties by depth for BH2 (NTGS2), from appendix B in Ensom et al. 2020. Note that samples collected from less than 2 m were collected in 2018 from boreholes that were immediately adjacent to the boreholes depicted here.

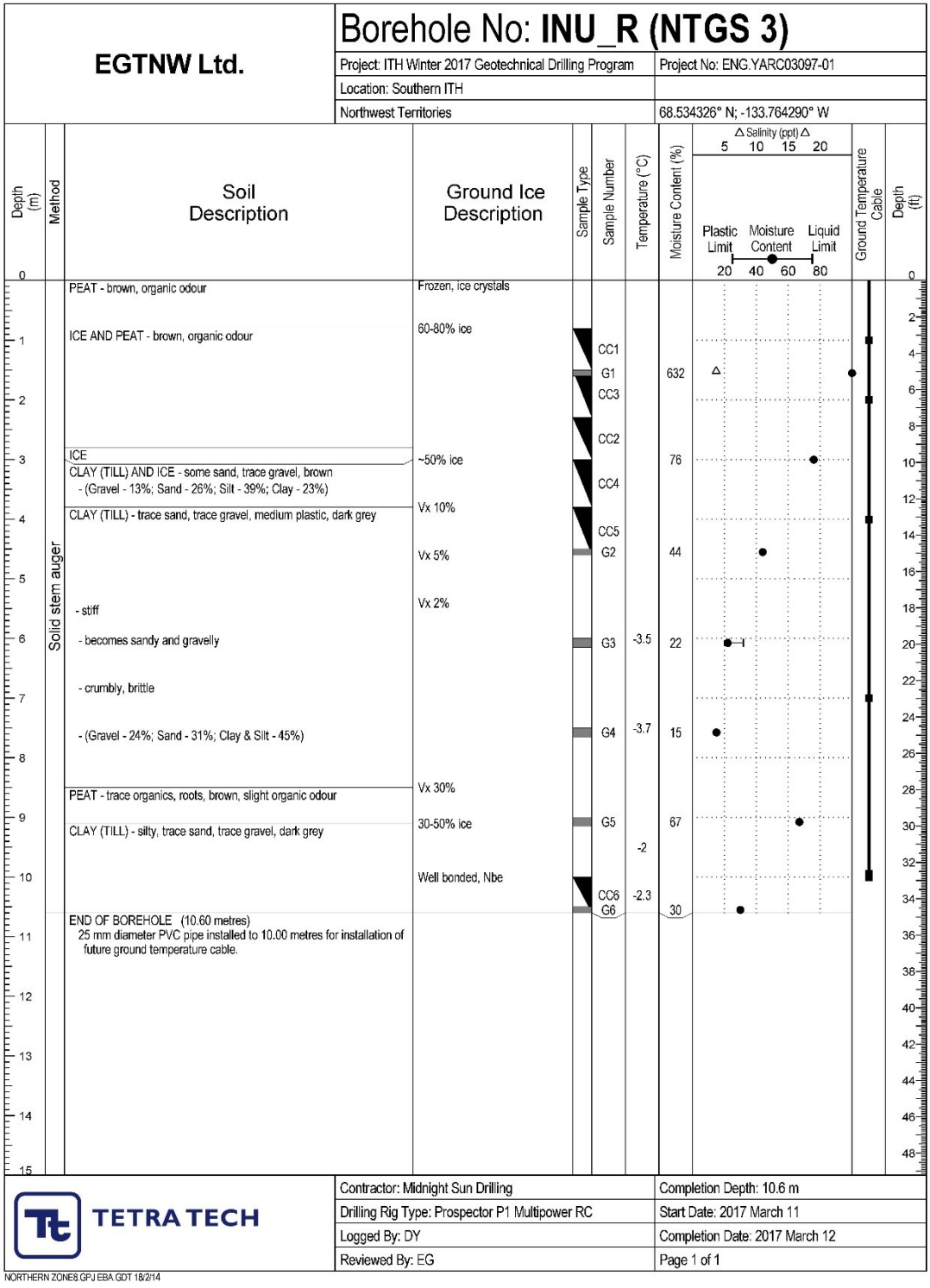

Figure A1-6. Sedimentological properties by depth for BH3 (NTGS3), from appendix B in Ensom et al. 2020. Note that samples collected from less than 2 m were collected in 2018 from boreholes that were immediately adjacent to the boreholes depicted here.

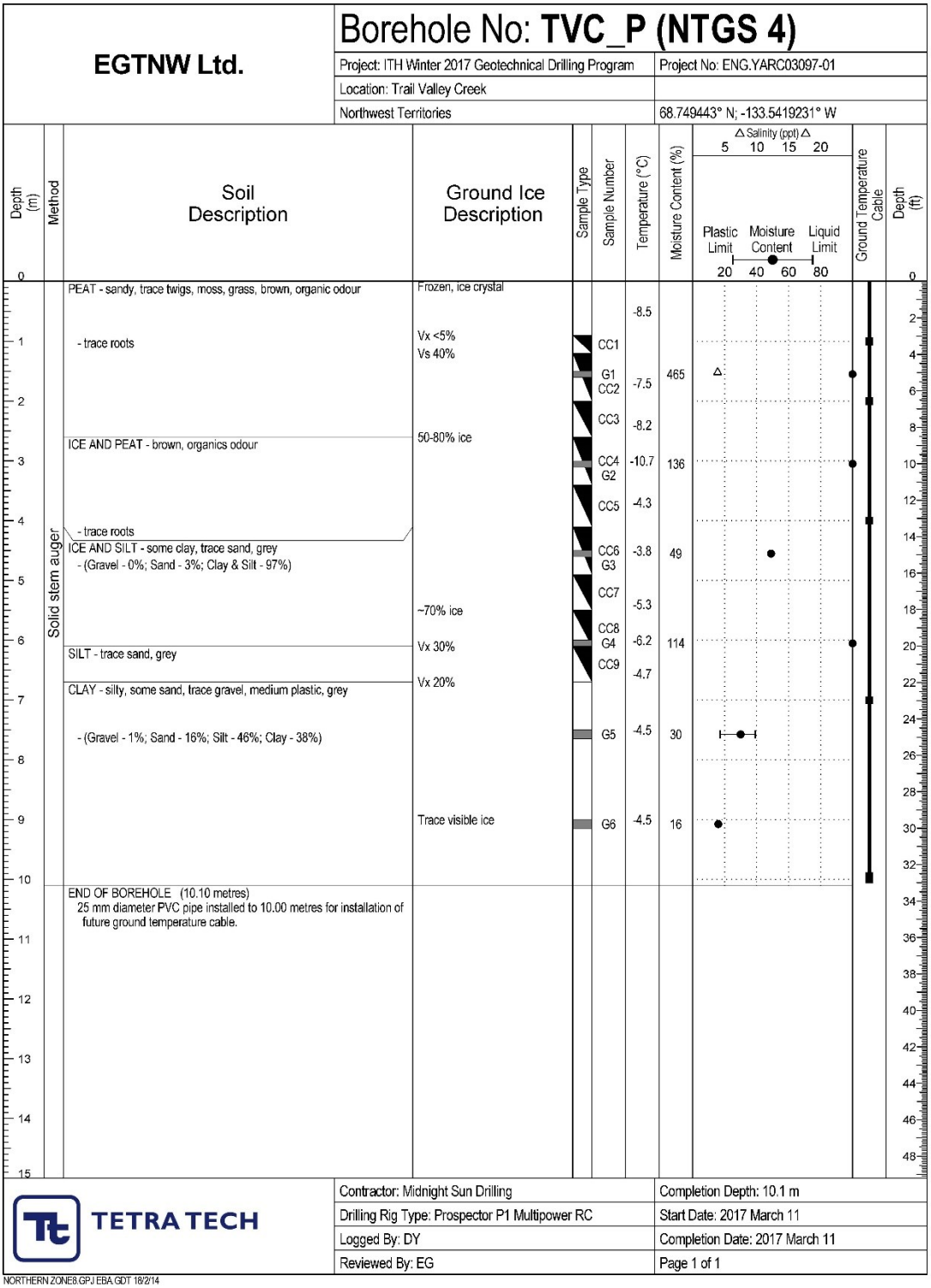

Figure A1-7. Sedimentological properties by depth for BH4 (NTGS4), from appendix B in Ensom et al. 2020.

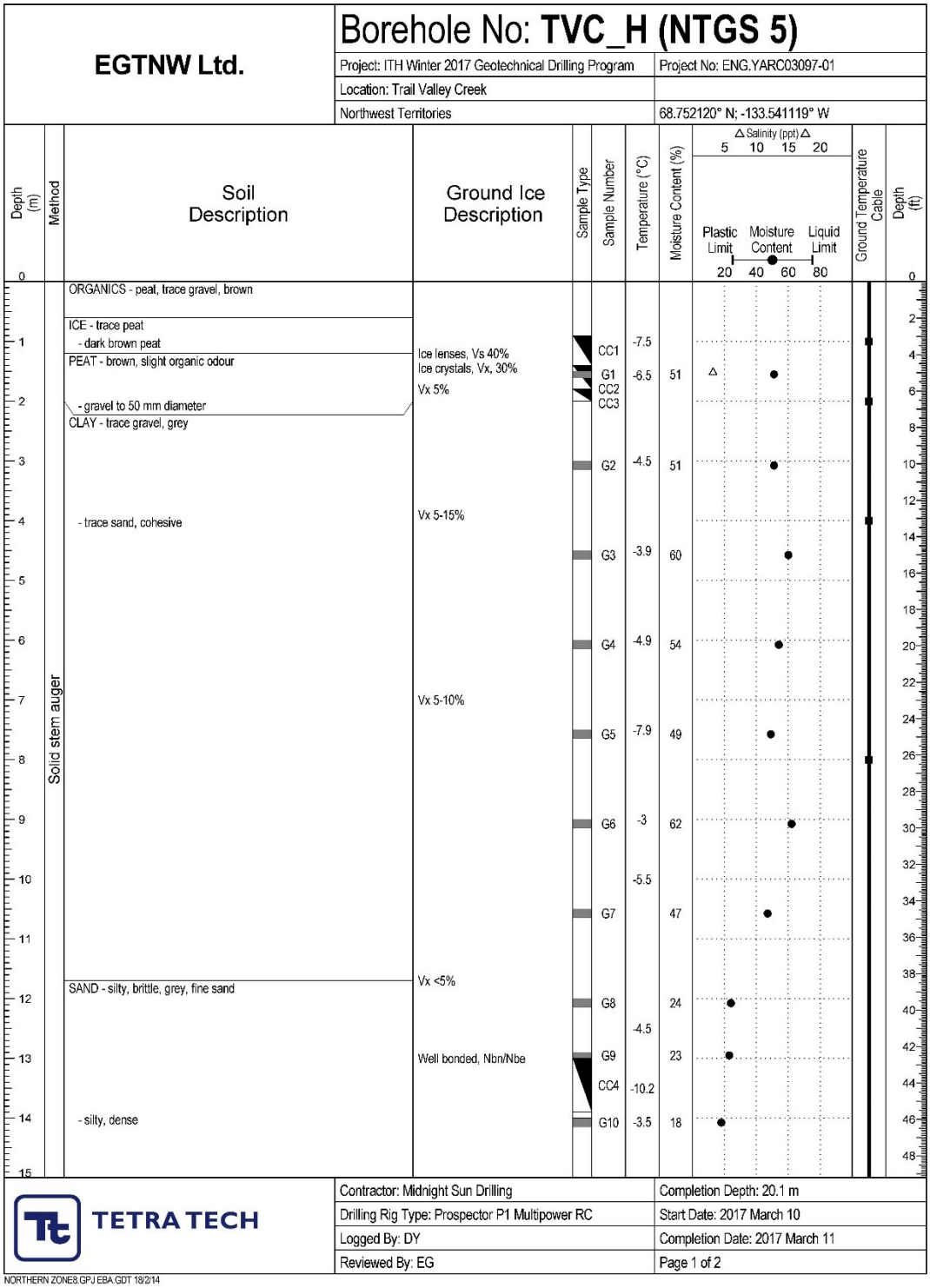

Figure A1-8. Sedimentological properties by depth for BH5 (NTGS5), from appendix B in Ensom et al. 2020.

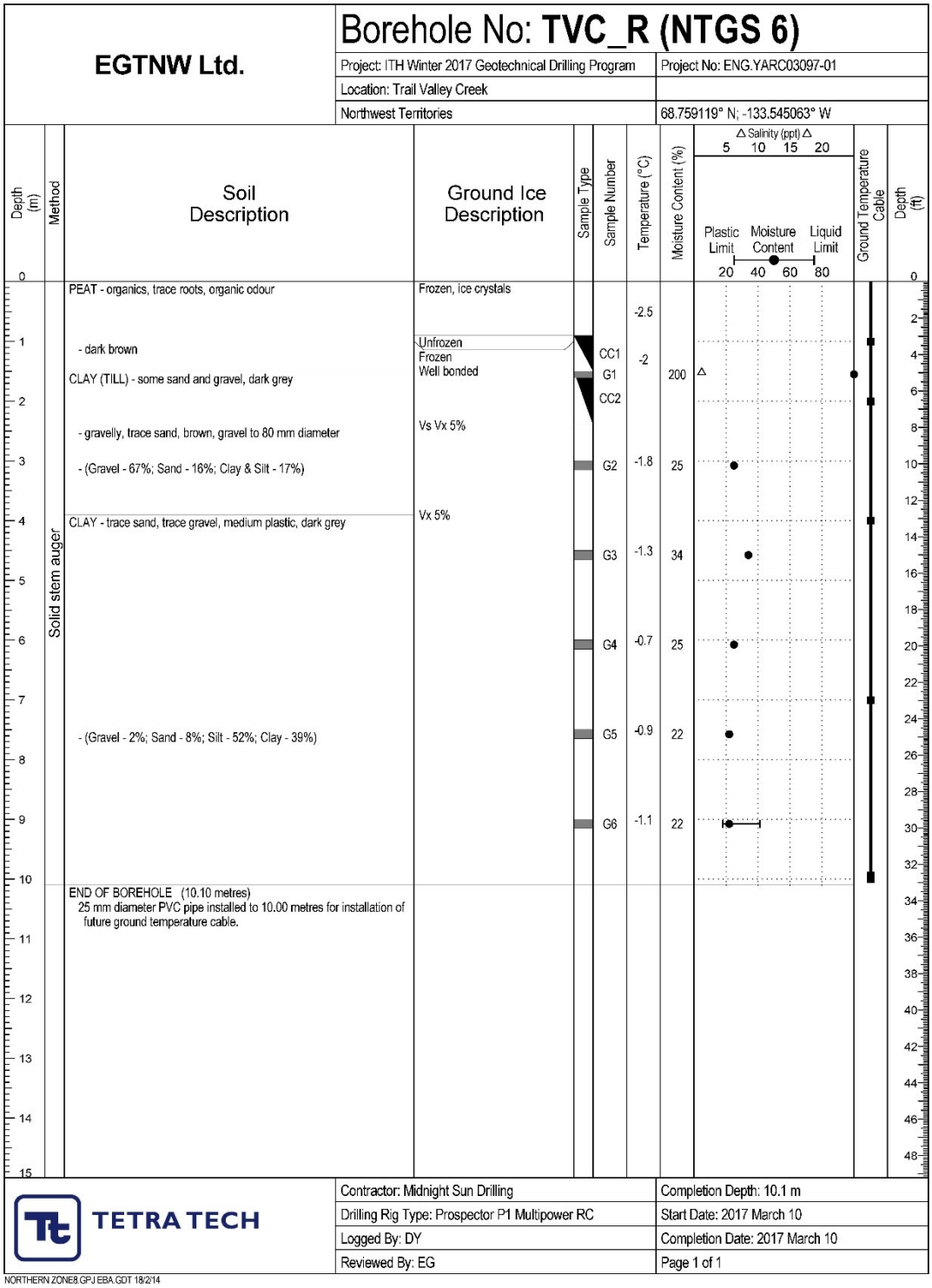

Figure A1-9. Sedimentological properties by depth for BH6 (NTGS6), from appendix B in Ensom et al. 2020. Note that samples collected from less than 2 m were collected in 2018 from boreholes that were immediately adjacent to the boreholes depicted here.

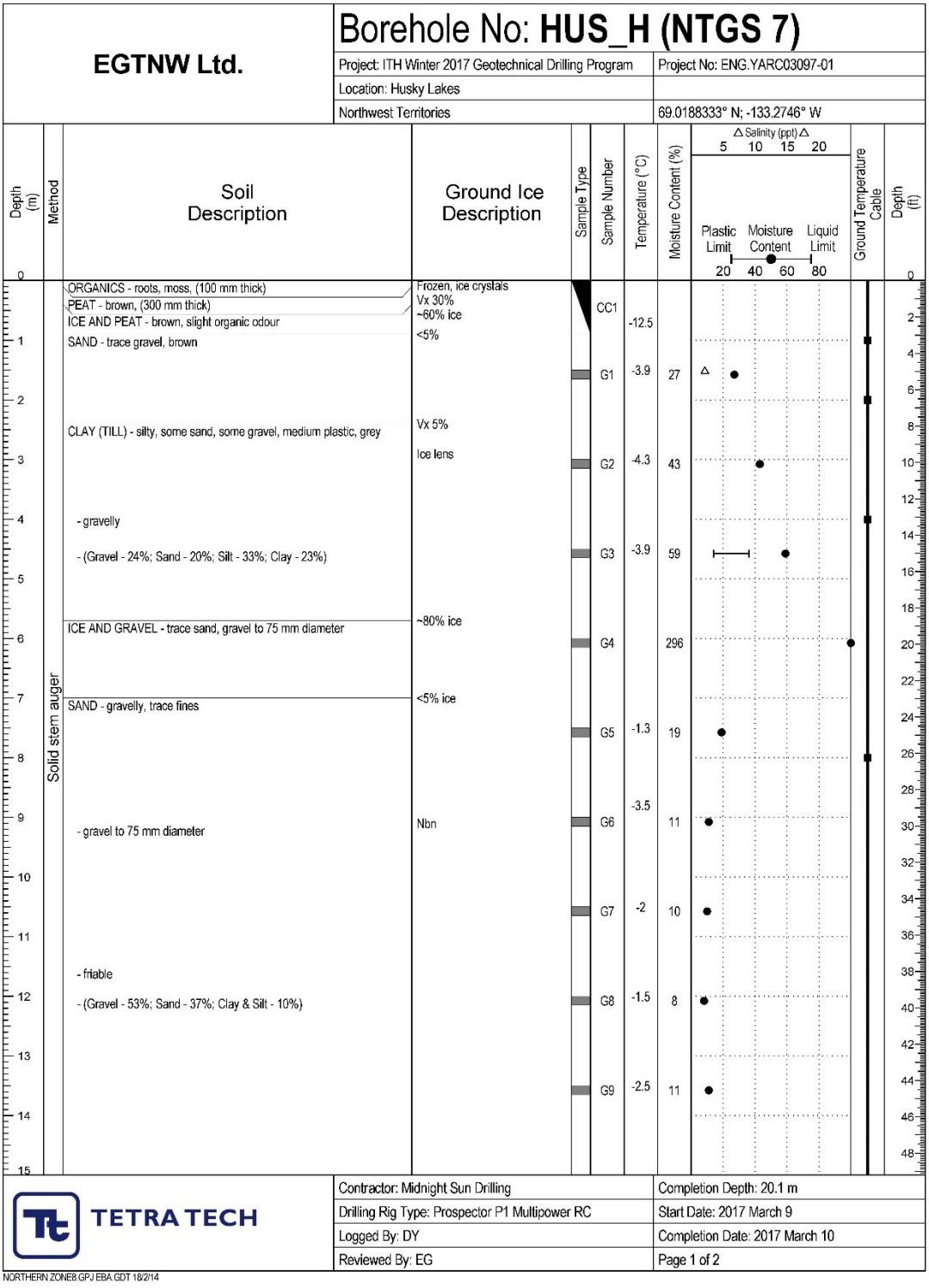

Figure A1-10. Sedimentological properties by depth for BH7 (NTGS7), from appendix B in Ensom et al. 2020. Note that samples collected from less than 2 m were collected in 2018 from boreholes that were immediately adjacent to the boreholes depicted here.

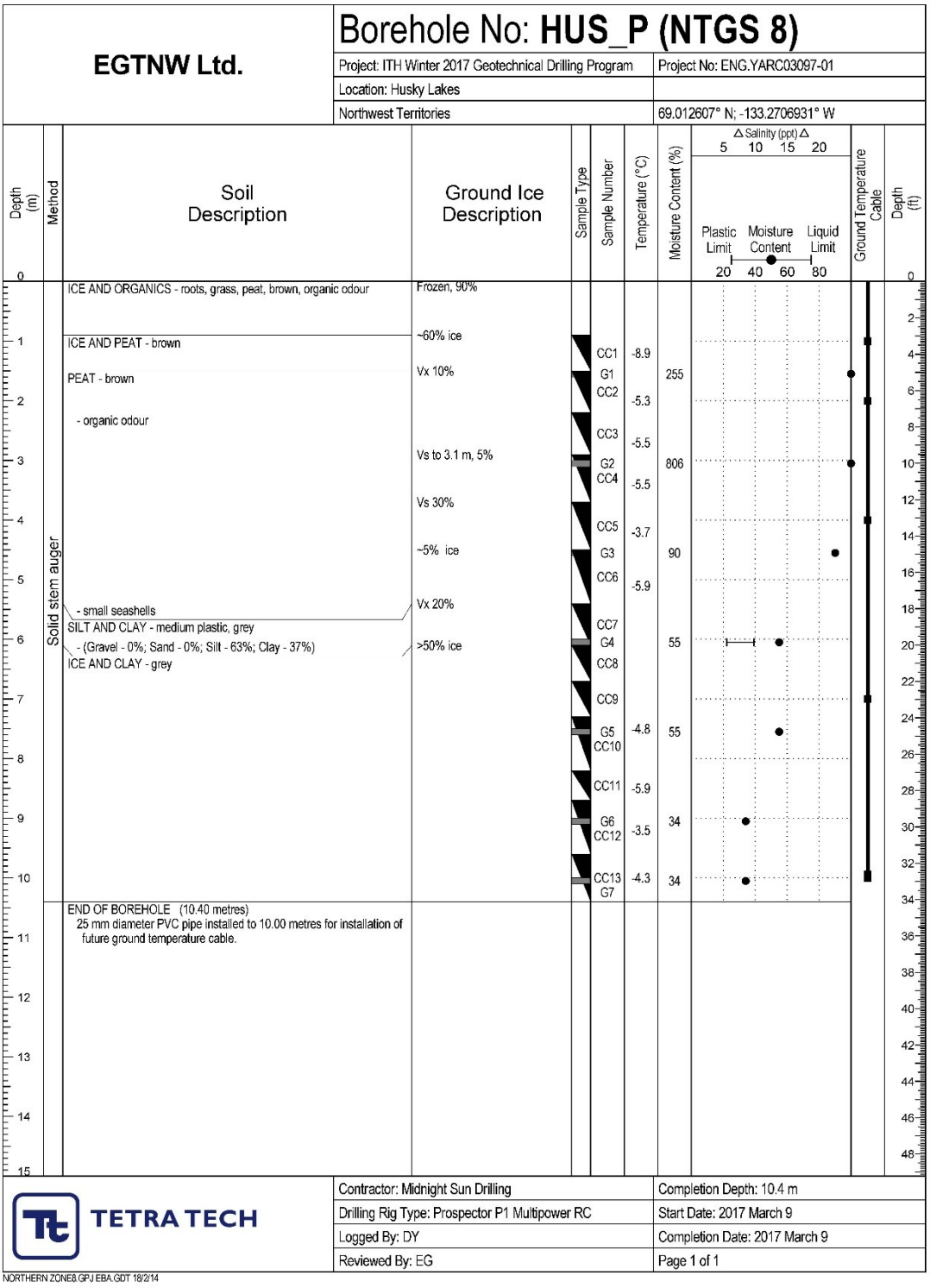

Figure A1-11. Sedimentological properties by depth for BH8 (NTGS8), from appendix B in Ensom et al. 2020. Note that samples collected from less than 2 m were collected in 2018 from boreholes that were immediately adjacent to the boreholes depicted here.

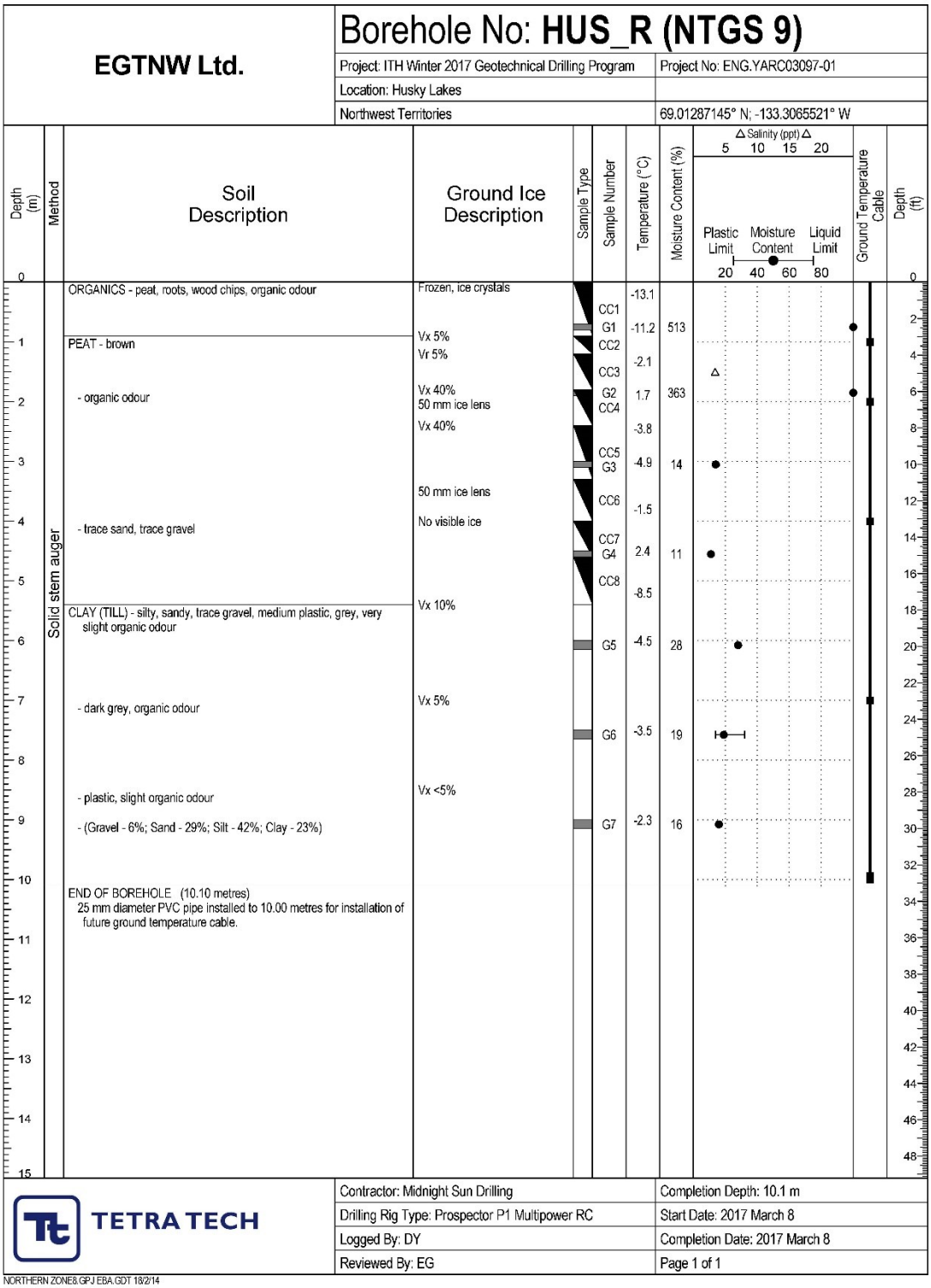

Figure A1-12. Sedimentological properties by depth for BH9 (NTGS9), from appendix B in Ensom et al. 2020. Note that samples collected from less than 2 m were collected in 2018 from boreholes that were immediately adjacent to the boreholes depicted here.

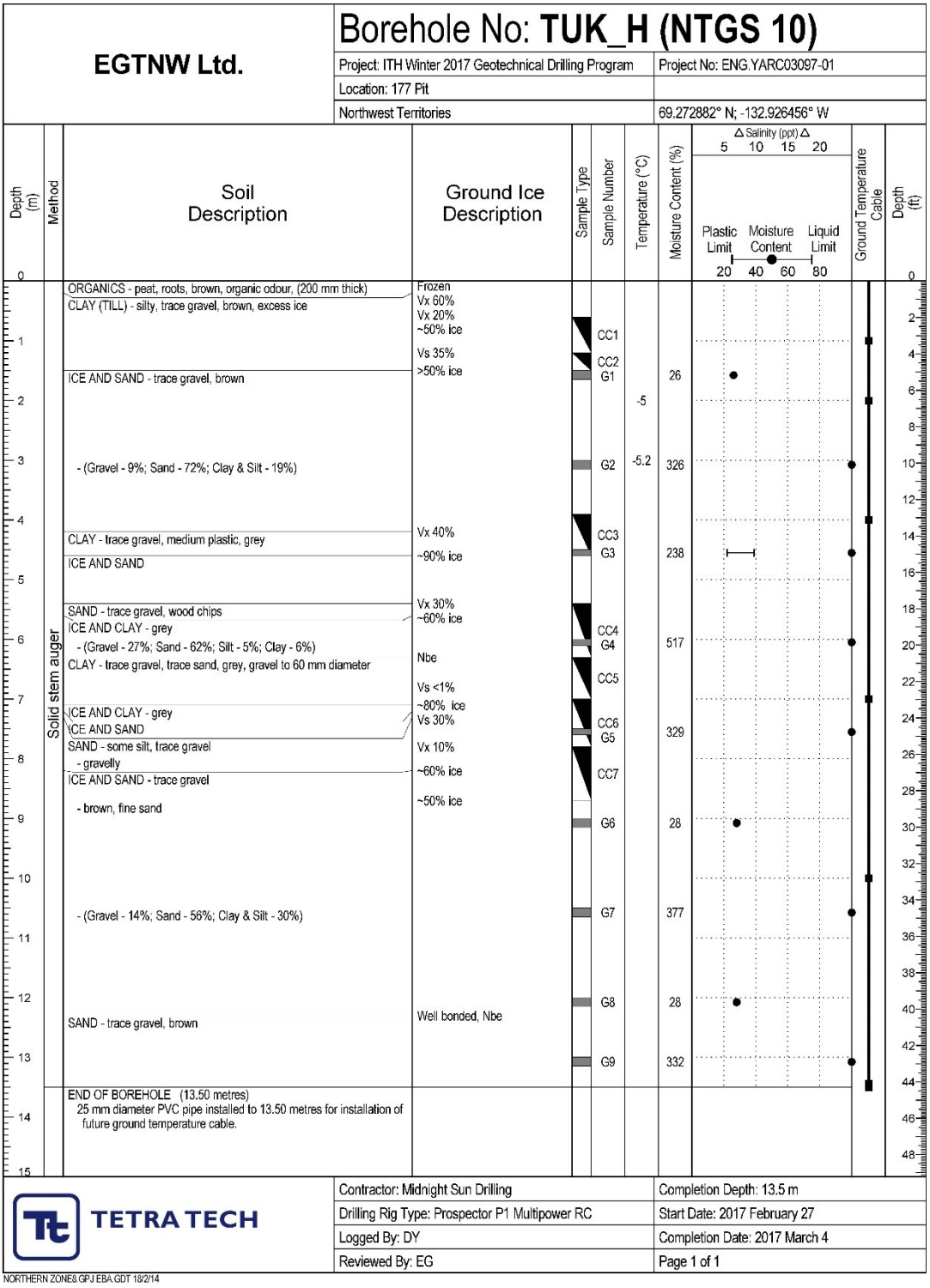

Figure A1-13. Sedimentological properties by depth for BH10 (NTGS10), from appendix B in Ensom et al. 2020.

Appendix 2. Supporting information for Chapter 3

Table A2-1. Description of fluorescence metrics with excitation (Ex) and emission (Em) wavelengths, including a brief description and the original reference for each metric (Gabor, McKnight, and Miller 2014). Note that the fluorescence index, humification index, freshness index, and slope ratio are calculated as ratios for the wavelengths specified.

Metric	Ex (nm)	Em (nm)	Description	Source
Peak B	275	310	Protein-like (tyrosine)	Coble 1996
Peak T	275	340	Protein-like (tryptophan)	Coble 1996
Peak A	260	380-460	Humic-like (fulvic acid)	Coble 1996
Peak M	312	380-420	Marine humic-like	Coble 1996
Peak C	350	420-480	Humic-like (terrestrial)	Coble 1996
Fluorescence Index (FI)	370	450 and 500	Increasing FI indicates more microbial (less terrestrial)	McKnight et al. 2001
Humification Index (HIX)	254	300-345 and 435-480	Increasing HIX indicates increasing humification	Ohno 2002
Freshness Index (BIX)	310	380 and 430	Increasing BIX indicates fresher material (microbially-produced)	Huguet et al. 2009
Slope Ratio (S_r)		275-295/350-400	Higher S_r indicates lower molecular weight	Helms et al. 2008

Table A2-2. Description of water chemistry parameters where sample time refers to the experimental time of collection. Filtration describes the filter nominal pore size and material*. Preservative refers to any additional acidification or treatmeant, while storage denotes the approximate temperate the samples were stored at prior to analysis.

Parameter	Sample Time	Filtration	Preservative	Storage	Analyzer
DOC	0, 28	0.7 GF/F	0.1% HCl	4°C	Shimadzu-TOC5000A
Abs/Fluor	0, 28	0.7 GF/F	None	4°C	Horiba Aqualog
TDP	0	0.7 GF/F	None	4°C	Lachat QuickChem QC8500 FIA Automated Ion Analyzer
TDN	0	0.7 GF/F	None	4°C	
DIN	0, 28	0.7 GF/F	None	-20°C	
Metals	28	0.7 GF/F	18% HNO_3	4°C	Thermo ICAP-6300 OES
$\delta^{18}O$	NA	none	No headspace	4°C	Los Gatos Liquid Water Isotope Analyzer
POC	0	0.1 Silver	0.1% HCl	4°C, room	Micro Cube elemental analyzer
DNA	0, 28	0.2 PES	1 mL RNALater	-20°C	

*For filtration, GF/F refers to Whatman Glass Fibre Filters, Silver refers to Sterlitech silver filters, PES refers to Millipore Sigma Polyethersulfone filters.

Table A2-3. Initial (time=0) DOM Compositional data for all experimental samples. ID represents samples using abbreviations that reference site (B=HB, D=HD, and C=FM3), stratigraphic layer (A=active layer, H=Holocene permafrost, P=Pleistocene permafrost) and inoculum type (U=Upstream, W=Within slump rill-water, N=Native, or K=Killed controls); EEE represent MilliQ controls. Input values of Sr, BIX, FI, and HIX represent the absolute value for these parameters, while input values of fluorescent peaks (PeakB, etc.) represent the contribution of each peak to the total fluorescent pool. Note that samples CAK, CAN, CAU, and CAW were removed from analyses as described in the methods 3.2.3 Leachate Preparation.

ID	Time	S_r	BIX	FI	HIX	PeakB	PeakT	PeakA	PeakM	PeakC
BAN	0	0.9	0.9	1.3	0.6	29.2	17.9	23.8	14.5	14.6
BAU	0	0.9	0.8	1.2	0.7	25.4	16.1	26.9	16.8	14.9
BAW	0	0.9	0.9	1.3	0.7	27.4	17.4	24.9	15.4	14.9
BPN	0	1.0	1.3	1.4	0.5	43.4	24.9	14.0	10.4	7.2
BPU	0	1.0	1.2	1.4	0.6	36.6	22.5	19.1	12.5	9.4
BPW	0	1.0	1.2	1.4	0.5	40.7	23.3	16.0	11.6	8.4
CAK	0	2.1	1.2	1.4	0.6	44.5	15.3	17.4	13.0	9.9
CAN	0	2.2	1.9	1.7	0.5	55.0	16.3	12.1	10.3	6.3
CAU	0	2.2	1.1	1.4	0.6	43.4	14.4	20.1	11.8	10.3
CAW	0	2.2	1.1	1.4	0.6	42.7	14.3	20.7	12.3	10.0
CHK	0	0.8	1.1	1.4	0.7	20.9	14.2	28.3	20.0	16.7
CHN	0	0.8	1.1	1.4	0.7	20.6	13.3	32.7	18.6	14.8
CHU	0	0.8	1.0	1.3	0.8	18.8	12.0	34.8	18.9	15.6
CHW	0	0.8	1.0	1.3	0.8	19.3	12.4	34.4	18.7	15.2
CPK	0	0.9	0.8	1.4	0.9	4.4	7.5	38.9	27.9	21.2
CPN	0	1.2	1.0	1.5	0.9	4.7	8.9	41.5	25.8	19.1
CPU	0	1.0	0.9	1.4	0.9	4.2	8.2	41.9	25.7	20.1
CPW	0	1.0	0.9	1.4	0.9	4.3	8.6	41.5	25.8	19.9
DAN	0	1.6	1.1	1.5	0.6	29.9	15.1	24.8	16.1	14.1
DAU	0	1.7	1.0	1.4	0.7	25.4	13.7	28.3	16.8	15.8
DAW	0	1.5	1.1	1.5	0.6	28.5	15.0	24.6	17.3	14.6
DHU	0	1.6	0.8	1.4	0.8	8.8	9.9	37.1	23.8	20.4
DHW	0	0.8	0.9	1.4	0.8	12.2	11.7	34.3	23.2	18.7
DPN	0	1.1	1.1	1.3	0.7	16.7	13.3	33.7	20.5	15.8
DPU	0	1.2	1.0	1.3	0.8	14.5	11.8	35.4	21.2	17.2
DPW	0	3.7	0.9	1.4	0.8	10.4	10.1	37.4	23.5	18.5
EEE	0	0.9	0.7	0.9	0.3	20.7	14.4	49.2	8.2	7.4

Table A2-4. Final (time=28) DOM compositional data for all experimental samples. Sample ID, parameter descriptions, and excluding CA- samples follow those described in Table A2-3.

ID	Time	Sr	BIX	FI	HIX	PeakB	PeakT	PeakA	PeakM	PeakC
BAN	28	0.8	0.8	1.3	0.7	24.8	15.0	26.8	16.8	16.5
BAU	28	0.8	0.7	1.2	0.8	17.7	12.0	31.5	20.8	18.0
BAW	28	0.8	0.8	1.3	0.7	22.3	14.4	27.9	18.2	17.2
BPN	28	0.9	1.2	1.4	0.6	37.5	21.0	18.7	13.3	9.5
BPU	28	0.8	0.9	1.3	0.7	25.3	18.1	26.8	16.4	13.4
BPW	28	0.9	1.1	1.4	0.6	33.4	20.0	21.2	14.2	11.1
CAK	28	0.6	0.7	1.3	0.8	6.4	8.6	39.0	24.9	21.1
CAN	28	0.9	1.4	1.5	0.5	46.9	18.0	15.1	12.2	7.8
CAU	28	0.9	1.0	1.3	0.6	34.9	14.8	24.3	14.0	12.1
CAW	28	0.9	1.0	1.3	0.6	34.8	14.5	24.5	14.3	11.8
CHK	28	0.6	0.8	1.4	0.8	5.5	8.8	37.4	27.0	21.3
CHN	28	0.7	0.9	1.4	0.9	9.3	9.4	41.0	22.2	18.1
CHU	28	0.7	0.9	1.3	0.8	10.6	9.3	39.8	22.0	18.4
CHW	28	0.7	0.9	1.3	0.9	10.1	9.2	39.9	22.4	18.5
CPK	28	0.5	0.8	1.4	0.9	4.6	7.5	38.0	28.3	21.7
CPN	28	0.7	1.0	1.4	0.9	4.4	8.7	41.6	26.4	18.9
CPU	28	0.8	0.9	1.4	0.9	3.8	7.5	40.8	27.1	20.8
CPW	28	0.8	0.9	1.4	0.9	3.8	8.0	41.8	26.6	19.8
DAN	28	0.7	1.0	1.5	0.7	26.0	13.9	27.3	17.2	15.7
DAU	28	0.7	0.9	1.4	0.8	20.3	11.5	31.4	19.3	17.6
DAW	28	0.7	0.8	1.4	0.8	5.4	9.4	36.3	27.4	21.4
DHU	28	0.7	0.8	1.3	0.9	3.8	8.0	40.1	26.6	21.6
DHW	28	0.6	0.9	1.4	0.9	5.3	9.5	37.8	26.8	20.7
DPN	28	0.7	1.0	1.4	0.8	11.1	10.9	37.8	22.5	17.6
DPU	28	0.7	0.9	1.3	0.8	10.0	10.1	38.6	23.0	18.3
DPW	28	0.9	0.9	1.4	0.9	4.7	8.5	40.5	26.2	20.1
EEE	28	0.9	-0.3	2.8	0.3	34.9	16.3	28.3	11.4	9.0

Table A2-5. Final (time=28) metal concentrations (Al, Ca, Fe, K, Mg, Na, Ba; units in heading) for experimental samples. Sample abbreviations and excluding CA- samples follow those described in Table A2-3.

ID	Al (µg/L)	Ca (mg/L)	Fe (mg/L)	K (mg/L)	Mg (mg/L)	Na (mg/L)	Ba (µg/L)
BAN	1275.0	4.7	2.7	2.8	1.9	1.0	740.2
BAU	836.0	16.4	1.8	2.8	6.0	2.3	586.1
BAW	1292.0	6.3	2.9	2.9	2.5	1.8	717.7
BPN	1581.0	1.9	3.0	0.8	1.1	1.0	307.5
BPU	1323.0	13.9	2.4	1.1	5.4	2.5	258.3
BPW	1758.0	3.9	3.3	1.2	2.0	2.0	353.3
CAK	na	na	na	na	na	na	na
CAN	16760.0	3.2	34.0	1.9	3.4	1.6	1614.0
CAU	15230.0	12.0	30.4	2.1	7.6	3.6	1789.0
CAW	16250.0	25.4	32.7	2.9	13.2	10.4	2112.0
CHK	na	na	na	na	na	na	na
CHN	256.9	25.7	0.4	6.6	10.1	10.9	545.0
CHU	711.1	24.6	1.3	6.0	9.6	9.8	542.2
CHW	1115.0	26.2	2.2	6.4	10.4	11.0	516.1
CPK	na	na	na	na	na	na	na
CPN	10.4	67.4	0.01	8.4	28.3	50.3	105.4
CPU	18.0	61.9	0.0	7.5	25.2	43.6	144.0
CPW	na	na	na	na	na	na	na
DAN	1818.7	2.1	5.5	1.4	1.4	1.2	969.9
DAU	na	na	na	na	na	na	na
DAW	601.6	14.6	1.0	2.4	6.8	13.5	433.8
DHU	na	na	na	na	na	na	na
DHW	9.3	97.8	0.01	8.1	28.4	35.7	93.2
DPN	271.4	49.5	0.5	8.1	17.0	95.5	114.2
DPU	271.0	46.2	0.6	6.5	14.8	75.3	143.7
DPW	9.2	56.5	0.01	7.7	20.3	90.9	87.5
EEE	na	na	na	na	na	na	na

Table A2-6. Final (time=28) metal concentrations (Cd, Co, Cr, Cu, Ni, Sr, V, Zn; units in heading) for experimental samples. Sample abbreviations and excluding CA- samples follow those described in Table A2-3.

ID	Cd (µg/L)	Co (µg/L)	Cr (µg/L)	Cu (µg/L)	Ni (µg/L)	Sr (µg/L)	V (µg/L)	Zn (µg/L)
BAN	0.15	11.2	1.8	7.0	14.1	32.8	5.8	120.6
BAU	0.4	3.7	1.8	4.4	8.9	53.5	2.8	79.4
BAW	0.6	10.2	2.2	7.3	13.8	38.4	6.4	100.3
BPN	0.7	4.1	4.9	12.2	5.0	18.6	7.3	60.0
BPU	0.4	4.4	4.3	10.1	5.3	43.5	4.8	48.8
BPW	0.7	2.1	5.5	12.8	7.9	28.3	7.4	54.5
CAK	na	na	na	na	na	na	na	na
CAN	0.15	52.0	21.0	47.0	30.0	157.0	55.0	361.0
CAU	5.0	20.0	24.0	51.0	30.0	157.0	57.0	311.0
CAW	0.15	26.0	16.0	46.0	29.0	157.0	51.0	237.0
CHK	na	na	na	na	na	na	na	na
CHN	0.15	1.0	0.9	4.6	0.8	57.3	2.4	7.15
CHU	0.15	1.7	2.5	8.9	1.9	69.8	3.7	25.2
CHW	0.4	1.5	2.6	15.7	3.4	89.2	6.1	50.4
CPK	na	na	na	na	na	na	na	na
CPN	0.15	2.6	0.4	0.7	0.8	46.1	0.95	22.6
CPU	0.15	0.45	0.4	1.5	1.7	43.6	0.95	19.3
CPW	na	na	na	na	na	na	na	na
DAN	0.8	7.7	3.9	17.0	13.4	44.7	8.7	70.0
DAU	na	na	na	na	na	na	na	na
DAW	0.9	13.4	1.1	11.0	27.1	52.5	0.95	182.5
DHU	na	na	na	na	na	na	na	na
DHW	0.15	7.7	1.6	0.7	13.6	176.0	0.95	28.4
DPN	0.5	1.4	1.8	6.0	0.8	104.7	0.95	23.9
DPU	0.15	0.45	1.7	5.0	2.3	95.0	2.6	23.0
DPW	0.15	9.8	0.4	0.7	11.0	107.7	0.95	23.9
EEE	na	na	na	na	na	na	na	na

Table A2-7. Oxygen loss (initial-final), initial total organic carbon (TOC), pH, nutrients, and carbon-normalized loss (Oxygen loss / TOC) for experiment samples. CA- samples were included for oxygen loss comparisons, but were excluded for all other parameters, as described in methods section 3.2.3. Sample abbreviations follow those described in Table A2-3.

ID	O loss (mg/L)	TOC (mg/L)	C-Normalized Loss (mg/L)	pH	TDP (ug/L)	TDN (ug/L)
BAN	1.55	18.73	8.3	5.1	145	597
BAU	4.08	5.15	79.2	5.2	136	537
BAW	2.27	8.64	26.3	5.2	134	688
BPN	2.37	5.55	42.6	6.3	129	237
BPU	3.44	4.75	72.3	6.4	109	219
BPW	3.18	5.25	60.6	6.4	117	371
CAK	-0.04	19.03	-0.2	1.1	1590	1460
CAN	0.47	35.04	1.4	4.5	1770	1340
CAU	0.57	34.63	1.6	4.8	1560	1310
CAW	0.58	33.55	1.7	5.0	1440	1260
CHK	0.18	4.39	4.0	2.2	328	555
CHN	2.36	8.50	27.7	7.4	338	523
CHU	2.41	3.92	61.6	7.8	300	520
CHW	3.08	8.51	36.3	7.7	299	507
CPK	0.10	4.46	2.2	2.2	15	1360
CPN	1.52	6.02	25.2	6.9	7	1480
CPU	1.60	4.62	34.6	7.4	6	1340
CPW	2.01	4.39	45.8	7.3	7	1360
DAK	0.03	12.09	0.3	na	na	na
DAN	0.68	10.14	6.7	4.4	304	328
DAU	1.69	12.02	14.0	4.4	278	308
DAW	2.95	14.59	20.2	4.4	292	762
DHU	6.54	10.88	60.1	6.7	36	2080
DHW	6.27	12.50	50.2	6.6	46	2330
DPK	1.84	11.88	15.5	na	na	na
DPN	2.26	6.42	35.2	7.0	149	1689
DPU	3.35	13.85	24.2	7.0	129	1395
DPW	3.60	17.68	20.4	5.7	162	1689
EEE	0.17	1.77	9.7	7.0	1	37

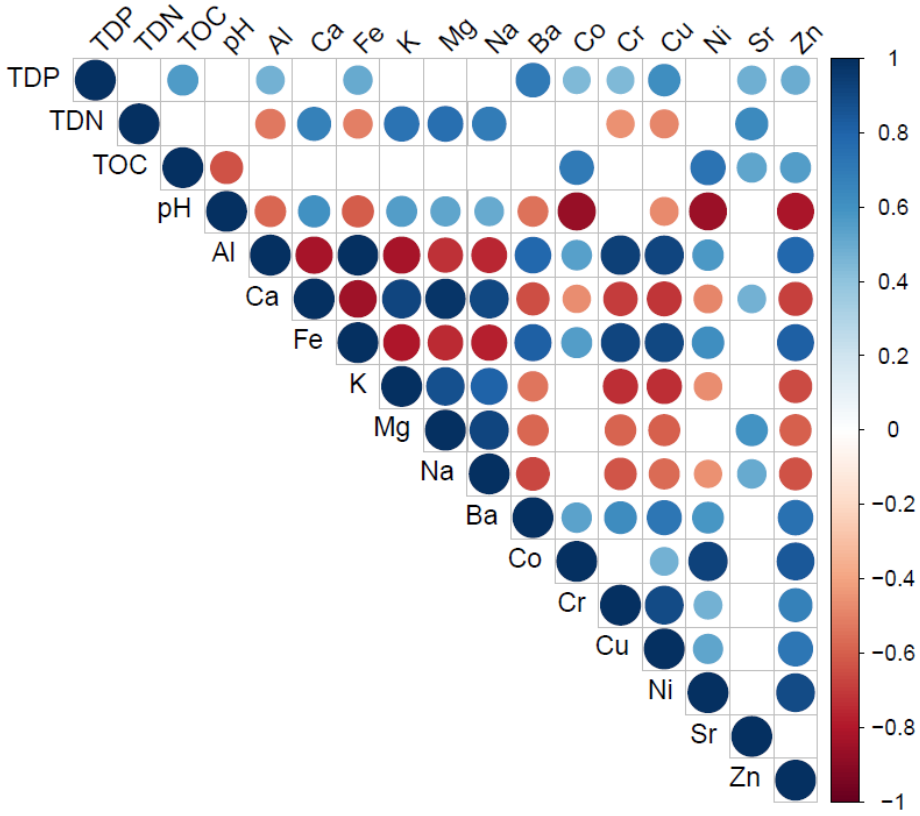

Figure A2-1. Correlation plot for water chemistry parameters including nutrients (measured from intial samples) and metals (measured from final samples). Only significant ($p<0.05$) correlation values are included, where colour indicates the sign (positive or negative) and size and shading indicates the correlation strength (larger is closer to 1).

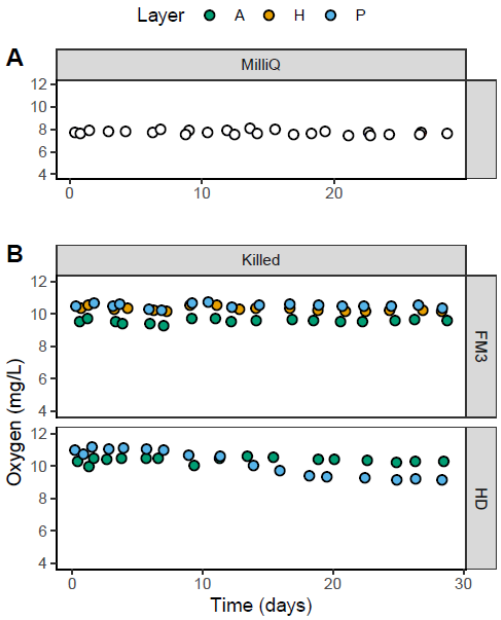

Figure A2-2. Oxygen concentrations by time for MilliQ and killed (1% volume concentration HCl) controls during the experiment, where horizontal sections represent sites and colour denotes layer (A=active layer, H=Holocene, and P=Pleistocene). Data points represent the mean and standard error (often smaller than height of symbol) of triplicate experiment bottles, with slight jitter to improve visibility of similar points (e.g., FM3-H and -P).

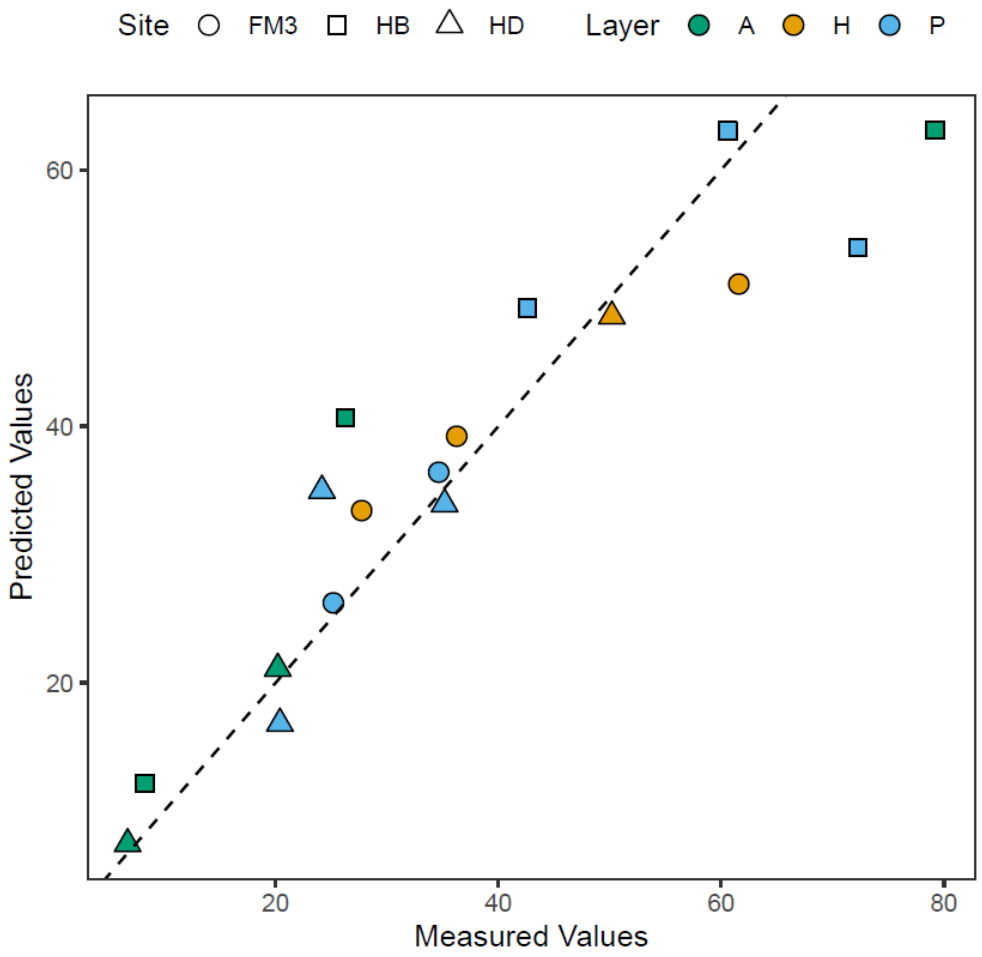

Figure A2-3. The predicted normalized oxygen loss using the LASSO regression against the actual normalized oxygen loss, where the dotted line represents a 1:1 relationship. Shape denotes the site and colour denotes the layer, where A=active layer, H=Holocene, and P=Pleistocene.

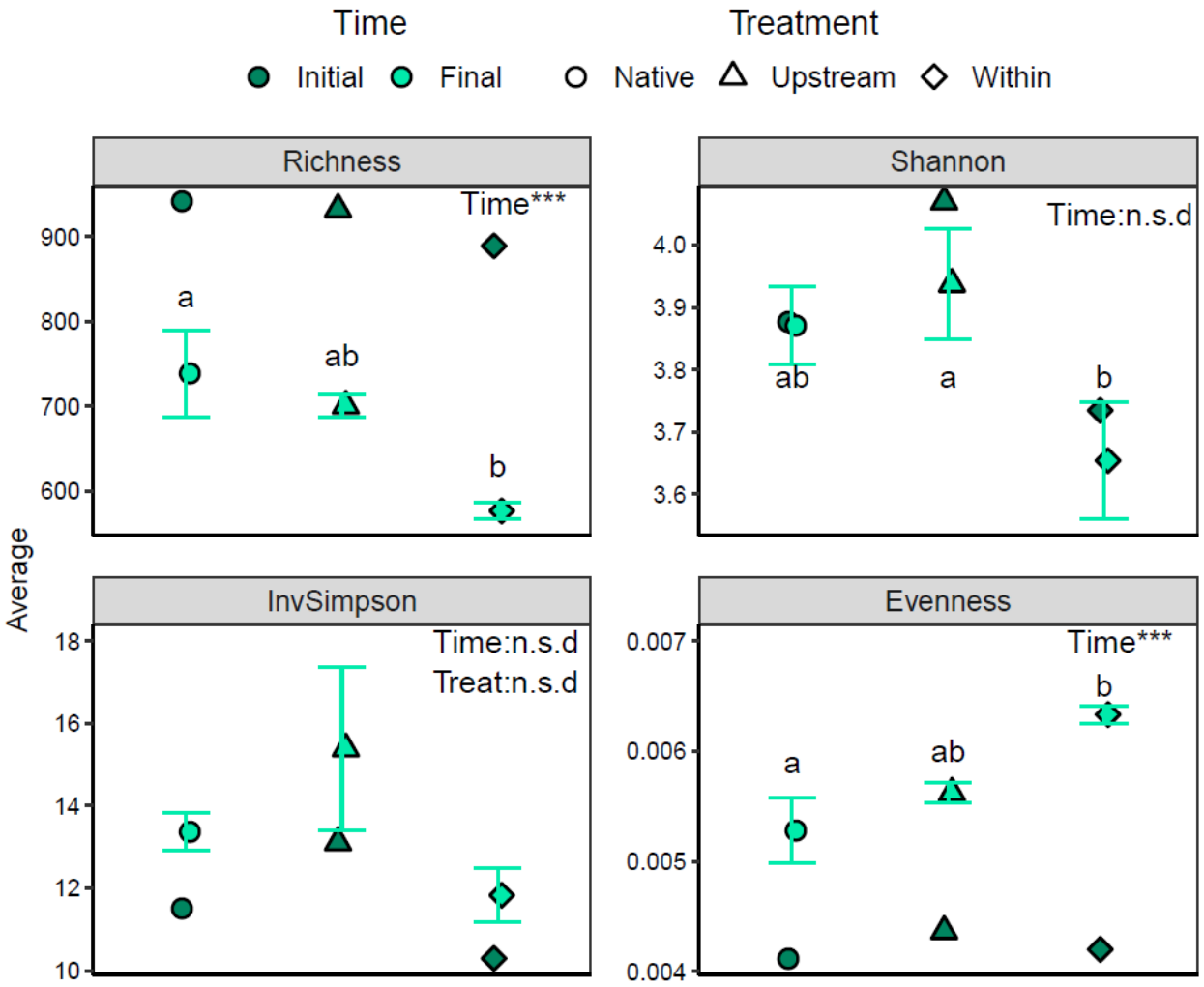

Figure A2-4. Diversity metrics to indicate bulk differences in microbial community between innocula treatments and over time. Final data points represent the mean with standard error bars from triplicate experimental bottles, where colour denotes time and shape denotes treatment. Letters and asterisks show significance for the two-way ANOVA with fixed effects of treatment (different letters show significant differences) and time (*** is significant), where n.s.d. means no significant difference. The index name is given in the header of each plot, with "free" y-axes to capture the appropriate range for each parameter.

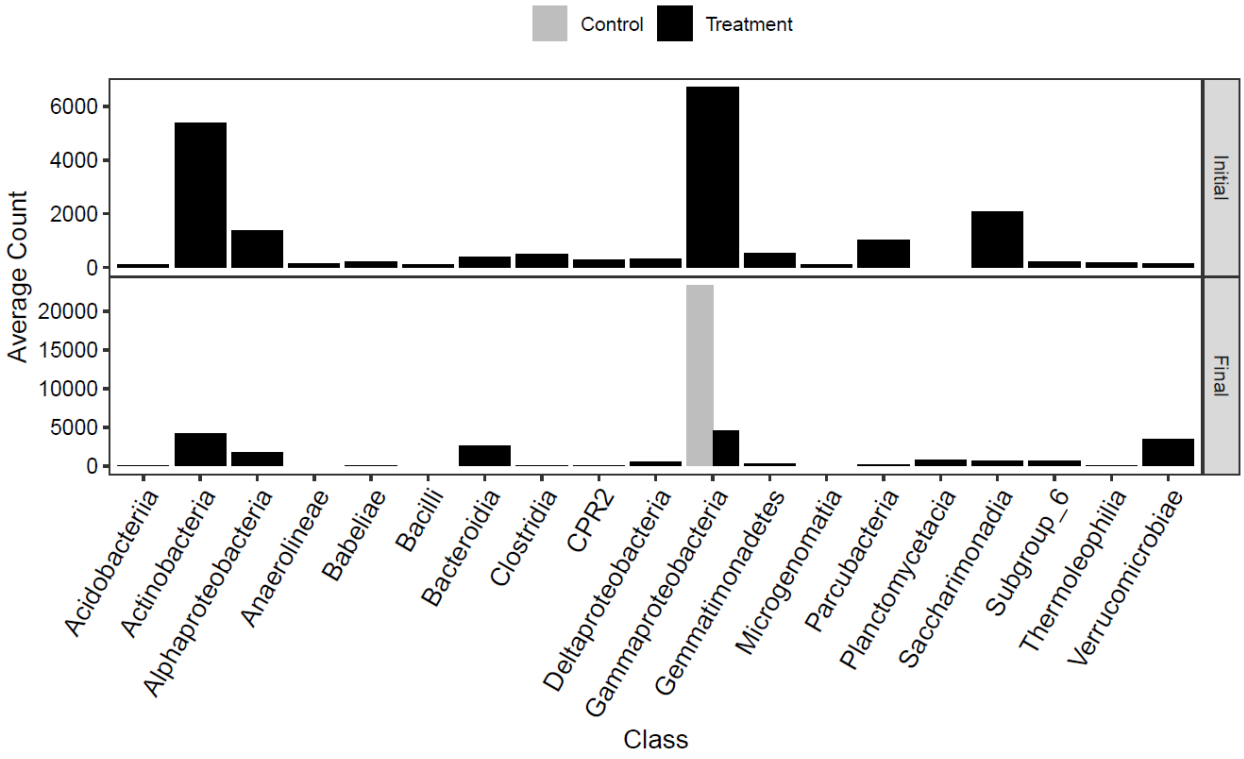

Figure A2-5. The average count of bacterial classes for the control and treatment bottles at the start (initial) and termination (final) of the experiment. The average represents the mean from triplicate treatment bottles for U-, W-, N-amended leachate sample, as well as a MilliQ control bottle. Results are based on the rarefied and decontaminated OTU table, presenting classes that had greater than 100 counts at either stage.